University of Alberta

Stability of Bilateral Teleoperation Systems: Effect of Sampled-data Control and Non-passivity or Strict-Passivity of Terminations

by

Seyed Ali Jazayeri Moghadas

A thesis submitted to the Faculty of Graduate Studies and Research

in partial fulfillment of the requirements for the degree of

Doctor of Philosophy

in

Control Systems

Department of Electrical and Computer Engineering

©Seyed Ali Jazayeri Moghadas

Fall 2013

Edmonton, Alberta

Abstract

A bilateral teleoperation system comprises a human operator, a teleoperator, and an environment. The teleoperator consists of a master robot, a slave robot, their controllers, and a communication channel between the master and the slave. Since the exact models of the teleoperator's terminations, namely the human operator and the environment, are typically unknown and/or time-varying, passivity or absolute stability of the two-port network teleoperator is considered in order to ensure the stability of the coupled teleoperation system. This stability analysis conventionally relies on two important assumptions: (a) all teleoperation system components operate in continuous-time, and (b) the teleoperator's terminations are passive. This dissertation studies the stability implications of violation of either assumption.

The stability of a bilateral teleoperation system may be jeopardized by controller discretization due to energy-distilling effects of a zero-order-hold. In this dissertation, a tool is developed to analyze the passivity of the sampled-data teleoperator. In the passivity framework, the teleoperation system is guaranteed to be passive and, therefore, stable for any passive and otherwise arbitrary terminations. Sufficient conditions for teleoperator passivity are derived for when position error based controllers are implemented in discrete-time and the rest of the system is in continuous-time. This new analysis is necessary because discretization does not necessarily preserve the passivity of a system. The proposed criterion for sampled-data teleoperator pas-

sivity imposes lower bounds on the teleoperator's robots dampings, an upper bound on the sampling time, and bounds on the control gains. The proposed criterion is verified through simulations and experiments. This constitutes Chapter 3 of this dissertation.

Teleoperator passivity is sufficient for the stability of the coupled teleoperation system including the terminations. A less conservative approach to guaranteeing the coupled system's stability is teleoperator's absolute stability. In the absolute stability framework, the teleoperation system is guaranteed to be stable for any passive and otherwise arbitrary terminations. This dissertation proposes a novel approach to analyzing the absolute stability of a sampled-data bilateral teleoperation system consisting of discrete-time controllers and continuous-time master, slave, operator, and environment. The proposed stability criterion permits scaling and delay in the master and the slave positions and forces. The absolute stability conditions impose bounds on the gains of the discrete-time controller, the damping terms of the master and the slave, and the sampling time. The resulting absolute stability condition has been verified via experiments with two Phantom Omni robots. This comprises Chapter 4 of this dissertation.

A design-related application of the above results is in proper selection of various control parameters and the sampling rate for stable teleoperation under discrete-time control. To explore the trade-off between the control gains and the sampling time, it is studied how large sampling times, which necessitate low control gains for maintaining stability, can lead to unacceptable teleoperation transparency and human task performance in a teleoperated switching task. This shows that the effect of sampling time must be taken into account because neglecting it undermines both the stability and transparency of teleoperation.

In the passivity and absolute stability analyses for investigating the coupled sta-

bility of a teleoperation system, the exact models for the teleoperator's terminations (the human operator and the environment) are not available. To make the stability analysis independent of the termination models, it is typically assumed that they are passive but otherwise arbitrary. However, the assumption of passivity of the terminations is less than accurate and may be violated in practice. Using Mobius transformations, in this dissertation we develop a new stability analysis tool for investigating the stability of a two-port network when coupled to an input strictly-passive, an output strictly-passive, an input non-passive, or a disc-like non-passive termination. While this new stability criterion is applicable to any two-port network, we apply it to bilateral teleoperation systems with position-error-based and direct-force-reflection controllers. Simulations and experiments are reported for a pair of Phantom haptic robots. This problem is presented in Chapter 5 of this dissertation.

Finally, Chapter 6 has concluding remarks and outlines possible future directions for this research. Specifically, it is suggested that in continuation of this research, other controllers are checked for sampled-data stability in bilateral teleoperation systems, non-passivity and strict-passivity of both of the terminations are considered in the absolute stability analysis, the previous analyses are extended to multi-lateral teleoperation systems and finally, the integral quadratic constraints formulation is used to analyze the teleoperation system stability.

Acknowledgments

First of all, I would like to thank my supervisor Dr. Mahdi Tavakoli for his great help and encouragement throughout the course of my PhD. I am sincerely grateful to Dr. Tavakoli for his excellent guidance and supervision. My sincere thanks goes to my friends in the Telerobotic and Biorobotic Systems Research Group and the Advanced Control Systems laboratory. In particular, I would appreciate the great company of Matthew Dyck, Meaghan Bowthopre, Jian Lee, Victor Mendez, Sean Hudgson, Alireza Mohammadi, Aerefeh Boroomand, Noushin Miandashti and Ran Tao. Lastly, I would like to thank my family for encouragement and support. Thank you.

Contents

List of Tables

List of Figures

List of Acronyms

LTI	Linear time-invariant
PEB	Position error based
DFR	Direct force reflection
DFR(PD)	Force-position with PD position controller
DFR(P+D)	Force-position with P+D position controller
RHP	Right half plane
LHP	Left half plane
ISP	Input strictly-passive
OSP	Output strictly-passive
INP	Input non-passive
ONP	Output non-passive
DNP	Disc-like non-passive
EOP	Excess of passivity
SOP	Shortage of passivity

OER Operator emulating robot

ZOH Zero Order Hold

FF Free-motion/free-motion

FC Free-motion/clamped

LFT Linear fractional transformation

DOF Degrees-of-freedom

Nomenclature

f_m Control signal for the master

f_s Control signal for the slave

f_h Operator's force

f_e Environment's force

x_m Master position

x_s Slave position

$C_m(s)$ Position controller for master

$C_s(s)$ Position controller for slave

k_{p_m}, k_{v_m} Proportional and derivative gains of C_m

k_{p_s}, k_{v_s} Proportional and derivative gains of C_s

Z_m Impedance of the master

Z_s Impedance of the slave

μ Position scaling factor of DFR controller

λ Force scaling factor of DFR controller

β Initial energy of a passive system

δ EOP of an ISP system

ϵ EOP of an OSP system

η SOP of an INP system

υ SOP of an ONP system

ρ SOP of a DNP system

Z_{ij} The i-th row and j-th column element of an impedance matrix

R_{ij} Real part of Z_{ij}

I_{ij} Imaginary part of Z_{ij}

z_2 Impedance coupled to port 2 of a two-port network

Z_{a1} Driving-point impedance at port 1 of a two-port network

A, B, C Parameters of a generalized circle in the complex plane

m_m Master mass

m_s Slave mass

m_m Master damping

m_s Slave damping

$\tilde{f}_h$ Exogenous input force from the operator's hand

$\tilde{f}_e$ Exogenous input force from the environment

n_p Position scaling factor of PEB controller

Chapter 1

Introduction

A teleoperation system consists of a human operator interacting with a master robot and remotely controlling a slave robot to perform a task in a remote environment [1, 2, 3, 4]. A teleoperation system is useful for performing tasks when the task environment is hazardous, has a large distance from the operator, is confined, and/or has a considerably different scale compared to the human hands natural range of motion. In a unilateral teleoperation system, the master's motion command is transmitted to the slave so that the slave mimics the motions of the master. In a bilateral teleoperation system, there is also force feedback from the environment to the operator. Ideally, bilateral teleoperation is transparent in the sense that the human operator feels the same as he/she would feel when operating directly on the environment. This is a significant advantage over unilateral teleoperation where the human operator is provided only with visual feedback from the remote environment.

1.1   Organization of the thesis

Briefly, this dissertation mainly focuses on investigating the consequences of two practical imperfections in the context of bilateral teleoperation control theory: (1) The impact of sampled-data control on the stability of bilateral teleoperation systems,

and (2) the impact of non-passivity of the operator or the environment on the stability of bilateral teleoperation systems. In the following, a brief summary of each chapter of the dissertation is given and conceptual connections between the chapters are described.

Chapter 2 presents the required background information that is used throughout the future chapters. A brief history of teleoperation systems is first given, followed by a short description about the current applications of bilateral teleoperation systems. Next, several widely-used control architectures for teleoperation systems are reviewed. For these control architectures, the stability of the teleoperation system is addressed next. The last two sections of this chapter discuss the preliminaries for studying the impacts of controller discretization and termination non-passive/strictly-passivity on teleoperation system stability in the rest of the thesis.

Chapters 3 tackles the passivity analysis problem in a sampled-data teleoperation system. It gives a criterion for passivity of the teleoperator when the controllers are modeled by discrete-time systems while the rest of the system is in continuous-time. In fact, in this analysis, the environment, the human operator, the master, and the slave are modeled in continuous-time and the teleoperation controllers are modeled in discrete-time. The proposed passivity criterion is verified through simulations and experiments involving a pair of Phantom Premium robots.

Chapter 4 proposes a criterion for absolute stability of a sampled-data operator. Absolute stability of the teleoperator guarantees the stability of the overall teleoperation system without requiring the teleoperator to be passive. In other words, in the absolute stability framework, the teleoperator can be non-passive while the coupled teleoperation system is stable. As a result, the proposed absolute stability criterion is less conservative than its passivity counterpart and, therefore, provides more flexibility in the controller design stage. Again, the proposed criterion has been tested on an experimental setup that consists of a pair of Phantom Premium robots.

In Chapter 5, by giving simple practical examples, it is argued that the common

assumption that the human operator in a teleoperation system is passive may be violated. Conversely, the assumption of passivity may be too relaxed for a strictly-passive environment. In Chapter 5, the well-known Llewellyn's absolute stability criterion has been extended to cases where the teleoperator is terminated to systems that are either non-passive or strictly-passive. Once again, experimental verification is performed on a pair of Phantom Premium robots.

Finally, Chapter 6 discusses the concluding remarks. Also, in this chapter, suggestions for continuation of this research are proposed. These suggestions include applying the sampled-data approach to different control architectures, including non-passivity and/or strict-passivity of both of the terminations of the two-port network in absolute stability analysis, applying the analysis of non-passivity and strict-passivity of termination to multi-port network and last but not least using integral quadratic constraints in unifying the analysis formulation.

1.2   Publications

A short version of Chapter 3 has been published in the IEEE Transactions on Haptics [5] while parts of this chapter have been presented in the 2011 IEEE World Haptics conference, Istanbul, Turkey [6]. A paper based on the results of Chapter 4 has been published in the Control Engineering Practice - a Journal of IFAC [7]. A shorter version of the work in Chapter 4 has been presented in the 2010 IEEE Conference on Decision and Control, Atlanta, Georgia, USA [8]. In the process of performing the experiments in Chapter 4, there was a need to develop a MATLAB toolbox to interface the Phantom Omni robots in Simulink. The development of this toolbox was presented in the 2011 Canadian Congress on Applied Mechanics, Vancouver, BC, Canada. From Chapter 5, the non-passive termination results have been presented in the 2012 IEEE/RSJ International Conference on Intelligent Robots and Systems, Vilamoura, Portugal [9]. Also, from Chapter 5, the strictly-passive termination results

will be presented in the 2013 IEEE World Haptics Conference in Daejeon, Korea, 2013 [10]. A long version of Chapter 5 has been submitted to the IEEE Transactions on Control Systems Technology [11]. Lastly, in a collaborative project, additional experiments demonstrating the human arms non-passivity will be presented in another paper in the 2013 IEEE World Haptics Conference in Daejeon, Korea [12].

1.3   Contributions of the thesis

In Chapter 3, the main contribution is a teleoperator passivity analysis that accounts for the exact models of discretization components in a sampled-data teleoperation system. Converting the time-domain passivity definition to frequency domain and manipulating the condition result in a closed-form criterion for sampled-data teleoperator passivity. This condition imposes lower bounds on the teleoperator's robots dampings, an upper bound on the sampling time, and bounds on the control gains. As such, it is a useful tool in designing stabilizing discrete-time controllers for teleoperation systems.

In Chapter 4, the main contribution is a teleoperator absolute stability analysis that accounts for the exact models of discretization components in a sampled-data teleoperation system. In a similar manner as the passivity analysis, but with different mathematical tools, the absolute stability of the teleoperation system is analyzed considering the exact models of the discrete-time controllers combined with the continuous-time models for the terminations and the robots. Expectedly, the resulting absolute stability condition is less conservative than the passivity counterpart in Chapter 3. This is also a useful tool in designing stabilizing discrete-time controllers for teleoperation systems with the difference that it can result in better teleoperation transparency compared to the passivity criterion.

The novel contribution of Chapter 5 is to extend the traditional absolute stability analysis of a bilateral teleoperator to cases where the human operator or the envi-

ronment is non-passive or strictly-passive. The non-passivity in the termination of a teleoperator can potentially destabilize the teleoperation system, if it is not accounted for. Conversely, strict passivity of a termination gives more flexibility in the control design and should be utilized. The proposed stability criterion helps to realize this flexibility and obtain more transparent teleoperation controllers.

Chapter 2

Background

In this chapter, the background related to bilateral teleoperation systems is presented. We begin by a brief historical overview of teleoperation systems in Section 2.1. In Section 2.2, some contemporary applications of teleoperation systems are discussed followed by an overview of common controller architectures for bilateral teleoperation systems in Section 2.3. Then, passivity and absolute stability of bilateral teleoperation systems are discussed in Section 2.4. Finally, a brief introduction is given to the main two topics of this thesis. These two topics are (a) analysis of the effect of sampled-data control on the stability of a teleoperation system (Section 2.5), and (b) analysis of the effect of non-passivity and strict-passivity of a teleoperator terminations on the stability of the teleoperation system (Section 2.6).

2.1   A historical review of teleoperation systems

The first teleoperation system was developed by Raymond C. Goertz in 1945 in order to handle hazardous materials remotely [13]. Emergence of electrical servomechanism helped Goertz to develop a telerobotic system that was accompanied by a closed-circuit TV. Teleoperation research was fueled by the space exploration activities in 1960's and 1970's. Landing on the surface of the moon in 1966 motivated the need for

research on teleoperation systems that suffer from time delay in the communication channel between the master and the slave robots. Ever since, the need to design teleoperation systems in such a way that they are capable of handling potentially time-varying delays in their communication channels has been felt by the research community. In 1967, as a partial solution to this problem, Ferrell and Sheridan proposed supervisory control where the human operator submits high-level commands and the slave is given autonomy to locally accomplish these high-level commands [14]. Predictive display was proposed by Bejczy and Kim in 1990 to deal with time delay in teleoperation systems, whereby the human operator sees the slave-sides response in a predictive manner [15]. Since 1990's, the Internet has been used as a communication channel and new challenge such as time-varying delays and packet loss have been considered [16].

In 1980's and 1990's, the control systems theory began to influence the theoretical and controller design aspects of teleoperation systems [17]. This led to the application of teleoperation systems to offshore operations such as pipeline monitoring, well-head completion, and similar oil-and-gas industrial applications [18]. It was in 1982 that the first bilateral teleoperation system was implemented in a joint project between the Central Research Laboratory and the Oak Ridge National Laboratory in the United States. Parallel to the development of modern computers, application of teleoperation systems was extended to new areas including undersea manipulation [1]. Relatively recent advances in teleoperation systems have led to the development of reliable teleoperation systems for robotically-assisted surgical procedures [19]. In a breakthrough in the history of teleoperation systems, in 2001, a robotically-assisted minimally invasive surgery was performed in which a surgeon in New York, U.S., remotely removed gallbladder of a patient in Strasbourg, France, using a ZEUS surgical robot [20, 21].

2.2 Contemporary applications of teleoperation systems

As a result of widespread availability of the Internet as a communication channel, teleoperation systems are used in many of today's applications. A summary of selected recent applications of teleoperation systems is given in the following.

Teleoperation systems are widely used in space teleoperation [22, 23, 24, 25, 26, 27, 28, 29]. In a major project in 1993, the first computer-controlled space telerobot was launched by the German Aerospace Center (DLR) [30, 31] for the NASA Space Shuttle [32, 33]. Another major development in space teleoperation involved the Space Station Freedom in the Japanese Experimental Module [34]. Perhaps the most challenging aspect of space teleoperation is the substantial time-delays in the communication channel, which are typically around seven seconds round-trip [35].

In another application of teleoperation systems, undersea manipulators have been controlled with telerobots since 1973 [36, 37, 38, 39]. For instance, construction machines were controlled remotely with a "scaled" teleoperator [40]. Some applications require mounting a teleoperator on a remotely-operated vehicle.

Another application of teleoperation systems is in robot-assisted surgery and tele-surgery [41, 42, 43]. Perhaps the most well-reputed robotically-assisted surgery system is the da Vinci Surgical System (Intuitive Surgical Inc., Sunnyvale, CA) [44, 45], which is equipped with laparoscopic tools in the slave side while the surgeon interacts with a user console. The minimally-invasive surgery procedures being performed using this teleoperation system include surgeries for prostate cancer [46], hysterectomy [47], and mitral valve repair [48, 49]. In another example of robotically-assisted surgery systems, in the neuroArm project, an MR-compatible teleoperated robot is developed for image-guided neurosurgery in the presence of magnetic fields of up to 3.0 tesla [50].

There are many other applications for bilateral teleoperation systems. These in-

clude handling hazardous material [51, 52], mobile robotics [53, 54, 55, 56, 57, 58, 59, 60], flying robots [61, 62, 63], and tele-rehabilitation [64, 65].

2.3 Controllers for bilateral teleoperation systems

2.3.1 Controller architectures

A bilateral teleoperation system may use different control architectures. A position-error-based (PEB) control architecture involves transmitting the position of each robot to the opposite robot of the teleoperation system. As such, the PEB architecture does not require force measurement. Conversely, a direct force reflecting (DFR) control architecture requires the contact force of the slave/environment to be measured and transmitted to the human operator. Combining the two aforementioned architectures, in a 4-channel (4-CH) architecture, both positions and forces of the master and the slave are transmitted to the other end of the teleoperation system [66, 67].

2.3.2 Control design objectives

The controllers of a teleoperation system are designed to achieve two objectives. First, the closed-loop system should have stability, which is defined as the boundedness of the signals in the system. Second, the teleoperation system should be transparent meaning that the positions/forces of the master and the slave should be similar. Equivalently, transparency ensures that the human operator receives an undistorted perception of the environment properties, e.g., impedance. There is a tradeoff between transparency and stability of a teleoperation system [66, 68, 69] – the best transparency is achieved by the least-conservative stabilizing controller [70]. Teleoperation passivity may be studied in the context of passivity as explained next.

2.4 Teleoperation stability vs. passivity

2.4.1 Stability

To analyze the closed-loop stability of a teleoperation system using conventional stability analysis approaches, the operator and the environment models must be known. While this assumption will significantly simplify the stability analysis, it cannot be made in practice because the dynamic parameters of the human operator change in response to the specific requirements of the task at hand, and the dynamic parameters of the environment are also usually uncertain, time-varying and/or nonlinear. To tackle the stability analysis of a teleoperation system without known models for the environment and the operator, two approaches have been proposed: Teleoperator passivity and teleoperator absolute stability. In the following, we discuss this beginning with modeling a teleoperator as a two-port network.

2.4.2 Two-port network modelling

Both the passivity and the absolute stability approaches break down a teleoperation system to three main blocks as shown in Fig. 2.1: A human operator (one-port network) and an environment (one-port network) interacting with a teleoperator (two-port network). The teleoperator comprises the communication channel, the master, the slave and the local controllers. The teleoperator passivity concerns the energy dissipation of the teleoperator and makes sure that the teleoperator is not generating energy. If so, the concatenation of a passive teleoperator and passive environment and operator terminations will be passive, i.e., the overall teleoperation system will be passive. On the other hand, the absolute stability is concerned with the stability of the overall teleoperation system for any passive but otherwise arbitrary operator and environment. Absolute stability of a two-port network has been shown to be equivalent to the passivity of the input impedance at a port of the two-port network when the other port is connected to a passive termination (Fig. 2.2). In turn, passivity

of a one-port network has been shown to be equivalent to positive-realness of its impedance. Positive realness of a system is defined as follows.

Positive Realness Definition: A single-input/single-output system with transfer function $Z(s)$ is positive real if and only if [71]

1. $Z(s)$ has no pole in the right half plane.

2. Any poles of $Z(s)$ on the imaginary axis are simple with real and positive residues.

3. $\text{Re}\{Z(j\omega)\} \geq 0$ for all $\omega > 0$.
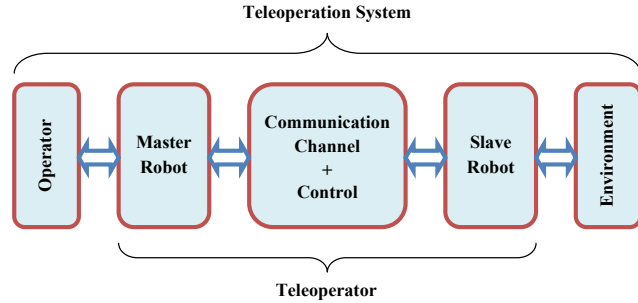
Figure 2.1: The teleoperation system versus the teleoperator.
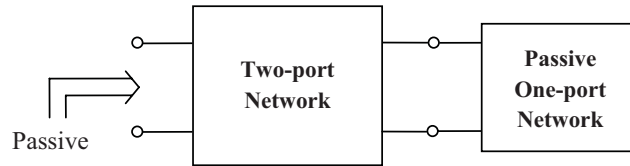
Figure 2.2: Connecting a passive one-port network to any port of an absolutely stable two-port network results in the passivity of the remaining one-port network

2.4.3 Two-port network passivity

Ensuring passivity of the two-port network teleoperator along with the assumed passivity of its two terminations will guarantee the passivity of the resulting interconnection and thus the closed-loop stability of the teleoperation system [72]. The human

operator impedance has been argued to be passive in relaxed arm tasks [73]. Passivity of the two-port teleoperator can be investigated via the scattering framework or Raisbeck's criterion [71, 74]. For a two-port network expressed in terms of its immitance matrix $\mathbf{P}$, the Raisbeck's conditions is presented in the following.

Raisbeck's passivity criterion: A two-port network with immitance matrix $\mathbf{P}$ is passive if and only if

1. P_{ij}'s have no pole in the right half plane.

2. Pure imaginary poles of P_{ij}'s are simple and have positive residue. Also, the residues P_{ij} satisfy $P_{11}P_{22} - P_{12}P_{21} \geq 0$ with $P_{21} = P_{12}^*$.

3. For all real positive frequencies ω,

$$R_{11} \geq 0$$
$$R_{22} \geq 0$$
$$4R_{11}R_{22} - (R_{12} + R_{21})^2 - (\text{Im}\{P_{12}\} - \text{Im}\{P_{21}\})^2 \geq 0 \qquad (2.1)$$

where $R_{ij} = \text{Re}P_{ij}$.

2.4.4 Two-port network absolute stability

To investigate the stability of a teleoperation system, a less conservative condition compared to teleoperator passivity is the teleoperator absolute stability. For a two-port network expressed in terms of its immitance matrix $\mathbf{P}$, the Llewellyn's conditions give the criterion for absolute stability of the network [71, 8].

Llewellyn's absolute stability criterion: A two-port network with immitance matrix $\mathbf{P}$ is absolutely stable if and only if

1. P_{11} and P_{11} have no pole in the right half plane.

2. Pure imaginary poles of P_{11} and P_{22} are simple and have positive residue.

3. For all real positive frequencies ω,

$$R_{11} \geq 0$$

$$R_{22} \geq 0$$

$$2R_{11}R_{22} - \text{Re}\{P_{12}P_{21}\} - |P_{12}P_{21}| \geq 0 \tag{2.2}$$

2.5 Effect of sampled-data control on teleoperators absolute stability and passivity

A teleoperation system controller is typically implemented via discrete-time components while the rest of the teleoperation system (the human operator, the environment, and the robots) operates in the continuous-time. Most stability analyses for teleoperation systems assume that the system is entirely in the continuous-time. In order to analyze the stability of the system using conventional methods, i.e., passivity and absolute stability, disregard the discrete-time nature of the components. For instance, modeling the system entirely in continuous-time neglects the energy leaks caused by the Zero Order Hold (ZOH) [75, 76]. Thus, the passivity or absolute stability of the teleoperation system is not guaranteed. The ZOH also accounts for half-sample delay (not to be confused with the communication channel delay) and has energy-instilling effects [77, 78, 75]. We provide an intuitive explanation for this energy leak using the example below.

Consider haptic teleoperation on a finite-impedance, passive physical object where the slave-environment interaction forces are measured by a force sensor, sampled and fed back to the user by a discrete-time controller (Fig. 2.3). As the slave robot penetrates the environment, the sampled slave/environment contact forces will be less than the real contact forces during each sampling intervals, resulting in the forces reflected to the user to be too low. By contrast, as the slave robot moves out of

the environment, the reflected forces will be too high compared to reality. Thus, the users legitimate expectation that a passive environment would not generate energy is violated. Indeed, as the user utilizes the teleoperation system to probe the passive environment by pushing and letting go of the user interface, the energy-instilling sampled-data controller presents the environment to the user as one emitting energy and causing vibrations - an effect never observed when touching the same environment directly by hand.

In our work, to fully account for the continuous-time and the discrete-time nature of various signals in the analysis of passivity and absolute stability of a teleoperator, a sampled-data analysis is applied (Chapter 3 and Chapter 4).
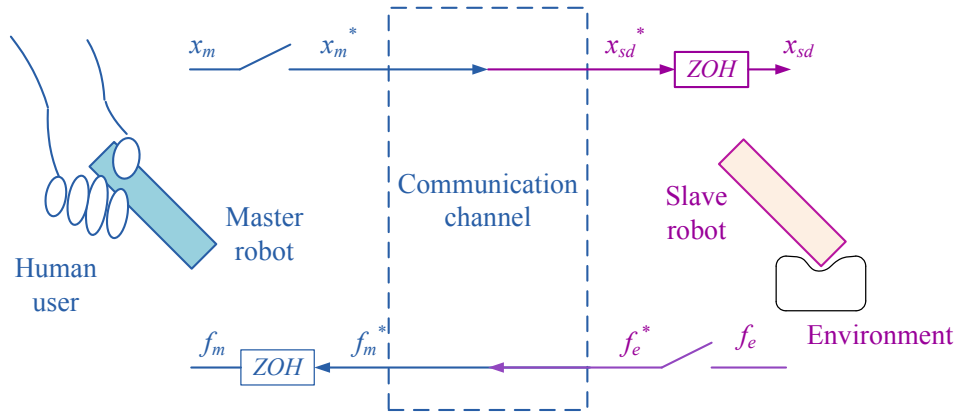
Figure 2.3: The operator is indenting a soft object remotely and receives force feedback

2.6 Effect of termination non-passivity and strict-passivity on stability of teleoperation systems

In both the passivity and the absolute stability analyses of a two-port network teleoperator, the assumption is that the terminations for both ports of the two-port network are passive. Interconnecting a non-passive termination to a passive two-port may cause instability even if the other port of the two-port network is terminated

to a passive one-port network. There are several practical examples when the termination of a teleoperation system becomes non-passive. For instance, consider a bilateral teleoperation system in which the two-port network teleoperator is designed to stay passive. Suppose that the system input/output are force/velocity, and hence the mathematical notion of passivity corresponds to the system's physical energy. Suppose that the environment of the slave robot is also passive. In this system, the source of energy must be the human operator; otherwise, the system never moves. This means the human operator is not always passive as it is assumed widely in the literature.

Conversely, a teleoperators termination can be overly passive in some applications. When the environment involves no source of energy or external forces, the environment is a strictly-passive one-port network. Considering th excess of passivity of the termination allows us to have some shortage of passivity in the teleoperator while the coupled system is stable. This notion resembles the excess of passivity and shortage of passivity of feedback interconnected systems [79]. When systems G_1 and G_2 are connected in a negative feedback look, having both of the systems passive ensures stability of the coupled system. If G_1 has a certain level of excess of passivity, G_2 can have a shortage of passivity lower than or equal to the excess of passivity of G_1 without jeopardizing the stability of the coupled system. The importance of this analysis is that it allows the designer to use the extra passivity of one of the terminations to change the controller gains of the two-port network teleoperator to values outside the absolute stability range and yet the coupled system is guaranteed to be stable. This can be leveraged to improve the teleoperation system transparency. The notions of "how much passive?" or "how much non-passive?" about terminations can be leveraged to develop a powerful tool for stability analysis of two-port network systems (Chapter 5).

Chapter 3

Passivity Analysis of Sampled-data Bilateral Teleoperation Systems [1]

3.1 Introduction

Due to the unknown, time-varying and sometimes nonlinear dynamics of the environment and/or the operator, it is easier to analyze the passivity of the teleoperator in lieu of the stability of the closed-loop teleoperation system (Fig. 2.1). Indeed, the interconnection of a passive teleoperator and passive environment and operator terminations will be passive and consequently the overall teleoperation system will be passive [80].

For a bilateral teleoperation system in continuous-time, the teleoperator is modelled as a two-port network and its passivity condition is related to the scattering matrix of the two-port network [81]. Alternatively, the passivity of the teleoperator can be analyzed by Raisbeck's condition (see Section 2.4.3) [71, 74].

The passivity of a teleoperation system is not guaranteed if the continuous-time controllers are substituted with their discrete-time counterparts because of energy

---

[1]This chapter has been published in the IEEE Transactions on Haptics [5] while parts of this chapter have been presented in the 2011 IEEE World Haptics conference, Istanbul, Turkey [6].
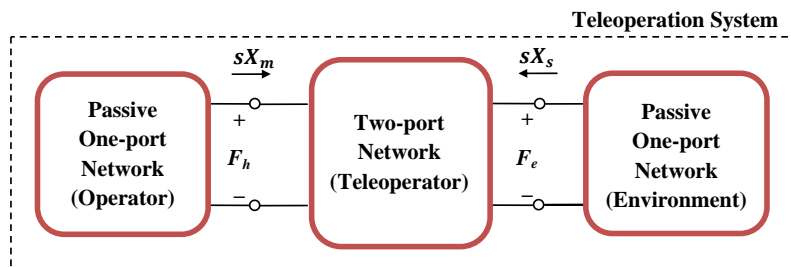
Figure 3.1: The passivity of the teleoperation system is guaranteed when a two-port network teleoperator is passive and is connected to two passive one-port network terminations.

leaks caused by the Zero Order Hold (ZOH) [76] (See Section 2.5).

Similar to bilateral teleoperation, in a force-reflective virtual reality simulation system the operator feels virtual contact forces while applying position commands through the haptic user interface. Colgate and Schenkel have found a passivity condition for such a system considering the discrete-time components of the system [82]. The passivity condition for the discrete simulation of a virtual wall $K + sB$ is found to be $b > KT/2 + B$, where b is the haptic interface damping and T is the sampling time. The stability of the virtual wall system has also been investigated using the Routh-Hurwitz method [83]; the condition for the stability of the same system is $b > KT/2 - B$, which is clearly less conservative than the passivity condition. Previous research has also considered the impact of other non-idealities such as quantization and friction on the stability of the virtual wall system [84, 85]. As discussed above, energy leaks caused by discretization have been investigated for haptic interaction with a virtual wall. The analysis of this chapter considers the haptic interaction with a physical environment via a computer-controlled teleoperation system. The resulting passivity condition can be used in control design to achieve maximum transparency and enable the human to stably teleoperate in the presence of discretization components.

In some approaches, the whole teleoperation system is converted to the discrete-time domain [76, 86] or the continuous-time domain [87], which simplifies the stability

analysis for known models of the environment and the operator. Also, Hannaford et al. proposed a passivity observer / passivity controller for monitoring and controlling the energy in the communication channel of a discrete-time teleoperation system [88]. In addition, Stramigioli et al. proposed a geometric method to investigate the problem of having both continuous-time and discrete-time signals in a single system where the teleoperation system is represented by a continuous-time port-Hamiltonian system [89, 78].

In this chapter, the passivity analysis starts with considering the dynamics of the master and the slave controllers as well as the dynamics of the master and the slave robots. The analyses presented in this chapter will lead to a passivity condition for a sampled-data teleoperation with position-error-based controller architecture and delay-free communication channel. The condition will impose bounds on the system parameters such as the sampling time, the controller gains and the robots damping terms. It is important to determine the lower bound on the damping term of the robots as most of the newly designed haptic devices intentionally have low damping terms to deliver touch sensitivity and fidelity to the operator. The upper bounds on the controller gains give a useful guideline for control design. For a stable teleoperation, system the transparency of the system is degraded if the controller gains are small in the stable region. Thus, this chapter gives the conditions that can be used as design guidelines for achieving high transparency and passive teleoperation systems.

The rest of this chapter is organized as follows. First, the prerequisite lemmas and their proofs are given in Section 3.2. The sampled-data teleoperation system is modeled in Section 3.3. This model is used in Section 3.4 to find a condition for the passivity of the teleoperator system. The derived passivity condition has been tested via computer simulations in Section 3.5, which allows the flexibility to change the damping terms of the robots (they are fixed in the experiments). Then, the experimental results using two Phantom Omni robots are reported in Section 3.6, and concluding remarks are given in Section 3.7.

18

3.2 Lemmas

This section includes the proofs of the lemmas that are used in Section 3.4.

Lemma 3.1. *For any arbitrary function $V(j\omega)$ and $\bar{C}(\omega)$*

$$\int_{-\infty}^{\infty} \bar{C}(\omega) \sum_{n=-\infty}^{\infty} \frac{V(j\omega + jn\omega_s)}{j\omega + jn\omega_s} \left[\frac{V(j\omega)}{j\omega}\right]^c d\omega \tag{3.1}$$

The integral (3.1) does not change if $\bar{C}(\omega)$ is replaced with its real part $\mathrm{Re}\{\bar{C}(\omega)\}$.

Proof. The integral limits are broken to two parts. Also, The integration and the summation in (3.1) are interchangeable. Then, (3.1) can be written as two summations

$$\sum_{n=-\infty}^{\infty} \int_{-\infty}^{-n\omega_s/2} \bar{C}(\omega) \frac{V(j\omega + jn\omega_s)}{j\omega + jn\omega_s} \left[\frac{V(j\omega)}{j\omega}\right]^c d\omega$$

$$+ \sum_{n=-\infty}^{\infty} \int_{-n\omega_s/2}^{\infty} \bar{C}(\omega) \frac{V(j\omega + jn\omega_s)}{j\omega + jn\omega_s} \left[\frac{V(j\omega)}{j\omega}\right]^c d\omega \tag{3.2}$$

In the first summation of (3.2), the variable ω can be changed by defining $\omega_1 = -\omega - n\omega_s$ and (3.2) is equal to

$$\sum_{n=-\infty}^{\infty} \int_{-n\omega_s/2}^{\infty} \bar{C}(-\omega_1) \frac{V(-j\omega_1)}{-j\omega_1} \left[\frac{V(-j\omega_1 - jn\omega_s)}{-j\omega_1 - jn\omega_s}\right]^c d\omega_1$$

$$+ \sum_{n=-\infty}^{\infty} \int_{-n\omega_s/2}^{\infty} \bar{C}(\omega) \frac{V(j\omega + jn\omega_s)}{j\omega + jn\omega_s} \left[\frac{V(j\omega)}{j\omega}\right]^c d\omega \tag{3.3}$$

Knowing that $V(j\omega)$ is Fourier transform of a real signal implies that $V^c(j\omega) = V(-j\omega)$. As a result, the two terms in (3.3) can be merged to

$$\sum_{n=-\infty}^{\infty} \int_{-n\omega_s/2}^{\infty} \left[\bar{C}(-\omega) + \bar{C}(\omega)\right] \frac{V(j\omega + jn\omega_s)}{j\omega + jn\omega_s} \left[\frac{V(j\omega)}{j\omega}\right]^c d\omega \tag{3.4}$$

19

Because of having $\bar{C}(-\omega) = \bar{C}^c(\omega)$, (3.4) can be rearranged as

$$\sum_{n=-\infty}^{\infty} \int_{-n\omega_s/2}^{\infty} 2\text{Re}\{\bar{C}(\omega)\} \frac{V(j\omega + jn\omega_s)}{j\omega + jn\omega_s} \left[\frac{V(j\omega)}{j\omega}\right]^c d\omega \qquad (3.5)$$

The integral is symmetric around $\omega = -\frac{n\omega_s}{2}$ and (3.5) can be rewritten as

$$\sum_{n=-\infty}^{\infty} \int_{-\infty}^{\infty} \text{Re}\{\bar{C}(\omega)\} \frac{V(j\omega + jn\omega_s)}{j\omega + jn\omega_s} \left[\frac{V(j\omega)}{j\omega}\right]^c d\omega \qquad (3.6)$$

Now, (3.6) is equal to (3.1) and this fact completes the proof. $\qquad\square$

Lemma 3.2. *For any arbitrary function $V(j\omega)$ and positive definite $\bar{C}^+(\omega)$*

$$\int_{-\infty}^{\infty} \bar{C}^+(\omega) \sum_{n=-\infty}^{\infty} \frac{V(j\omega + jn\omega)}{j\omega + jn\omega} \left[\frac{V(j\omega)}{j\omega}\right]^c d\omega > 0 \qquad (3.7)$$

Proof. Let us define ζ as

$$\zeta(\omega) = \left[\bar{C}^+(\omega)\right]^{1/2} \frac{V(j\omega)}{j\omega} \qquad (3.8)$$

The left hand side of (3.7) can be written as

$$\int_{-\infty}^{\infty} \sum_{n=-\infty}^{\infty} \zeta(\omega + n\omega)\zeta(\omega)^c d\omega$$

$$= \int_{-\infty}^{\infty} z(t) \sum_{n=-\infty}^{\infty} z(t)e^{-jn\omega_s t} dt$$

$$= T \int_{-\infty}^{\infty} z^2(t) \frac{1}{T} \sum_{n=-\infty}^{\infty} e^{-jn\omega_s t} dt$$

$$= T \int_{-\infty}^{\infty} z^2(t) \sum_{n=-\infty}^{\infty} \delta(t - kT) dt$$

$$= T \sum_{n=-\infty}^{\infty} z^2(t - kT) dt \qquad (3.9)$$

The last equation in (3.9) will be positive all the time that proves the claim. $\qquad\square$

20

Lemma 3.3. *For $V(j\omega)$ as in (3.45) and any arbitrary negative definite $\bar{C}^-(\omega)$ we have*

$$\int_{-\infty}^{\infty} \bar{C}^-(\omega) \sum_{n=-\infty}^{\infty} \frac{V(j\omega + jn\omega)}{j\omega + jn\omega} \left[\frac{V(j\omega)}{j\omega}\right]^c d\omega >$$
$$\int_{-\infty}^{\infty} \bar{C}^-(\omega) \sum_{n=-\infty}^{\infty} \frac{1}{(\omega + n\omega_s)^2} V(j\omega)V^c(j\omega)d\omega \qquad (3.10)$$

Proof. The summation and the integration are interchangeable in the left hand side of (3.10)

$$\sum_{n=-\infty}^{\infty} \int_{-\infty}^{\infty} \bar{C}^-(\omega)\frac{V(j\omega + jn\omega)}{j\omega + jn\omega} \left[\frac{V(j\omega)}{j\omega}\right]^c d\omega \qquad (3.11)$$

The summation in (3.11) can be split to three parts

$$\int_{-\infty}^{\infty} \bar{C}^-(\omega)\frac{V(j\omega + jn\omega)}{j\omega + jn\omega} \left[\frac{V(j\omega)}{j\omega}\right]^c d\omega + \sum_{n=1}^{\infty} \int_{-\infty}^{\infty} \bar{C}^-(\omega)\frac{V(j\omega + jn\omega)}{j\omega + jn\omega} \left[\frac{V(j\omega)}{j\omega}\right]^c d\omega$$
$$+ \sum_{n=1}^{\infty} \int_{-\infty}^{\infty} \bar{C}^-(\omega)\frac{V(j\omega - jn\omega)}{j\omega - jn\omega} \left[\frac{V(j\omega)}{j\omega}\right]^c d\omega \qquad (3.12)$$

The variable change of $\omega_1 = \omega - n\omega_s$ in the summation (3.12) results in

$$\int_{-\infty}^{\infty} \bar{C}^-(\omega)\frac{V(j\omega + jn\omega_s)}{j\omega + jn\omega_s} \left[\frac{V(j\omega)}{j\omega}\right]^c d\omega + \sum_{n=1}^{\infty} \int_{-\infty}^{\infty} \bar{C}^-(\omega)\frac{V(j\omega + jn\omega_s)}{j\omega + jn\omega_s} \left[\frac{V(j\omega)}{j\omega}\right]^c d\omega$$
$$+ \sum_{n=1}^{\infty} \int_{-\infty}^{\infty} \bar{C}^-(\omega_1)\frac{V(j\omega_1)}{j\omega_1} \left[\frac{V(j\omega_1 + jn\omega_s)}{j\omega_1 + jn\omega_s}\right]^c d\omega_1 \qquad (3.13)$$

In (3.11), the argument of $\bar{C}^-$ did not alter because the integration covers all frequencies. The last two summations in (3.11) can be merged.

$$\int_{-\infty}^{\infty} \bar{C}^-(\omega)\frac{V(j\omega + jn\omega_s)}{j\omega + jn\omega_s} \left[\frac{V(j\omega)}{j\omega}\right]^c d\omega + \sum_{n=1}^{\infty} \int_{-\infty}^{\infty} \bar{C}^-(\omega)V_1(\omega)d\omega \qquad (3.14)$$

21

where

$$V_1(\omega) = \frac{V(j\omega + jn\omega_s)}{j\omega}\left[\frac{V(j\omega)}{j\omega + jn\omega_s}\right]^c + \frac{V(j\omega)}{j\omega + jn\omega}\left[\frac{V(j\omega + jn\omega_s)}{j\omega}\right]^c \quad (3.15)$$

Similar to Lemma 3.4, it can be shown that for any arbitrary complex numbers X and Y, $XY^c + X^cY < XX^c + YY^c$. Considering that the function $\bar{C}^-$ is negative definite, (3.14) will be greater than

$$\int_{-\infty}^{\infty} \bar{C}^-(\omega)\frac{V(j\omega + jn\omega_s)}{j\omega + jn\omega_s}\left[\frac{V(j\omega)}{j\omega}\right]^c d\omega + \sum_{n=1}^{\infty}\int_{-\infty}^{\infty}\bar{C}^-(\omega)V_2(\omega)d\omega \quad (3.16)$$

where

$$V_2(\omega) = \frac{V(j\omega + jn\omega)}{j\omega}\left[\frac{V(j\omega + jn\omega_s)}{j\omega}\right]^c + \frac{V(j\omega)}{j\omega + jn\omega}\left[\frac{V(j\omega)}{j\omega + jn\omega_s}\right]^c \quad (3.17)$$

Inequality (3.16) is simplified to

$$\int_{-\infty}^{\infty}\bar{C}^-(\omega)\left|\frac{V(j\omega)}{j\omega}\right|^2 d\omega + \sum_{n=1}^{\infty}\int_{-\infty}^{\infty}\bar{C}^-(\omega)\left\{\left|\frac{V(j\omega + jn\omega_s)}{j\omega}\right|^2 + \left|\frac{V(j\omega)}{j\omega + jn\omega_s}\right|^2\right\} d\omega$$
$$(3.18)$$

$$= \int_{-\infty}^{\infty}\bar{C}^-(\omega)\left\{\left|\frac{V(j\omega)}{j\omega}\right|^2 + \sum_{n=1}^{\infty}V_3(\omega)\right\} d\omega \quad (3.19)$$

where

$$V_3(\omega)\left|\frac{V(j\omega)}{j\omega - jn\omega_s}\right|^2 + \left|\frac{V(j\omega)}{j\omega + jn\omega_s}\right|^2 \quad (3.20)$$

Integral (3.19) is equal to

$$\int_{-\infty}^{\infty}\bar{C}^-(\omega)\sum_{n=-\infty}^{\infty}\left|\frac{V(j\omega)}{j\omega + jn\omega_s}\right|^2 d\omega \quad (3.21)$$

$$\int_{-\infty}^{\infty} \bar{C}^-(\omega) \sum_{n=-\infty}^{\infty} \frac{1}{(\omega + n\omega_s)^2} V(j\omega)V^c(j\omega)d\omega \tag{3.22}$$

The last equation in (3.16) is the right side of (3.10). □

Lemma 3.4. *For any arbitrary complex numbers of X and Y,*

$$-XY^c - X^cY \leq XX^c + YY^c \tag{3.23}$$

where superscript c stands for complex conjugate.

Proof. The complex numbers X and Y have real and imaginary parts:

$$X = X_r + jX_i, Y = Y_r + jY_i \tag{3.24}$$

Inequality (3.23) holds if and only if

$$X_r^2 + X_i^2 + Y_r^2 + Y_i^2 + 2X_rY_r + 2X_iY_i \geq 0 \tag{3.25}$$

Inequality (3.25) can be rearranged as

$$(X_r + Y_r)^2 + (X_i + Y_i)^2 \geq 0 \tag{3.26}$$

Inequality (3.26) holds all the time and also the steps are necessary and sufficient in the proof and this fact completes the proof. □

Lemma 3.5. *The passivity condition (3.61) gives the sufficient condition of the passivity of the system to be (3.62).*

Proof. Based on (3.59) and (3.61), the sufficient condition for the passivity is

23

$$\int_{-\infty}^{\infty} \left[b_m + (n_p{}^2 + n_p)\bar{C}^-(\omega) \sum_{n=-\infty}^{\infty} \frac{1}{(\omega + n\omega_s)^2} \right] \times V_m(j\omega)V_m^c(j\omega)d\omega +$$

$$\int_{-\infty}^{\infty} \left[b_s + (1 + n_p)\bar{C}^-(\omega) \sum_{n=-\infty}^{\infty} \frac{1}{(\omega + n\omega_s)^2} \right] \times V_s(j\omega)V_s^c(j\omega)d\omega > 0 \qquad (3.27)$$

On the other hand,

$$\sum_{n=-\infty}^{\infty} \frac{1}{(\omega + n\omega_s)^2} = \frac{T^2}{2} \frac{1}{1 - \cos \omega T} \qquad (3.28)$$

Substituting (3.28) into (3.27), the conditions that guarantee the teleoperator passivity will be

$$b_m + (n_p{}^2 + n_p)\bar{C}^-(\omega)\frac{T^2}{2} \frac{1}{1 - \cos \omega T} > 0$$

$$b_s + (1 + n_p)\bar{C}^-(\omega)\frac{T^2}{2} \frac{1}{1 - \cos \omega T} > 0 \qquad (3.29)$$

Or

$$b_m > (n_p{}^2 + n_p)\mathrm{Re}\{\bar{C}(\omega)\}\frac{T^2}{2} \frac{1}{1 - \cos \omega T}$$

$$b_s > (1 + n_p)\mathrm{Re}\{\bar{C}(\omega)\}\frac{T^2}{2} \frac{1}{1 - \cos \omega T} \qquad (3.30)$$

Substituting (3.49) into (3.30) gives the passivity condition to be

$$b_m > \frac{T}{2} \frac{n_p{}^2 + n_p}{1 - \cos \omega T}\mathrm{Re}\left\{ (1 - e^{-j\omega T})C(e^{j\omega T}) \right\}$$

$$b_s > \frac{T}{2} \frac{1 + n_p}{1 - \cos \omega T}\mathrm{Re}\left\{ (1 - e^{-j\omega T})C(e^{j\omega T}) \right\} \qquad (3.31)$$

Finally, conditions (3.31) can be expressed as (3.62) $\qquad\qquad \square$

3.3 Teleoperation system modelling

The block diagrams of a position-error-based sampled-data teleoperation is shown in Fig. 3.2. The master and the slave robots are modelled as 1-DOF, linear time invariant systems

$$
\begin{aligned}
f_h - f_m &= m_m \ddot{x}_m + b_m \dot{x}_m \\
f_e - f_s &= m_s \ddot{x}_s + b_s \dot{x}_s
\end{aligned}
\tag{3.32}
$$

where f_h and f_e are the operator and the environment forces, respectively. The subscripts m and s indicate the master and the slave robots, respectively. In (3.32), f_i's are the controller output forces and x_i's are the robots positions. Also, m and b denote the mass and the damping of each robot after linearization. It is also assumed that the robots do not include link or joint flexibility. As depicted in Fig. 3.2, the positions of the master and slave robots are discretized using sampler blocks. The superscript * denotes sampled signals. The sampled signals are converted back to the continuous-time domain using zero-order-hold blocks. The environment and the operator are modelled as impedances $Z_e(s)$ and $Z_h(s)$, which are assumed to be passive but otherwise arbitrary. In Fig. 3.2, $\tilde{f}_h$ is the exogenous input force from the operator's hand and $\tilde{f}_e$ is the exogenous input force from the environment.

The environment and the operator models of Fig. 3.2 can be converted to the Laplace domain as

$$
\begin{aligned}
\tilde{F}_h(s) - F_h(s) &= Z_h(s) s X_m(s) \\
\tilde{F}_e(s) - F_e(s) &= Z_e(s) s X_s(s)
\end{aligned}
\tag{3.33}
$$
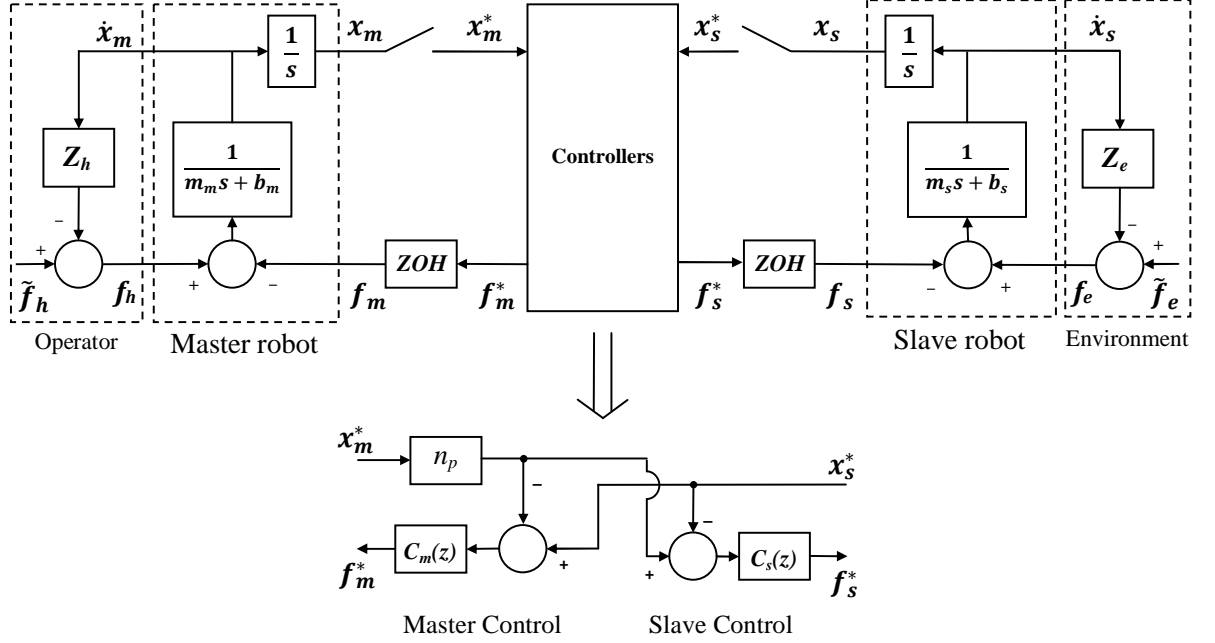
Figure 3.2: The block diagrams of a teleoperation system, which includes discretized controller models.

The robots' dynamics (3.32) can be rewritten in the Laplace domain as

$$
\begin{aligned}
sX_m(s) &= \frac{1}{m_m s + b_m}(-F_m(s) + F_h(s)) \\
sX_s(s) &= \frac{1}{m_s s + b_s}(-F_s(s) + F_e(s))
\end{aligned}
\tag{3.34}
$$

The output of the sampler is a sampled signal and can be mathematically represented as a Dirac comb weighted by the sampled signal [90]

$$
x^*(t) = \sum_{k=0}^{\infty} x(kT)\delta(t - kT)
\tag{3.35}
$$

The mathematical representation of the sampled signal (3.35) in the Laplace domain is

$$
X^*(s) = \mathcal{L}\{x^*(t)\} = \sum_{k=0}^{\infty} x(kT)e^{-skT}
\tag{3.36}
$$

The z-domain equivalent of (3.36) is

$$X(z) = \mathcal{Z}\{x^*(t)\} = X^*(s)|_{s=1/T \ln z} \tag{3.37}$$

The ZOH block transfer function relating its discrete-time input to its continuous-time output is [91]

$$\begin{aligned} F_m(s) &= \frac{1 - e^{-sT}}{sT} F_m^*(s) \\ F_s(s) &= \frac{1 - e^{-sT}}{sT} F_s^*(s) \end{aligned} \tag{3.38}$$

The PEB controller blocks in Fig. 3.2 subtract the position signals and apply forces based on the master/slave position difference. Note that it is assumed that there is no delay in the communication channel between the master and the slave. The position error in the slave robot is

$$e = x_m - x_s \tag{3.39}$$

Based on the error, the discrete-time controllers of the master and the slave sides implement the following control laws

$$\begin{aligned} F_m^*(s) &= C_m(z)|_{z=e^{sT}}[X_s^*(s) - X_m^*(s)] \\ F_s^*(s) &= C_s(z)|_{z=e^{sT}}[X_m^*(s) - X_s^*(s)] \end{aligned} \tag{3.40}$$

3.4 Passivity condition for the sampled-data teleoperator

The teleoperator passivity condition in the time domain is based on the dissipated energy in the equivalent two-port network of the teleoperator, which can be measured by the input-output energy integral at the two network ports (Fig. 3.1). For the two-

port network at the initial rest, the passivity condition is

$$\int_0^t f_m(\tau)\dot{x}_m(\tau)d\tau + \int_0^t f_s(\tau)\dot{x}_s(\tau)d\tau \geq 0 \tag{3.41}$$

The system is passive if and only if, for all time $t > 0$, (3.41) holds. Condition (3.41) will be satisfied if

$$\int_0^t f_m(\tau)\dot{x}_m(\tau)d\tau + \int_0^t f_s(\tau)\dot{x}_s(\tau)d\tau \geq \frac{1}{2}m_m\dot{x}_m^2 + \frac{1}{2}m_s\dot{x}_s^2 \tag{3.42}$$

Clearly, (3.42) is sufficient but not necessary for (3.41). The dynamic of the master robot in (3.32) implies that

$$f_h - f_m = m_m\frac{d\dot{x}_m}{dt} + b_m\dot{x}_m \tag{3.43}$$

Finding f_h from (3.43) and substituting in (3.42), along with similar simplifications for the slave robots simplifies (3.42) to

$$\int_0^t f_m(\tau)\dot{x}_m(\tau)d\tau + \int_0^t f_s(\tau)\dot{x}_s(\tau)d\tau \ + \int_0^t b_m\dot{x}_m^2(\tau)d\tau + \int_0^t b_s\dot{x}_s^2(\tau)d\tau > 0 \tag{3.44}$$

Generalization of the Parseval theorem [92] can be used to take (3.44) to the frequency domain as

$$\int_{-\infty}^{\infty} F_m(j\omega)V_m^c(j\omega)d\omega + \int_{-\infty}^{\infty} F_s(j\omega)V_s^c(j\omega)d\omega+$$
$$\int_{-\infty}^{\infty} b_m V_m(j\omega)V_m^c(j\omega)d\omega + \int_{-\infty}^{\infty} b_s V_s(j\omega)V_s^c(j\omega)d\omega > 0 \tag{3.45}$$

where V_i and F_i (for $i = m, s$) are the Fourier transform of $\dot{x}_i$ and f_i, respectively and the superscript ^{c} denotes the complex conjugate operator.

Using (3.38) and (3.40), the control signals for the master and the slave are

$$F_m(j\omega) = \frac{1 - e^{-j\omega T}}{j\omega T} C_m(e^{j\omega T}) X_m^*(j\omega) - \frac{1 - e^{-j\omega T}}{j\omega T} C_m(e^{j\omega T}) X_s^*(j\omega)$$

$$F_s(j\omega) = \frac{1 - e^{-j\omega T}}{j\omega T} C_s(e^{j\omega T}) X_m^*(j\omega) - \frac{1 - e^{-j\omega T}}{j\omega T} C_s(e^{j\omega T}) X_s^*(j\omega) \qquad (3.46)$$

Position signals in (3.46) can be found from (3.36)

$$X_m^*(j\omega) = \frac{1}{T} \sum_{n=-\infty}^{\infty} \frac{V_m(j\omega + jn\omega_s)}{j\omega + jn\omega_s}$$

$$X_s^*(j\omega) = \frac{1}{T} \sum_{n=-\infty}^{\infty} \frac{V_s(j\omega + jn\omega_s)}{j\omega + jn\omega_s} \qquad (3.47)$$

where $\omega_s = 2\pi/T$. Substituting (3.46) and (3.47), the first two terms of (3.45) become

$$\int_{-\infty}^{\infty} \bar{C}_m(\omega) \sum_{n=-\infty}^{\infty} \frac{V_m(j\omega + jn\omega_s) - V_s(j\omega + jn\omega_s)}{j\omega + jn\omega_s} \times \left[\frac{V_m(j\omega)}{j\omega} \right]^c d\omega$$

$$+ \int_{-\infty}^{\infty} \bar{C}_s(\omega) \sum_{n=-\infty}^{\infty} \frac{V_s(j\omega + jn\omega_s) - V_m(j\omega + jn\omega_s)}{j\omega + jn\omega_s} \times \left[\frac{V_s(j\omega)}{j\omega} \right]^c d\omega \qquad (3.48)$$

where

$$\bar{C}_m(j\omega) = -\frac{1 - e^{-j\omega T}}{T} C_m(e^{j\omega T})$$

$$\bar{C}_s(j\omega) = -\frac{1 - e^{-j\omega T}}{T} C_s(e^{j\omega T}) \qquad (3.49)$$

To further simplify (3.48), the master and the slave controllers are selected to be equal to each other

$$C_m(j\omega) = C_s(j\omega) = C(j\omega) \qquad (3.50)$$

In a special case in this section the assumption of (3.50) will be changed to cover a more general case where the controllers are proportional to each other with the same scaling factor as the position scaling.

For simplicity of notation let us define $\bar{C}(j\omega) = \bar{C}_m(j\omega)$. The first two integral terms in (3.48) can be rewritten as

$$\int_{-\infty}^{\infty} \bar{C}(j\omega) \sum_{n=-\infty}^{\infty} \frac{V(j\omega + jn\omega)}{j\omega + jn\omega} \left[\frac{V(j\omega)}{j\omega}\right]^c d\omega \qquad (3.51)$$

where $V(j\omega)$ is defined as

$$V(j\omega) = V_m(j\omega) - V_s(j\omega) \qquad (3.52)$$

Using Lemma 3.1 (see Section 3.2 for proof), $\bar{C}(j\omega)$ can be replaced by its real value

$$\int_{-\infty}^{\infty} \text{Re}\{\bar{C}(\omega)\} \sum_{n=-\infty}^{\infty} \frac{V(j\omega + jn\omega)}{j\omega + jn\omega} \left[\frac{V(j\omega)}{j\omega}\right]^c d\omega \qquad (3.53)$$

Now, (3.53) can be split to two parts based on the sign of the real part of the transfer function $\bar{C}$

$$\int_{-\infty}^{\infty} \bar{C}^+(j\omega) \sum_{n=-\infty}^{\infty} \frac{V(j\omega + jn\omega)}{j\omega + jn\omega} \left[\frac{V(j\omega)}{j\omega}\right]^c d\omega$$
$$+ \int_{-\infty}^{\infty} \bar{C}^-(j\omega) \sum_{n=-\infty}^{\infty} \frac{V(j\omega + jn\omega)}{j\omega + jn\omega} \left[\frac{V(j\omega)}{j\omega}\right]^c d\omega \qquad (3.54)$$

The positive and negative parts of the real part of the controller are defined as

$$\bar{C}^+(j\omega) = \begin{cases} \text{Re}\{\bar{C}(j\omega)\} & \text{, if } \text{Re}\{\bar{C}(j\omega)\} > 0 \\ 0 & \text{, otherwise} \end{cases} \qquad (3.55)$$

$$\bar{C}^-(j\omega) = \begin{cases} \text{Re}\{\bar{C}(j\omega)\} & \text{, if } \text{Re}\{\bar{C}(j\omega)\} < 0 \\ 0 & \text{, otherwise} \end{cases} \qquad (3.56)$$

Lemma 3.2 in Section 3.2 shows that the first integral in (3.54) is positive at all time.

Using (3.48) and (3.54) the sufficient condition for the passivity becomes

$$\int_{-\infty}^{\infty} \bar{C}^-(\omega) \sum_{n=-\infty}^{\infty} \frac{V(j\omega + jn\omega)}{j\omega + jn\omega} \left[\frac{V(j\omega)}{j\omega}\right]^c d\omega +$$

$$\int_{-\infty}^{\infty} b_m V_m(j\omega) V_m^c(j\omega) d\omega + \int_{-\infty}^{\infty} b_s V_s(j\omega) V_s^c(j\omega) d\omega > 0 \qquad (3.57)$$

Using Lemma 3.3 (see Section 3.2 for proof), the first integral in (3.57) is greater than

$$\int_{-\infty}^{\infty} \bar{C}^-(\omega) \sum_{n=-\infty}^{\infty} \frac{1}{(\omega + n\omega_s)^2} V(j\omega) V^c(j\omega) d\omega \qquad (3.58)$$

Thus, for passivity of the teleoperator it is sufficient to have

$$\int_{-\infty}^{\infty} \bar{C}^-(\omega) \sum_{n=-\infty}^{\infty} \frac{1}{(\omega + n\omega_s)^2} V(j\omega) V^c(j\omega) d\omega +$$

$$\int_{-\infty}^{\infty} b_m V_m(j\omega) V_m^c(j\omega) d\omega + \int_{-\infty}^{\infty} b_s V_s(j\omega) V_s^c(j\omega) d\omega > 0 \qquad (3.59)$$

The definition of $V(j\omega)$ can be substituted from (3.52) in (3.59). The first integral in (3.59) becomes

$$\int_{-\infty}^{\infty} \bar{C}^-(\omega) \sum_{n=-\infty}^{\infty} \frac{1}{(\omega + n\omega_s)^2} V_m(j\omega) V_m^c(j\omega) d\omega$$

$$+ \int_{-\infty}^{\infty} \bar{C}^-(\omega) \sum_{n=-\infty}^{\infty} \frac{1}{(\omega + n\omega_s)^2} V_s(j\omega) V_s^c(j\omega) d\omega$$

$$- \int_{-\infty}^{\infty} \bar{C}^-(\omega) \sum_{n=-\infty}^{\infty} \frac{1}{(\omega + n\omega_s)^2} \times \{V_m(j\omega) V_s^c(j\omega) + V_m^c(j\omega) V_s(j\omega)\} d\omega \qquad (3.60)$$

Applying Lemma 3.4 (from Section 3.2) to the last integral in (3.60), it can be

said that (3.60) is less than

$$\int_{-\infty}^{\infty} \bar{C}^-(\omega) \sum_{n=-\infty}^{\infty} \frac{1}{(\omega+n\omega_s)^2} V_m(j\omega)V_m^c(j\omega)d\omega+$$

$$\int_{-\infty}^{\infty} \bar{C}^-(\omega) \sum_{n=-\infty}^{\infty} \frac{1}{(\omega+n\omega_s)^2} V_s(j\omega)V_s^c(j\omega)d\omega$$

$$+ \int_{-\infty}^{\infty} \bar{C}^-(\omega) \sum_{n=-\infty}^{\infty} \frac{1}{(\omega+n\omega_s)^2} \times \{V_m(j\omega)V_m^c(j\omega) + V_s^c(j\omega)V_s(j\omega)\} \, d\omega \qquad (3.61)$$

Lemma 3.5 in Section 3.2 proves that (3.61) and the last two integrals of (3.59) give the sufficient condition for passivity of the teleoperator to be

$$\boxed{\begin{aligned} b_m &> \frac{T}{1-\cos\omega T}\mathrm{Re}\left\{(1-e^{-j\omega T})C_m(e^{j\omega T})\right\} \\ b_s &> \frac{T}{1-\cos\omega T}\mathrm{Re}\left\{(1-e^{-j\omega T})C_s(e^{j\omega T})\right\} \end{aligned}} \qquad (3.62)$$

For verification, the Raisbeck's criterion for passivity of a continuous-time PEB-controller teleoperator was determined. The Raisbeck's criterion is given in Section 2.4.3. In the following it will be shown that for a continuous-time teleoperation system, the above Raisbeck's condition will be always satisfied which is consistent with the passivity condition (3.62) when the sampling time T is substituted by zero. The hybrid matrix of a continuous-time teleoperation system with PEB controllers is [93]

$$\mathbf{H}_{PEB} = \begin{bmatrix} Z_m(s) + C_m \frac{Z_s(s)}{Z_s(s)+C_s(s)} & \frac{C_m(s)}{Z_s(s)+C_s(s)} \\ -\frac{C_s(s)}{Z_s(s)+C_s(s)} & \frac{1}{Z_s(s)+C_s(s)} \end{bmatrix} \qquad (3.63)$$

To test (2.1), one may replace the continuous-time controllers of (3.63) by $C_m(s) = C_s(s) = K + Bs$, and the master and slave impedances of (3.63) by $Z_m(s) = Z_s(s) = ms$, and the Raisbeck's conditions (2.1) become $m^2\omega^4 B/[B^2\omega^2+(m\omega^2-K)^2]$, $B\omega^2/[B^2\omega^2 + (m\omega^2 - K)^2]$ and zero, respectively. Thus, all three conditions (2.1) are satisfied, which means that the two-port network teleoperator for a continuous-time, PEB-controlled system is passive. Despite the continuous-time counterpart,

32

for a sampled-data teleoperation system increasing the controller gain may incur non-passivity, which emphasizes importance of modeling the discretization effect in passivity analysis of the teleoperation system. Special case I: Unequal controllers

The assumption on the master and the slave controllers to be equal (3.50) can be changed to

$$\frac{C_m(j\omega)}{n_p} = C_s(j\omega) = C(j\omega) \tag{3.64}$$

where n_p is the position scaling factor. It should be noted that setting the controllers the same proportion as the position signals is practically justifiable. For instance, in micro-surgery, the slave's micro-surgical tools undergo fine motions and need a high-gain controller compared to the master's handle whose range of motion spans the human hand's workspace (i.e., $C_m < C_s$ and $x_m > x_s$). In the unequal controller case, the position error (3.39) becomes

$$e = n_p x_m - x_s \tag{3.65}$$

The analysis is repeated for the cases where the value of n_p is non-unity and the controllers have the relationship of (3.64). The derivation for non-unity scaling is given Lemma 1 in the following. The passivity condition in the unequal controller case becomes

$$\boxed{\begin{aligned} b_m &> \frac{T}{2}\frac{n_p+1}{1-\cos\omega T}\mathrm{Re}\left\{(1-e^{-j\omega T})C_m(e^{j\omega T})\right\} \\ b_s &> \frac{T}{2}\frac{n_p+1}{1-\cos\omega T}\mathrm{Re}\left\{(1-e^{-j\omega T})C_s(e^{j\omega T})\right\} \end{aligned}} \tag{3.66}$$

Remark 1. *This lemma includes derivations of the passivity condition for the case where the position error of (3.39) is replaced by the scaled version of (3.65), and the master and the slave controllers of (3.50) is replaced by (3.64). To keep the derivation concise, only the steps that are different have been presented in the following steps.*

Using the definition of error (3.65), (3.40) becomes

$$F_m^*(s) = C_m(z)|_{z=e^{sT}}[X_s^*(s) - n_p X_m^*(s)]$$
$$F_s^*(s) = C_s(z)|_{z=e^{sT}}[n_p X_m^*(s) - X_s^*(s)] \qquad (3.67)$$

And, (3.46) becomes

$$F_m(j\omega) = n_p \frac{1 - e^{-j\omega T}}{j\omega T} C_m(e^{j\omega T}) X_m^*(j\omega) - \frac{1 - e^{-j\omega T}}{j\omega T} C_m(e^{j\omega T}) X_s^*(j\omega)$$
$$F_s(j\omega) = n_p \frac{1 - e^{-j\omega T}}{j\omega T} C_s(e^{j\omega T}) X_m^*(j\omega) - \frac{1 - e^{-j\omega T}}{j\omega T} C_s(e^{j\omega T}) X_s^*(j\omega) \qquad (3.68)$$

Also, (3.48) becomes

$$\int_{-\infty}^{\infty} \bar{C}_m(\omega) \sum_{n=-\infty}^{\infty} \frac{n_p V_m(j\omega + jn\omega_s) - V_s(j\omega + jn\omega_s)}{j\omega + jn\omega_s} \times \left[\frac{V_m(j\omega)}{j\omega}\right]^c d\omega$$
$$+ \int_{-\infty}^{\infty} \bar{C}_s(\omega) \sum_{n=-\infty}^{\infty} \frac{V_s(j\omega + jn\omega_s) - n_p V_m(j\omega + jn\omega_s)}{j\omega + jn\omega_s} \times \left[\frac{V_s(j\omega)}{j\omega}\right]^c d\omega \qquad (3.69)$$

The definition of $\bar{C}$ changes to $\bar{C}(j\omega) = \bar{C}_m(j\omega)/n_p$ and $V(j\omega)$ in (3.52) is re-defined as $V(j\omega) = n_p V_m(j\omega) - V_s(j\omega)$. Also, (3.60) and (3.61) should be changed to

$$\int_{-\infty}^{\infty} \bar{C}^-(\omega) \sum_{n=-\infty}^{\infty} \frac{1}{(\omega + n\omega_s)^2} n_p^2 V_m(j\omega) V_m^c(j\omega) d\omega$$
$$+ \int_{-\infty}^{\infty} \bar{C}^-(\omega) \sum_{n=-\infty}^{\infty} \frac{1}{(\omega + n\omega_s)^2} V_s(j\omega) V_s^c(j\omega) d\omega$$
$$- n_p \int_{-\infty}^{\infty} \bar{C}^-(\omega) \sum_{n=-\infty}^{\infty} \frac{1}{(\omega + n\omega_s)^2} \times \{V_m(j\omega) V_s^c(j\omega) + V_m^c(j\omega) V_s(j\omega)\} d\omega \qquad (3.70)$$

and,

$$\int_{-\infty}^{\infty} \bar{C}^-(\omega) \sum_{n=-\infty}^{\infty} \frac{1}{(\omega + n\omega_s)^2} n_p^2 V_m(j\omega) V_m^c(j\omega) d\omega +$$

$$\int_{-\infty}^{\infty} \bar{C}^-(\omega) \sum_{n=-\infty}^{\infty} \frac{1}{(\omega + n\omega_s)^2} V_s(j\omega) V_s^c(j\omega) d\omega$$

$$+ n_p \int_{-\infty}^{\infty} \bar{C}^-(\omega) \sum_{n=-\infty}^{\infty} \frac{1}{(\omega + n\omega_s)^2} \times \{V_m(j\omega) V_m^c(j\omega) + V_s^c(j\omega) V_s(j\omega)\} d\omega \quad (3.71)$$

The final passivity condition (3.62) becomes

$$\boxed{\begin{aligned} b_m &> \frac{T}{2} \frac{n_p + 1}{1 - \cos \omega T} \text{Re}\left\{(1 - e^{-j\omega T}) C_m(e^{j\omega T})\right\} \\ b_s &> \frac{T}{2} \frac{n_p + 1}{1 - \cos \omega T} \text{Re}\left\{(1 - e^{-j\omega T}) C_s(e^{j\omega T})\right\} \end{aligned}} \quad (3.72)$$

Special case II: PD controller

The passivity condition (3.62) is valid for all controllers. If the controller's structure is known, the condition can be further simplified. For instance, for a PD controller $K + Bs$, which can be discretized using bilinear transformation method as

$$C_s(z) = C_m(z) = K + B \frac{z - 1}{Tz} \quad (3.73)$$

the passivity condition (3.62) is simplified to

$$b > KT - 2B \cos \omega T \quad (3.74)$$

Condition (3.74) is dependent on the frequency ω. The term $\cos \omega T$ can vary between -1 and 1. Thus, a sufficient condition for teleoperator passivity over all frequencies will be

$$b > KT + 2B \quad (3.75)$$

which has to hold for both the master and the slave robots.

35

Condition (3.75) implies that increasing the sampling time and controller gains drive the system closer to non-passivity. The master or slave robot damping term b is a physical characteristic of the robot and cannot be easily changed whereas the other parameters in (3.75) can be appropriately set in the control design process.

In addition to the passivity of the teleoperator, it is desirable to have high teleoperation transparency. Condition (3.75) can be used to achieve as high transparency as possible while maintaining passivity.

In fact, in a continuous-time teleoperation system, it can be proved that increasing the controller gains moves the system closer to more transparent teleoperation. High controller gains lead the hybrid matrix of the PEB teleoperation system in continuous-time (3.63) to approach the ideal transparent hybrid matrix as follows

$$\mathbf{H}_{ideal} = \begin{bmatrix} 0 & 1 \\ -1 & 0 \end{bmatrix} \tag{3.76}$$

Comparison of (3.63) and (3.76) leads to the fact that for the stable teleoperation system, increasing the gains of C_m and C_s increases teleoperation transparency, although fully transparent teleoperation cannot be achieved using the PEB controller because of the first element of (3.63) which is always greater than zero. It is shown that to the full transparency of the teleoperation system can be achieved with either force-position controller [94] or three-channel architecture [95]. .

3.5 Simulation study

The teleoperation system of Fig. 3.2 has been simulated in MATLAB/Simulink and the passivity condition (3.75) has been tested for a teleoperator comprising a pair of 1-DOF robots modelled by mass-damping terms. These mass and damping parameters match those of Phantom Premium 1.5A robots used in the experiments, the details of which will be described in Section 3.6. The simulation allows for variation of

parameters that cannot be altered in experiments such as the robot damping term b.

To determine the passivity of the teleoperator, a passivity observer, which calculates the dissipated energy, has been incorporated into the simulations. The dissipated energy is represented by the input-output energy integral in (3.41). For a passive teleoperator, the energy integral is non-negative at all times.

For selected model parameters, first the passivity borderline is theoretically determined via condition (3.75) and shown in Fig. 3.3 by red lines. Next, the simulation is repeated for various model parameters changed over a grid in the parameter space. The system is simulated for a chosen passive model (a first-order positive-real transfer function) for the human operator and the environment. Changing the model of the human operator and the environment – zero impedance, infinite impedance, or other positive-real transfer functions yields similar simulation results. In each point of the grid of parameters values, the energy integral is monitored to detect non-passive teleoperator cases; if the energy integral becomes negative at any time, it signals a non-passive teleoperator. The dark pixels in Fig. 3.3 indicate where in the parameter space the energy integral becomes negative (i.e., the teleoperator is non-passive). As it can be seen, the regions indicated by the passivity condition (3.75) closely match the simulation results. There is a gap between the filled area and the red line, which corresponds to cases where condition (3.75) is conservative for detecting the teleoperator non-passivity. The conservatism of condition (3.75) was predictable due to the fact that it was found as a sufficient condition for passivity.

Fig. 3.4 shows an example of the observer output for a teleoperation system simulation, in which the controller gain has switched from $K = 160$ to $K = 250$ at $t = 50^{\text{sec}}$, making the system non-passive. Before the change, the passivity observer output stayed non-negative. As shown in Fig. 3.4, while the observer detected non-passivity of the system at $t = 109^{\text{sec}}$ (when the passivity observer output crossed zero), the teleoperation system became non-passive soon after the gain change happened at $t = 50^{\text{sec}}$. In fact, the passivity observer can only determine if the system is non-
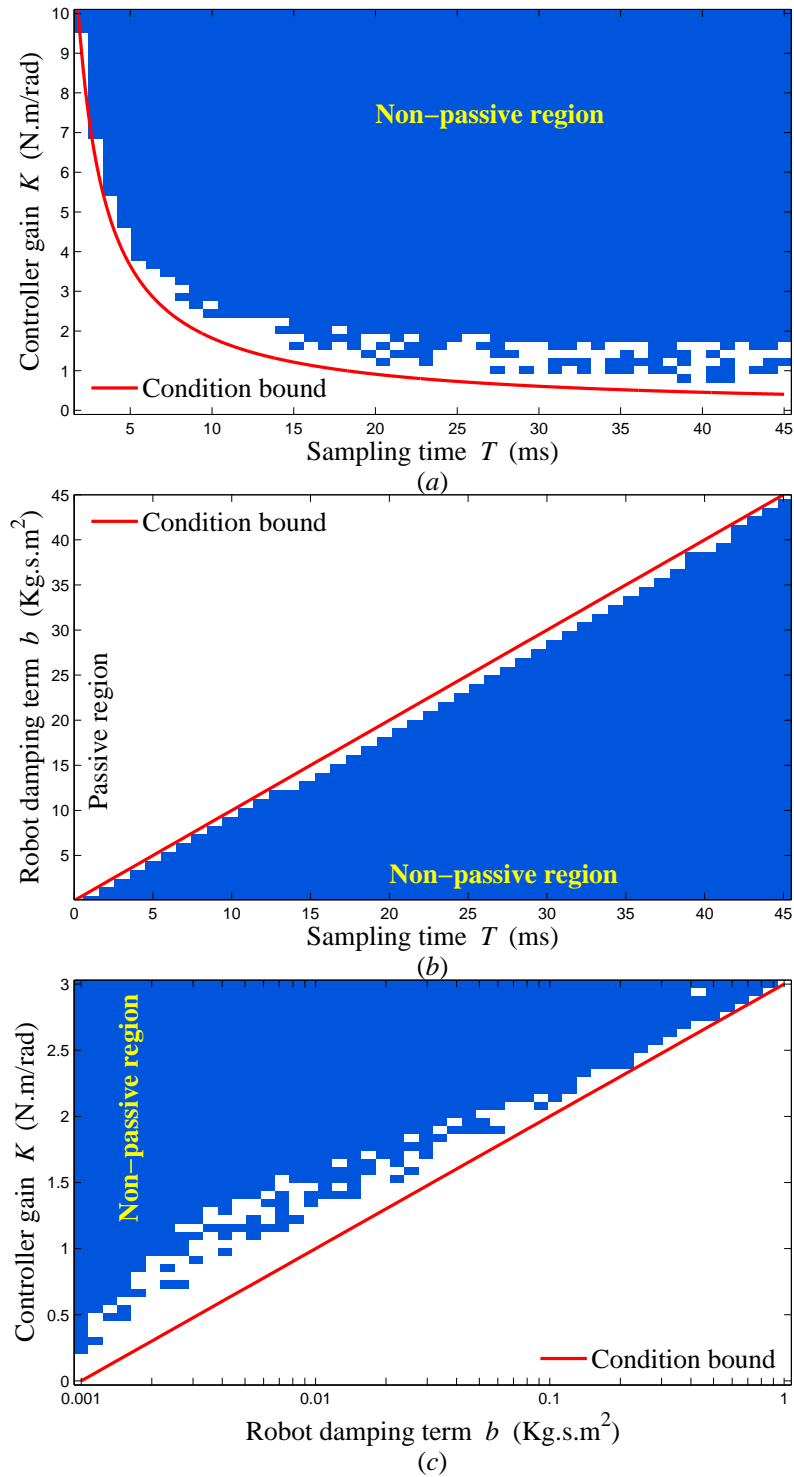
Figure 3.3: Passive and non-passive regions (a) in $K-T$ plane for $B=0$ $m=0.015$ and $b=0.01822$, (b) in $b-T$ plane for $K=1$, $m=0.015$ and $B=0$, and (c) in $K-b$ plane for $B=0$, $m=0.015$ and $T=1^{\mathrm{ms}}$.
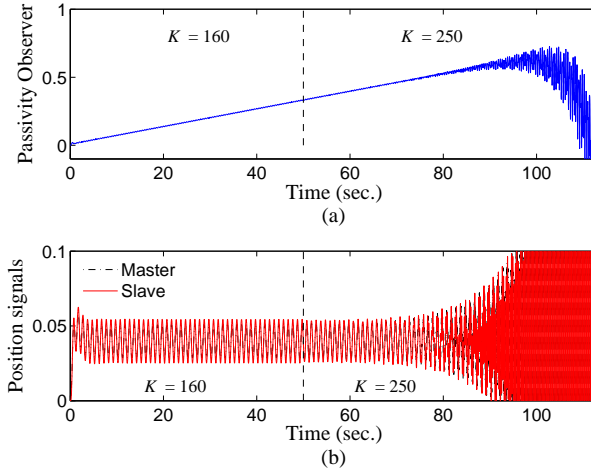
Figure 3.4: Passivity observer output in simulations for a teleoperator with a changing controller gain. The controller gain changes from $K = 160$ to $K = 250$ at $t = 50^{\text{sec}}$ and makes the teleoperator non-passive. The other system parameters are $T = 5^{\text{ms}}$, $b = 1$ and $B = 0$.

passive if the index becomes negative. In case the energy integral remains positive, the passivity observer is not able to produce any conclusion about whether the system is passive or non-passive. On the other hand, the passivity condition (3.75) determines the passivity of the system analytically and more accurately.

3.6 Experimental results

3.6.1 Teleoperation system setup

To verify the passivity condition (3.75) experimentally, the stability condition has been tested for a teleoperation system consisting of a pair of Phantom Premiums 1.5A robots (Sensable Technologies/Geomagic, Wilmington, MA) with JR3 force sensors (JR3, Inc., Woodland, CA) at their end-effectors. We consider the robots to work in the joint space – angular position and torque are the output and input of each joint of each robot. Out of the three actuated joints of each robot, the first one is used in the experiment while the second and the third joints, which form a parallel mechanism,

39

are locked using high gain controllers.

3.6.2 Choice of terminations: Free-motion/free-motion (FF) vs. free-motion/clamped (FC)

The experiments have set up to include two extreme cases of zero and infinitely-stiff impedances corresponding to free-motion and a clamped coupling for each termination. This results in four combinations for the two terminations.

- Case 1: Both master and slave in free motion (FF)

- Case 2: Master in free motion and slave clamped (FC)

- Case 3: Master clamped and slave in free motion (FC)

- Case 4: Both master and slave clamped (CC)

Since our teleoperation system including its controllers is symmetric with respect to the master and the slave, Cases 2 and 3 are similar experiments (FC). In contrast to Cases 1 to 3 for the termination choices where at least one of the robots is able to move and potentially show the instability of the teleoperation system, Case 4 does not serve our experiment objectives. Having clamped robots allows for non-zero forces, but does not allow for the investigation of stability in our position-error-based teleoperation system. Thus, Case 4 has been excluded from our experiments. Case 4 (CC) can be important as one of the extreme cases for termination choices especially in control architectures with force sensor feedback (e.g., the 4-channel method) where the destabilizing effect of non-collocated sensing and link/joint flexibility are important. Fig. 3.5 shows the experimental setup for the FC termination arrangement, and the FF arrangement (not shown) is similar except that it involves no clamping of either robot.

It should be noted that the experimental protocol described above has the advantage that it is independent of any human operator's intervention (as master's cou-

Figure 3.5: Experimental setup for the case where the master arm (left) is in free motion and the slave arm (right) is clamped (FC).

pling), rendering the experiments highly reproducible. Similarly, it does not depend on any particular physical environment (as slave's coupling).

Within each of the two *cases* for the terminations (FF or FC), different *experiments* have been run for different values of the sampling time. Within each experiment (i.e., at a given sampling time), the controller gain has been altered in different *tests*. Within each test (i.e., at a given sampling time and a given controller gain), different *trials* have been conducted for different values of the initial condition.

3.6.3   Choice of initial conditions

In the experiments, when the master and/or the slave are in free motion, we provide them with initial conditions such that the teleoperation system is excited; otherwise, there will be no motion. The initial condition specifies the position difference between the master and the slave at the onset of a trial (within a test within an experiment) – the slave is placed at the origin of its coordinate system while the master has an initial angular position. Since a passive system should remain stable regardless of its initial condition, when investigating the passivity of the teleoperator, the initial condition has been changed over a series of trials in a large span only limited by

41

the physical constraints of the experimental setup. Instability in one trial is enough to indicate that the teleoperation system with the chosen parameters is potentially unstable. If none of the trials makes the teleoperation system unstable, the system is identified as passive at this particular test (with controller gain K) and experiment (with sampling time T).

3.6.4 Determination of passivity/non-passivity borderline

In both FF and FC cases, either the velocity or the contact force is zero in both the master and the slave sides. This makes the passivity definition according to the integral of power at the two ports, namely (3.41), impossible to check because the power at each port is always zero. Instead, to determine the non-passivity of the teleoperation system, its instability has been monitored as characterized by growing oscillations. It should be noted that the reverse conclusion is not valid; there are systems that are stable without being passive.

The procedure for experimentally determining the passivity/non-passivity border-line is as follows. A given sampling time T specifies a vertical line in the $K - T$ plane for different values of the controller gain K. The intersection of this vertical line with the theoretical passivity borderline determines the value of the controller gain below (above) which the teleoperator is expected – from a purely theoretical perspective – to be passive (non-passive). The objective of each experiment is to find the smallest and the largest controller gains that make the teleoperator non-passive and passive, respectively, at a given sampling time. Such an experiment is then repeated at different sampling times (vertical line locations). To find the smallest controller gain that makes the teleoperator non-passive, the controller gain is first set to the value given by the theoretical passivity borderline at that sampling time. Next, we perform a trial for a small initial condition, the results of which can be one of the following two possibilities.

- (A) If the teleoperation system is stable, the trial is repeated with a larger

initial condition. The increase in the initial condition is continued until either the system becomes unstable (reverting to Case B below) or the entire range of initial conditions has been tested. If no instability was observed across the trials, the data point corresponding to this test is marked as being passive in the $K - T$ plane. Then, the controller gain is increased slightly (by steps of less than 1% of the maximum gain) and the same test is repeated for this new gain, possibly adding one more passive data point to the $K - T$ plane. The increase in the controller gain is continued until the system becomes unstable, which corresponds to a non-passive teleoperation system.

- (B) If the teleoperation system is unstable, the data point corresponding to this test is marked as being non-passive in the $K - T$ plane. Then, following a procedure in the opposite direction, the controller gain is decreased slightly (by steps of less than 1% of the maximum gain) until the system becomes stable. Again, if no instability was observed across several trials, the data point corresponding to this test is marked as being passive in the $K - T$ plane.

The result of the above procedure is an accurate experimentally-obtained passivity borderline in the $K - T$ plane.

3.6.5   Results

The experimental borderlines found for FF and FC experiments are shown in Fig. 3.6 and 3.7, respectively. Thus, in Fig. 3.6, the teleoperator is coupled to two zero-impedance terminations. Also, in Fig. 3.7, the teleoperator is coupled to a zero-impedance termination and another infinite-impedance termination. The theoretical regions of passivity and (potential) non-passivity obtained from condition (3.75) are shown as separated by the theoretical borderline (blue line). Also, the result of each experiment is indicated either as a star (stable) or a circle (unstable) in these figures. For a given sampling time, many more tests were conducted but not shown in Fig. 3.6
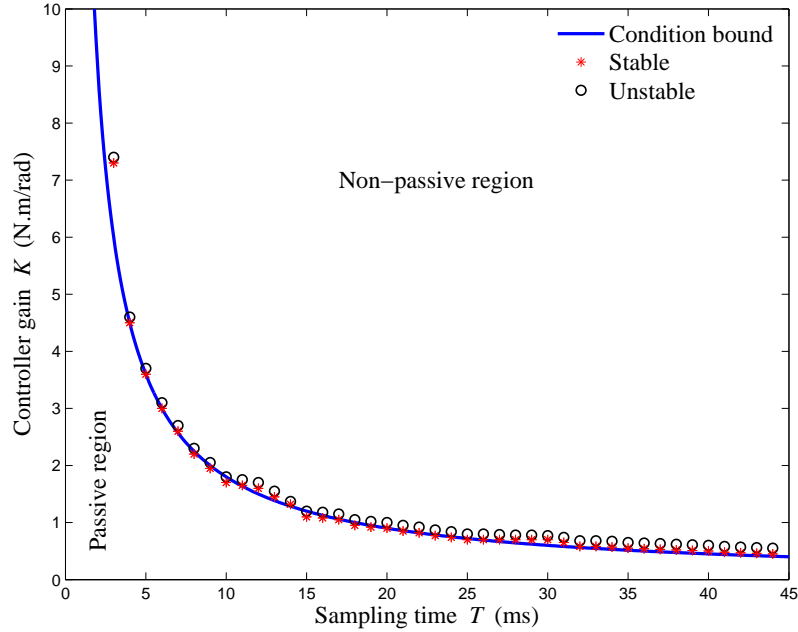
Figure 3.6: Free-motion/free-motion (FF) experiment data points and theoretical passivity borderline. Stars represent stable, and circles represent unstable systems.

and 3.7; only those data points corresponding to the previously-discussed "smallest and the largest controller gains" were shown.

As seen in Fig. 3.6, in the FF case, the theoretical teleoperator passivity/non-passivity borderline closely matches the experimentally-obtained borderline. The close match between the theoretical borderline (3.75) for the passivity of the teleoperator and the experimental borderline for the stability of the teleoperation system in the FF case (Fig. 3.6) demonstrates that the aforementioned theoretical condition is not overly conservative in the context of stability analysis. Also, this theoretical condition corresponds to a worst-case scenario in terms of termination choices the stability region for the teleoperation system in the FC case (Fig. 3.7) is bigger than that predicted by the passivity region for the teleoperator in the FF case (Fig. 3.6). From Fig. 3.7, in the FC case, it is seen that the theoretical teleoperator passivity/non-passivity borderline is more conservative than the experimentally-obtained borderline in the sense that, in the $K-T$ plane, certain theoretically non-passive points are found
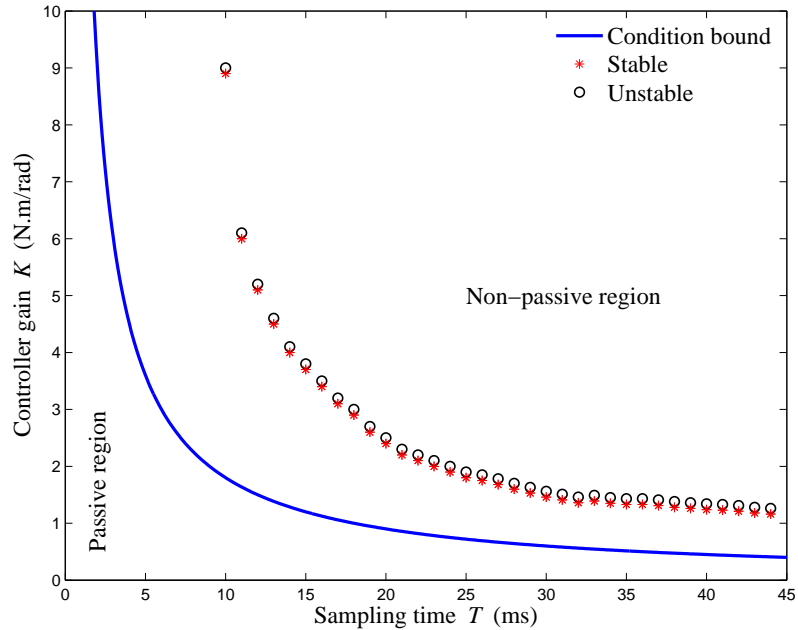
Figure 3.7: Free-motion/clamped (FC) experiment data points and theoretical passivity borderline. Stars represent stable, and circles represent unstable systems.

to be practically passive. Both of the above were expected for the reasons explained below. Recall that we defined a teleoperation system to consist of a teleoperator coupled to two terminations (a human operator and a remote environment). In the FF case, the teleoperation system and the teleoperator are the same and, therefore, the non-passivity of the teleoperation system (as assessed by the procedure outlined in Section 3.6.4) is tantamount to the (potential) non-passivity of the teleoperator (as assessed by condition (3.75)). However, in the FC case, the experimental procedure to determine passivity/non-passivity in Section 3.6.4 concerns that of the teleoperation system, which is now different from the teleoperator alone due to the presence of one infinitely-stiff termination for the teleoperator. In other words, while the choice of terminations cannot affect the passivity or nonpassivity of the teleoperator, it affects the stability of the overall teleoperation system, which is what is evaluated through the steps in Section 3.6.4. Thus, the theoretical passive region (3.75) for the teleoperator was expected to be different from the experimental non-passive region for the

45

Table 3.1: Mean-square-error of master-slave position tracking relative to the master position mean-square (percent).

T (ms)	$K = 0.4$	$K = 1.0$	$K = 2.0$	$K = 2.4$
7	10.2580	9.9864	3.0355	3.3159
15	13.2608	5.8948	Unstable	Unstable

teleoperation system with the gap between these two regions being affected by the passive behaviors of the terminations. The extreme FF and FC cases for terminations in Fig. 3.5 correspond to two of the possible extreme passivity/non-passivity borderlines.

3.6.6 Transparency comparison

From the passivity borderlines in Fig. 3.6 and Fig. 3.7, it can be concluded that the upper bound on the controller gain becomes smaller as the sampling time increases. For any given sampling time, one may choose the controller gain to be low enough to avoid instability of the teleoperation system. However, lowering the controller gain comes at a cost to transparency of the teleoperation system; to limit the transparency degradation, we need to use the largest stabilizing controller gain. Table 3.1 demonstrates this fact using free-motion experiments in which the controller gain K and the sampling time T are altered and master-slave position tracking error is measured: in most cases increasing K in the stable region of the $K - T$ plane results in smaller percent mean-square-error (MSE) in position tracking relative to the mean-square-error of master position. This is why knowing the passivity borderline is important.

3.7 Conclusions

In this chapter, a passivity condition has been found for a delay-free bilateral teleoperation system in which the position error based controllers are implemented in

discrete-time. To find this condition, the models of the zero-order-hold and the sampler are incorporated in an appropriate frequency-domain analysis. The condition imposes a lower bound on the robot damping, an upper bound on the sampling time, and bounds on the controller gains. For the special case of PD control, the bounds on the proportional and derivative controller gains have been found to be upper bounds. Thus, the passivity condition provides the designer with guidelines about how much the controller gain can be increased with no risk of instability. Supporting simulations and experiments demonstrating the validity of the passivity condition have been reported.

Chapter 4

Absolute Stability Analysis of Sampled-Data Scaled Bilateral Teleoperation Systems [1]

4.1 Introduction

4.1.1 Teleoperation stability analysis

To analyze the closed-loop stability of a teleoperation system, one can assume that the operator and the environment models are known, e.g. in [76]. While this assumption will simplify the stability analysis, it cannot be made in practice because the dynamic parameters of the human operator change in response to the specific requirements of the task at hand [96], and the dynamic parameters of the environment are uncertain, time-varying and nonlinear.

Modeling the teleoperation system as a two-port network (teleoperator comprising the master, the controller and communication channel, and the slave) coupled to two

---

[1]This chapter has been published in the Control Engineering Practice - a Journal of IFAC [7]. Parts of this chapter have also been presented in the 2010 IEEE Conference on Decision and Control, Atlanta, Georgia, USA [8] and in the 2011 Canadian Congress on Applied Mechanics, Vancouver, BC, Canada.

one-port networks (environment and operator) paved the way for ensuring closed-loop stability via teleoperator passivity, i.e., ensuring that the two-port network teleoperator is passive, which physically means the teleoperator is not generating any energy [97, 98] (see Section 2.4.3).

Absolute stability analysis relaxes the passivity assumption on the teleoperator meaning that it allows the teleoperator to be non-passive as long as the closed-loop stability of the teleoperation system is preserved. Similar to passivity, the absolute stability approach assumes that the environment and the operator are passive but otherwise arbitrary. The absolute stability of a *continuous-time* two-port network can be assessed using Llewellyn's criterion [99, 100, 101] (see Section 2.4.4). Recent studies have introduced geometric approaches inspired by criteria for unconditional stability of microwave systems to study the absolute stability of teleoperation systems [102]. The proposed method by Haddadi and Hashtrudi-zaad allows the environment and the operator to be non-passive with bounded impedance while the overall *continuous-time* teleoperation system is still stable.

As mentioned in Section 2.4.2, absolute stability breaks down the teleoperation system to three main blocks: A human operator (one-port network), an environment (one-port network), and a teleoperator (two-port network). The absolute stability of a two-port network is also equivalent to the passivity of the one-port network resulting from connecting the other port of the two-port network to a passive termination [102] (see Fig. 2.2). The challenge that is fully addressed in this chapter is how to ensure stability of the overall teleoperation system when the only information about the terminations (i.e., the human operator and the environment) is their passivity.

The assumption of passivity of the one-port network terminations can be expressed by their positive realness for linear systems (see Section 2.4.2). Positive realness of a transfer function corresponds to having its Nyquist diagram entirely in the right half of the complex plane. The assumption of termination passivity has been integrated into the stability analysis using the mapping of the positive real region to a unit

49

disc in the Nyquist plane by finding the proper linear fractional transformation. A simpler case of such mapping has been first introduced by Colgate and Schenkel [82] for a one-port system (i.e. the virtual wall) and in this chapter has been extended to two-port network by solving the combined dynamics of both the master and the slave robots in a teleoperation system.

The effect of position and/or force scaling on the stability and passivity of a teleoperation system is a nontrivial problem. The conventional two-port network passivity analysis cannot be directly used in a scaled teleoperation system with arbitrary position and force scaling factors for the following reason. The two-port network representing the teleoperator is passive if the work done by the operator and the environment on it is non-negative at all times and for all inputs and initial conditions:

$$\int_0^t f_h(\tau)\dot{x}_m(\tau)d\tau + \int_0^t f_e(\tau)\dot{x}_s(\tau)d\tau > 0 \qquad (4.1)$$

where f and $\dot{x}$ stand for force and velocity and subscript h, m, e and s correspond to hand, master, environment and slave, respectively. The above energy balance equation has relied on defining the power at the input and output ports as the multiplication of a velocity and a force. If x_m and x_s are scaled with respect to each other, then it is obvious that f_h and f_e need to be at the inverse scale to make the input and the output powers comparable in the conventional passivity definition of (4.1) (see [103, 104]). In other words, the conventional passivity definition (4.1) cannot hold if both velocity and force at one termination of a teleoperation are at a smaller scale than those at the other termination which is against the transparency requirement [105]. On the other hand, it will be elaborated that the proposed absolute stability approach is able to tackle the stability of a scaled teleoperation system with the same ease as when there is no power scaling.

4.1.2 Sampled-data teleoperation

A major challenge in stability analysis of teleoperation systems that is addressed in this chapter is the effect of controller discretization. The discretization of a stabilizing continuous-time controller does not necessarily preserve the stability (see Section 2.5 for detailed discussion) [77, 75]. In fact, the stability of the closed-loop system will be degraded due to the energy-instilling behaviour of the Zero Order Hold (ZOH) [77].

Past research dealing with the effect of discretization has either modified the teleoperation controllers to ensure the sampled-data system stability, or have analyzed the stability of the sampled-data system with discretized counterparts of the original continuous-time controllers [106]. In one of the first researches toward the controller design for a sampled-data teleoperation system, six low-pass filters were added to the control structure to stabilize the overall teleoperation system, which resulted in its sluggish performance [75]. It was shown that for step-invariant discretization of the sampled-data teleoperation system, there exists an upper bound on the sampling time to keep the system stable. As for stability analysis of the sampled-data teleoperation system, the research is focused either on the absolute stability of the discrete-time communication channel [86] or the stability of the overall teleoperation system for known models of the environment [70].

4.1.3 Sampled-data teleoperation stability analysis

Knowing the bounds on the parameters of the teleoperator model and the controller for ensuring absolute stability provides guidelines for designing controllers with high gains as needed for transparent teleoperation – it will be shown in this chapter that increasing the control gains beyond a limit jeopardizes stability. In addition, certain applications such as texture recognition require high-frequency force feedback, increasing the demand for transparency over high frequencies and shrinking the stability margin. In the controller design for such a system, knowing the boundaries between the stable and unstable regions will be very useful. Another reason to know

the bounds on the system parameters is that, as it will be shown later, there is a trade-off between the sampling time and the maximum environment stiffness for stable teleoperation. When the slave robot is in hard contact (i.e., the environment stiffness is very large), the system requires very small sampling times, which exceeds the physical constraints of the discrete-time control hardware. Knowing the minimum sampling time helps to determine the maximum environment stiffness for which the teleoperator will be absolutely stable. Lastly, the absolute stability condition becomes particularly important with robots that, for performance reasons, have been designed to have low dampings (e.g., by minimizing friction). As shown in this chapter, the stability condition puts a lower bound on the robot damping. Therefore, with a fixed robot damping, the controller is designed according to the absolute stability condition to ensure that the teleoperation system remains absolutely stable.

In this chapter, a new absolute stability condition is developed for a sampled-data teleoperator without assuming any model for the operator or the environment as long as they are passive. The effect of the zero order hold is considered in the absolute stability analysis of the system. The absolute stability permits the teleoperator to be passive or nonpassive, resulting in a less conservative condition compared to the teleoperator passivity condition, thus allowing for higher teleoperation transparency and inclusion of arbitrary position and force scaling factors between the master and the slave. Unlike most of absolute stability methods in the literature, this new analysis considers continuous-time robots working with *discrete-time controllers* with arbitrary scaling factors for position and force. The condition can be used as a guideline for designing stabilizing and high-transparency controllers for sampled-data teleoperation systems.

This chapter is organized as follows. A sampled-data bilateral teleoperation system is modeled in Section 4.2. This model is later used in Section 4.3 to derive a condition for absolute stability of the sampled-data teleoperator. A few special cases are considered in Section 4.4 to result in more practical conditions. Then, the ex-

perimental results on a pair of Phantom Omni robots are presented in Section 4.5 followed by the experimental results on a three-way slide switch in Section 4.6. Lastly, concluding remarks are given in Section 4.7.

4.2 Modelling of sampled-data teleoperation systems

To study absolute stability, the dynamic models of the master robot and the slave robot are required. The modelling of the sampled-data bilateral teleoperation given in (3.32)-(3.39) are valid for absolute stability analysis of the bilateral teleoperation system.

The control architecture in modelling of Fig. 3.2 assumes that the teleoperation system uses a position-error-based (PEB) controller. A PEB controller is chosen because, with a direct force reflection (DFR) controller, even the continuous-time teleoperation system will not be absolutely stable (Appendix A). As depicted in Fig. 3.2, the PEB controllers work based on the position error between the master and the slave. As also mentioned in (3.40), the outputs of the master and slave controllers F_m^* and F_s^* will be *sampled-data* signals

$$F_m^*(s) = C_m(z)[X_s^*(s) - n_p X_m^*(s)]$$
$$F_s^*(s) = C_s(z)[n_p X_m^*(s) - X_s^*(s)] \tag{4.2}$$

where n_p is the scaling factor between the master and the slave positions. Similar to the unity-scale teleoperation [8], as the controller drives the position error $e = x_s - n_p x_m$ to zero, the master and slave positions will have the following ratio

$$\frac{x_s}{x_m} = n_p \tag{4.3}$$

Here, the * superscript requires us to use the infinite impulse-train definition (3.35) of the sampler in the derivations that follow.

In order to be able to derive the closed-loop transfer function, from Fig. 3.2, the continuous-time transfer functions from f_m to x_m and from f_s to x_s can be found as

$$\frac{X_m}{F_m} = \frac{1}{s} \cdot \frac{\frac{1}{m_m s + b_m}}{1 + \frac{Z_h}{m_m s + b_m}} = \frac{1}{s} \cdot \frac{1}{m_m s + b_m + Z_h} \tag{4.4}$$

$$\frac{X_s}{F_s} = \frac{1}{s} \cdot \frac{\frac{1}{m_s s + b_s}}{1 + \frac{Z_e}{m_s s + b_s}} = \frac{1}{s} \cdot \frac{1}{m_s s + b_s + Z_e} \tag{4.5}$$

Note that the only knowledge about the transfer functions of the human operator Z_h and the environment Z_e is that they are passive. When the above continuous transfer functions are combined with the models of the two zero-order-holds in (3.38), the transfer functions from f_m^* to x_m and from f_s^* to x_s can be found as

$$\begin{aligned}
G_m(s) &= \frac{X_m(s)}{F_m^*} = \frac{1}{m_m s + b_m + Z_h(s)} \cdot \frac{1 - e^{-sT}}{sT} \cdot \frac{1}{s} \\
G_s(s) &= \frac{X_s(s)}{F_s^*} = \frac{1}{m_s s + b_s + Z_e(s)} \cdot \frac{1 - e^{-sT}}{sT} \cdot \frac{1}{s}
\end{aligned} \tag{4.6}$$

By substituting these into the model of the sampler (3.35), the overall system equations (4.2) become

$$\begin{aligned}
F_m^*(s) &= C_m(e^{sT})[-n_p G_m^*(s) F_m^*(s) + G_s^*(s) F_s^*(s)] \\
F_s^*(s) &= C_s(e^{sT})[-G_s^*(s) F_m^*(s) + n_p G_m^*(s) F_s^*(s)]
\end{aligned} \tag{4.7}$$

where $G_m^*(s)$ and $G_s^*(s)$ are the following discrete-time transfer functions:

$$G_m^*(s) = \frac{1}{T} \sum_k G_m(s + jk\omega_T)$$

$$G_s^*(s) = \frac{1}{T} \sum_k G_s(s + jk\omega_T) \tag{4.8}$$

And $\omega_T = 2\pi/T$ is the sampling frequency.

4.3 Absolute stability of sampled-data teleoperation

In section 4.2, the sampled-data teleoperation system was modelled and resulted in closed-loop equations (4.7). Our main theorem for testing absolute stability of the sampled-data teleoperation system will be given after the following definition and lemma.

Definition 4.1. *A teleoperator is called absolutely (or unconditionally) stable when coupling it to any passive but otherwise arbitrary environment and operator terminations results in a stable teleoperation system* [2].

Remark 2. *If a teleoperator is not absolutely stable, the teleoperation system is called potentially unstable. Note that a potentially unstable teleoperator does not necessarily amount to an unstable teleoperation system.*

Lemma 4.1. *The closed-loop characteristic equation of the sampled-data teleoperation system in Fig. 3.2 is*

$$1 + n_p C_m(e^{sT}) G_m^*(s) + C_s(e^{sT}) G_s^*(s) = 0 \tag{4.9}$$

---

[2] Stability of the teleoperation system is defined as BIBO stability of the system when the system input is the exogenous human operator force $\tilde{f}_h$ and the system output is the slave position x_m.

Proof. It is easy to see that the transfer function from $\tilde{F}_h$ to X_m is

$$\frac{X_m(s)}{\tilde{F}_h(s)} = \frac{(1 + C_s(e^{sT})G_s^*(s))H_m(s)}{1 + n_p C_m(e^{sT})G_m^*(s) + C_s(e^{sT})G_s^*(s)} \quad (4.10)$$

where

$$H_m(s) = \frac{1}{Z_m(s) + Z_h(s)} \cdot \frac{1}{s} \quad (4.11)$$

and the master robot impedance is defined by $Z_m = m_s s + b_m$. It can be shown that (4.9) is the also denominator of all transfer functions from inputs $\tilde{F}_h$ or $\tilde{F}_e$ to any other output. $\square$

The open-loop system equations (4.7) can be written as

$$\begin{bmatrix} 1 + n_p C_m G_m^* & -C_m G_s^* \\ -n_p C_s G_m^* & 1 + C_s G_s^* \end{bmatrix} \begin{bmatrix} F_m^* \\ F_s^* \end{bmatrix} = \begin{bmatrix} 0 \\ 0 \end{bmatrix}$$

The determinant of the above matrix gives the characteristic equation of the system to be (4.9).

Theorem 4.1. *The sampled-data teleoperator resulting from using the discrete-time control laws (4.2) with the continuous-time system (3.32) as in Fig. 3.2 will be absolutely stable if*

$$||M_m N_m + M_s N_s||_\infty < 1 \quad (4.12)$$

where M_m, M_s, N_m and N_s are linear fractional transformations defined as

$$N_m\{s, C_m(e^{sT})\} = \frac{n_p b_s C_m(e^{sT})r(s)}{2b_m b_s + n_p b_s C_m(e^{sT})r(s) + b_m C_s(e^{sT})r(s)}$$

$$N_s\{s, C_s(e^{sT})\} = \frac{b_m C_s(e^{sT})r(s)}{2b_m b_s + n_p b_s C_m(e^{sT})r(s) + b_m C_s(e^{sT})r(s)}$$

$$(4.13)$$

$$M_m\{s, G_m^*\} = -1 + \frac{2b_m}{r(s)}G_m^*(s)$$

$$M_s\{s, G_s^*\} = -1 + \frac{2b_s}{r(s)}G_s^*(s) \qquad (4.14)$$

and

$$r(j\omega) = \frac{T}{2}\frac{e^{-j\omega T} - 1}{1 - cos\omega T} \qquad (4.15)$$

Proof. For the sampled-data teleoperator's absolute stability, it is necessary and sufficient that the closed-loop characteristic equation (4.9) of the teleoperation system has all of its roots in the left half of the complex plane. The definition of absolute stability of a teleoperator assumes that the environment and the operator are passive and, therefore, their impedances are positive real functions. This is what the proof starts with.

In the Nyquist plane, Z_h and Z_e cover the entire right half plane due to their positive realness. Therefore, given that the master and slave robots have positive mass and damping, it is concluded that

$$1/(m_m s + b_m + Z_h(s)) \in \mathfrak{D}\{\frac{1}{2b_m}, \frac{1}{b_m}\} \doteq \mathbb{D}_m$$

$$1/(m_s s + b_s + Z_e(s)) \in \mathfrak{D}\{\frac{1}{2b_s}, \frac{1}{b_s}\} \doteq \mathbb{D}_s \qquad (4.16)$$

where $\mathfrak{D}\{x_1, x_2\}$ is a disk in the Nyquist plane with the center point of $(x_1, 0)$ and the diameter of x_2. The mappings in (4.16) are frequency-independent. Now, (4.16) can be replaced in (4.6) to ultimately determine the regions of G_m^* and G_s^* in (4.8). Because $\mathbb{D}_m$ and $\mathbb{D}_s$ are frequency-independent, they can be moved out of the sum-

mations in (4.8). The regions of G_m^* and G_s^* are, therefore, found as

$$
\begin{aligned}
G_m^* &\in r(j\omega)\mathbb{D}_m \\
G_s^* &\in r(j\omega)\mathbb{D}_s
\end{aligned}
\tag{4.17}
$$

where $r(j\omega)$ is the frequency-dependent part in the summation (4.8) and can be calculated as

$$
r(j\omega) = \frac{1}{T} \sum_{k=-\infty}^{+\infty} \frac{1 - e^{-(j\omega + jk\omega_T)T}}{(j\omega + jk\omega_T)^2}
\tag{4.18}
$$

Then, (4.18) will yield (4.15).

Consequently, the regions covered by G_m^* and G_s^* consist of a frequency-dependent part $r(j\omega)$ as in (4.15) and a frequency-independent part as in (4.16) that is shifted and scaled in the Nyquist plane. The areas in (4.17) can be mapped to the stable unit disc centered at the origin via the following transformations:

$$
\begin{aligned}
-1 + \frac{2b_m}{r(j\omega)} G_m^* &\in \mathfrak{D}\{0,2\} \\
-1 + \frac{2b_s}{r(j\omega)} G_s^* &\in \mathfrak{D}\{0,2\}
\end{aligned}
\tag{4.19}
$$

Based on (4.19), the linear fractional transformations (LFT) defined by M_m and M_s in (4.14) map the regions of G_m^* and G_s^* in (4.17) to two unit discs.

Now, transformations N_m and N_s can be found such that the transformed characteristic equation

$$
1 + M_m N_m + M_s N_s = 0
\tag{4.20}
$$

has the same roots as the original characteristic equation (4.9). To this end, replacing

M_m and M_s from (4.14) into (4.20) leads us to the condition

$$1 + \frac{-r(s) + 2b_m G_m^*}{r(s)} N_m\{s, C_m(e^{sT})\} + \frac{-r(s) + 2b_s G_s^*}{r(s)} N_s\{s, C_s(e^{sT})\}$$
$$= \kappa(1 + n_p C_m G_m^* + C_s G_s^*) \qquad (4.21)$$

Note that (4.21) should be valid for any G_m^* and G_s^* and the coefficient κ should be independent of G_m^* and G_s^*. By solving (4.21), the transformations N_m and N_s can be found as in (4.13). Finally, the small gain theorem provides a sufficient condition for the stability of the characteristic equation (4.20) as given by (4.12) [107].

$\square$

It is to note that the although (4.20) and (4.9) have similar form, they have very different interpretation and applying the small gain theorem on (4.9) gives an involve condition particularly due to the fact that the assumption on positive realness of the terminations will not be used and the it has the unknown models of the environment and the operator are still in the condition.

In Theorem 4.1, transformations M_m and M_s are unit discs in the Nyquist plane. Condition (4.12) is the general condition that the controllers C_m and C_s should meet to ensure that the sampled-data teleoperator is absolutely stable.

To achieve condition (4.12), a sufficient condition is

$$||M_m N_m||_\infty + ||M_s N_s||_\infty < 1. \qquad (4.22)$$

Since M_m and M_s are unit discs in the Nyquist plane, this sufficient condition for absolute stability reduces to

$$||N_m||_\infty + ||N_s||_\infty < 1 \qquad (4.23)$$

By substituting the definitions of N_m and N_s from (4.13) in the above, the sufficient

condition for teleoperator absolute stability becomes

$$\frac{|n_p b_s C_m(e^{j\omega T})r(j\omega)| + |b_m C_s(e^{j\omega T})r(j\omega)|}{|2b_m b_s + b_s n_p C_m(e^{j\omega T})r(j\omega) + b_m C_s(e^{j\omega T})r(j\omega)|} < 1 \tag{4.24}$$

where $r(j\omega)$ is defined in (4.15). Note that (4.24) gives an absolute stability condition that is not tied to any particular controller as long as the teleoperation system complies with PEB control architecture. For known models of the master and the slave robots, any given discrete-time controller can be tested using condition (4.24) to investigate the absolute stability of the sampled-data teleoperator. Also, note that although absolute stability is less conservative than passivity, some new conservativeness have been introduced by finding the stability condition using the small gain theorem.

Next, the communication channel is assumed to have constant delays in transmitting the signals and the absolute stability condition for such case has been derived as follows. The delay for the master side and the slave side are assumed to be independent and potentially different. Without loss of generality it is assumed that the position scaling is unity $n_p = 1$. Furthermore, it is assumed that the delays in the communication channel are integer multiple of the sampling time of the controllers.

Theorem 4.2. *For a position-error-based sample-data teleoperation system with the continuous-time open-loop dynamics (3.32), if there is a delay T_1 in communication path from the master to the slave and a delay T_2 in the opposite direction, the absolute stability condition is*

$$\frac{|D + b_s C_m r| + |D + b_m C_s r| + |D|}{|2b_m b_s C_m C_s + b_s C_m^2 C_s r + b_m C_s^2 C_m r + D|} < 1 \tag{4.25}$$

where

$$D = \frac{r^2(1 - e^{-(T_1+T_2)s})}{2} \tag{4.26}$$

Proof. Substituting the controller laws for the master and the slave into the open-loop

dynamics provides the following closed-loop dynamics for the time-delay sampled-data teleoperation system:

$$F_m^*(s) = C_m(e^{sT})[-G_m^*(s)F_m^*(s) + e^{-sT_2}G_s^*(s)F_s^*(s)]$$
$$F_s^*(s) = C_s(e^{sT})[-e^{-sT_1}G_s^*(s)F_m^*(s) + n_pG_m^*(s)F_s^*(s)]$$

(4.27)

Compared to (4.7) The two new terms e^{-sT_1} and e^{-sT_2} are due to the time delay in the communication channel. In the rest of the proof, the arguments (s) and (e^{sT}) of the transfer functions are omitted. Regrouping the controller outputs, the closed-loop equations can be written as

$$\begin{bmatrix} 1 + C_mG_m^* & -e^{-sT_2}C_mG_s^* \\ -e^{-sT_1}C_sG_m^* & 1 + C_sG_s^* \end{bmatrix} \begin{bmatrix} F_m^* \\ F_s^* \end{bmatrix} = \begin{bmatrix} 0 \\ 0 \end{bmatrix}$$

(4.28)

Similar to the delay-free derivation in (4.16) to (4.20), the absolute stability condition becomes

$$||M_mN_m + M_sN_s + M_mM_sN_d||_\infty < 1$$

(4.29)

where

$$N_m = \frac{r^2(1 - e^{-(T_1+T_2)s}) + 2C_m^2C_srb_s}{4b_mb_sC_mC_s + 2b_srC_m^2C_s + 2b_mrC_s^2C_m + r^2[1 - e^{-(T_1+T_2)s}]}$$

(4.30)

$$N_s = \frac{r^2(1 - e^{-(T_1+T_2)s}) + 2C_s^2C_mrb_m}{4b_mb_sC_mC_s + 2b_srC_m^2C_s + 2b_mrC_s^2C_m + r^2[1 - e^{-(T_1+T_2)s}]}$$

(4.31)

$$N_d = \frac{r^2(1 - e^{-(T_1+T_2)s})}{4b_mb_sC_mC_s + 2b_srC_m^2C_s + 2b_mrC_s^2C_m + r^2[1 - e^{-(T_1+T_2)s}]}$$

(4.32)

Also, M_m and M_s in (4.29) are the same unit discs defined in (4.14). Thus, a sufficient

condition for absolute stability is

$$||N_m||_\infty + ||N_s||_\infty + ||N_d||_\infty < 1 \tag{4.33}$$

Substituting the definitions of N_m, N_s and N_d from (4.30)-(4.32) in (4.33), the absolute stability condition, which is the delayed counterpart of (4.24), becomes what is shown in (4.25). $\qquad\square$

4.4   Special cases

Although condition (4.24) covers all controllers used in the PEB architecture of (4.2), verifying it can be difficult in the general case for arbitrarily controllers. In this section, certain assumptions on the controllers are shown to help to reduce the absolute stability condition (4.24) to useful bounds on the control parameters that make it easier to design stabilizing, high-performance controllers.

4.4.1   Proportionally selected controllers

Condition (4.24) includes both the master and the slave controllers, which can be arbitrarily selected. In practical design, an option is to select the controllers to be proportional to each other:

$$C_s(z) = n_c C_m(z) \tag{4.34}$$

where n_c is an arbitrary positive constant. There is no restriction on the controllers $C_s(z)$ and $C_m(z)$.

Substituting (4.34) into (4.24) results in the following absolute stability condition:

$$\frac{|n_p b_s C_m(e^{j\omega T}) r(j\omega)| + |n_c b_m C_m(e^{j\omega T}) r(j\omega)|}{|2 b_m b_s + b_s n_p C_m(e^{j\omega T}) r(j\omega) + n_c b_m C_m(e^{j\omega T}) r(j\omega)|} < 1 \tag{4.35}$$

Replacing the complex term $C_m(e^{j\omega T})r(j\omega)$ by $p + jq$ in (4.35) gives

$$\frac{n_p b_s \sqrt{p^2 + q^2} + n_c b_m \sqrt{p^2 + q^2}}{\sqrt{(2b_m b_s + n_p b_s p + n_c b_m p)^2 + (n_p b_s q + n_c b_m q)^2}} < 1 \qquad (4.36)$$

which can be further manipulated to conclude the following absolute stability condition:

$$\boxed{\frac{b_m b_s}{n_p b_s + n_c b_m} > -\mathrm{Re}\{C_m(e^{j\omega T})r(j\omega)\}} \qquad (4.37)$$

It should be noted that in (4.37) the ratio of the master and the slave controllers n_c is not necessarily related to the position scaling n_p. This means that (4.37) covers the most general case while certain applications may require specific relationships between the two.

For the sake of simplicity in the following discussion, let us assume that $n_c = n_p = 1$. With this assumption, the absolute stability condition (4.37) becomes

$$\frac{b_m b_s}{b_m + b_s} > -\mathrm{Re}\{C_m(e^{j\omega T})r(j\omega)\} \qquad (4.38)$$

Let us compare the absolute stability condition (4.38) against the passivity condition for a similar sampled-data teleoperator (i.e., when there is no position or controller scaling). As shown in [6], the sampled-data teleoperator passivity conditions are $b_m > -2p$ and $b_s > -2p$ to be satisfied simultaneously. When the robot dampings are equal ($b_m = b_s$), the absolute stability condition (4.38) reduces to $b_m = b_s > -2p$, which is the same as the passivity condition. However, when the dampings are not equal ($b_m \neq b_s$), the absolute stability condition (4.38) allows the dampings to vary as long as they satisfy $1/b_m + 1/b_s < -1/p$ whereas the passivity conditions require each of $1/b_m$ and $1/b_s$ to be less than $-1/(2p)$. In other words, the absolute stability condition is less conservative than the passivity condition under similar circumstances. For instance, as shown in Fig. 4.1, where the slave robot damping violates the passivity condition $b_s > -2p$, the absolute stability condition (4.38) will be satisfied if the

master robot has a high enough damping.
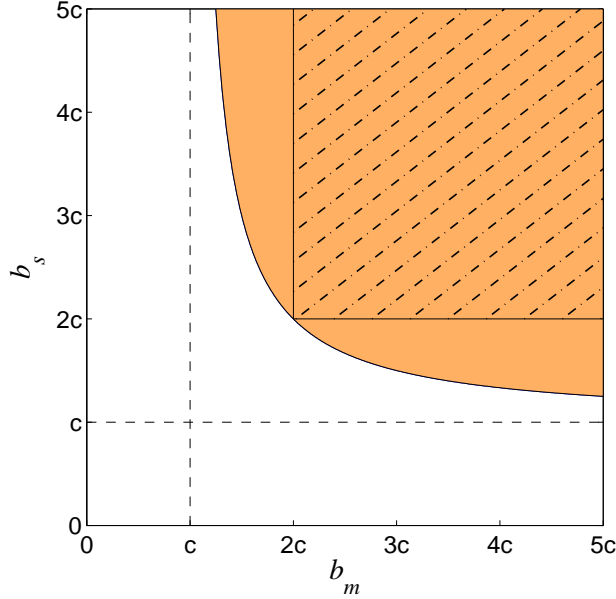
Figure 4.1: Absolute stability and passivity regions in the plane of the master robot damping b_m versus the slave robot damping b_s. Blue shows the absolute stability region and hatched corresponds to the passivity region and c is the right hand side of (4.37).

In another analysis on the absolute stability condition (4.37), consider a micro/macro teleoperation scenario where the slave robot is substantially heavier/larger than the master robot, e.g., the remote manipulation of an excavator robot by a lighter/smaller haptic device. The slave damping is much higher than the master damping ($b_s \gg b_m$), and (4.37) can be approximated as $b_m/n_p > -p$. First, this new condition only puts a lower bound on the master damping as the slave damping is already large enough. Second, the condition will be relieved further if $n_p = x_s/x_m$ is large, which is indeed the case in the tele-excavation application. Conversely, in macro/micro teleoperation, the slave robot has significantly smaller scale and weight than the master robot, implying that the passivity condition lower bounds the damping of the slave robot.

While the above were two illustrative examples, in general the absolute stability condition found in this chapter presents improvements over the passivity condition. First, as described above through an illustrative example, the condition (4.37) allows the master and slave dampings to vary in a more flexible and less conservative manner. Second, the absolute stability condition (4.37) allows to include arbitrary position scaling n_p (and controller scaling n_c) in the system that meet the practical requirements of the task at hand at no cost.

4.4.2 PD controllers

The absolute stability condition (4.37) is valid for all controllers in the position error based structure of (4.2). For a known controller structure, this condition can be further simplified. In the following, a continuous-time PD controller $C_m(s) = K + Bs$ is discretized using the bilinear transformation method to $C_m(z) = K + B(z-1)/Tz$ [90]. Substituting the PD controller in (4.37) yields the following absolute stability condition:

$$\frac{b_m b_s}{n_p b_s + n_c b_m} > \frac{KT}{2} - B \cos \omega T \tag{4.39}$$

Condition (4.39) depends on the frequency ω. Since $\cos \omega T$ varies between -1 and 1, a sufficient condition for absolute stability of the teleoperator over all frequencies will be

$$\frac{b_m b_s}{n_p b_s + n_c b_m} > \frac{KT}{2} + B \tag{4.40}$$

The absolute stability condition (4.40) indicates that the higher the sampling time and the controller gains, the closer the system is to potential instability. In a practical teleoperation system, the robot dampings b_m and b_s are physical characteristics of the robots and are typically fixed. The controller scaling n_c, which in PEB control also reflects the force scaling, and the position scaling n_p and are determined by the physical requirements of the teleoperation system and the task at hand. Typically, the sampling time T is lower bounded as a result of the limited A/D conversion,

D/A conversion, and computation speeds of the control hardware. Therefore, the parameters in (4.40) that can most easily be set are the PD controller gains.

On the other hand, as mentioned in Section 4.1, besides stability the teleoperation control design has to strive for transparency. Higher transparency can be achieved by increasing the controller gains, as shown in the following Remark.

Remark 3. *In a continuous-time PEB teleoperation system, increasing the controller gains will result in a higher teleoperation transparency. Indeed, if the continuous-time counterpart of Fig. 3.2 is modelled in the hybrid matrix form,*

$$
\begin{bmatrix} F_m(s) \\ -V_s(s) \end{bmatrix} = H(s) \begin{bmatrix} V_m(s) \\ F_s(s) \end{bmatrix}
\tag{4.41}
$$

the hybrid matrix $H(s)$ is

$$
H(s) = \begin{bmatrix} Z_m + C_m \frac{Z_s}{Z_s + C_s} & \frac{C_m}{Z_s + C_s} \\ -\frac{C_s}{Z_s + C_s} & \frac{1}{Z_s + C_s} \end{bmatrix}
\tag{4.42}
$$

where $Z_m(s) = m_m s + b_m$ and $Z_s(s) = m_s s + b_s$. For perfect master/slave position and force matching, the transparent hybrid matrix must be

$$
H_{ideal} = \begin{bmatrix} 0 & 1 \\ -1 & 0 \end{bmatrix}
\tag{4.43}
$$

Comparison of (4.42) and (4.43) leads to the fact that increasing the controller gains of C_m and C_s increases teleoperation transparency.

By analogy, in a sampled-data teleoperation system, higher gains will deliver higher transparency. On the other hand, the absolute stability condition (4.40) imposes upper bounds on the controller gains, indicating a tradeoff between transparency and absolute stability. In the next section, these boundaries are tested via experiments designed to get the highest transparency while remaining stable.

4.4.3 Impact of time delay

The absolute stability condition (4.25) for delayed teleoperation systems has been verified for a given teleoperation system. A nominal teleoperation system has been defined to have the system parameters $K = 1000$, $B = 0$, $T = 1^{ms}$ and $b_m = b_s = b = 1$. A stability index has been defined as the left hand side of (4.25) minus one, which should be negative to ensure the absolute stability of the delayed-teleoperation system. The resulting stability index has been plotted against changes in the system parameters, e.g., the controller gain and the time delay. The results have been shown in Fig. 4.2 and 4.3.
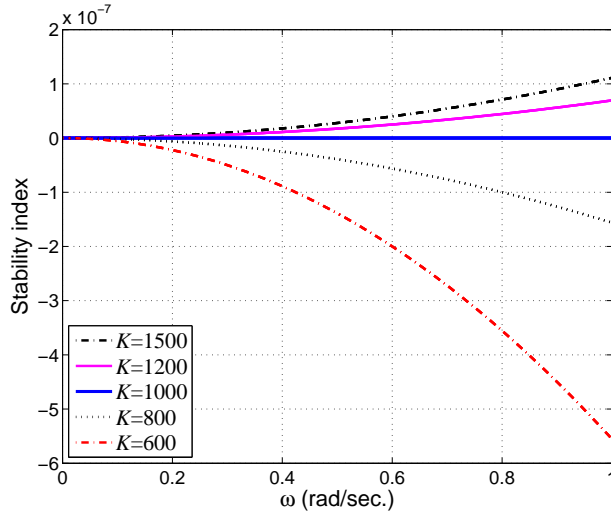
Figure 4.2: Stability index vs. the controller gain when the delays $T_1 = T_2 = 0$. As long as the controller gain K satisfies (4.37), which is $K < 1000$, the stability index remains negative (i.e., the teleoperation system remains absolutely stable).

As depicted in Fig. 4.2, by changing the controller gain in the absence of time delay, the absolute stability of the system is affected. A gain of $K = 1000$ is the border line for stability; lower gains make the stability index negative and the teleoperation system absolutely stable. Fig. 4.3 shows that the delay can cause the stability index to become positive and consequently the teleoperation system not absolutely stable (i.e., potentially unstable). Furthermore, from Fig. 4.3 it is concluded that the
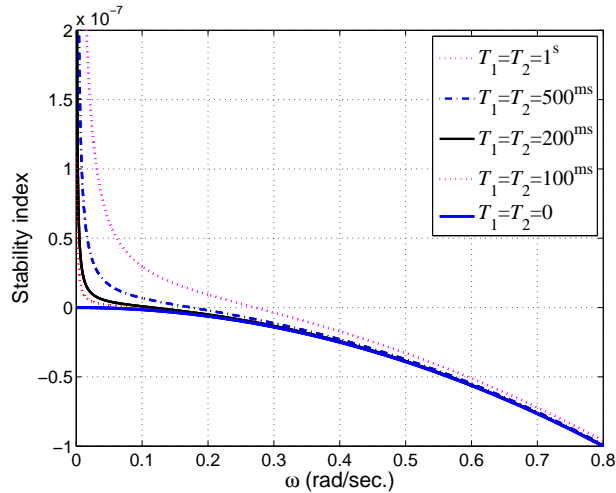
Figure 4.3: Stability index vs. time delay when the controller gain $K = 800$. As long as the delays satisfy (4.25), the stability index remains negative (i.e., the teleoperation system remains absolutely stable).

absolute stability condition is violated for any non-zero delay.

4.5 Experiments on a scaled dual Phantom Omni

To verify the absolute stability condition, an experiment has been set up with two identical Phantom Omni robots from Sensable Technologies, Inc., which are 6-DOF haptic devices with 3 actuated and 3 free-running joints. Out of the three actuated joints of the robot, the first joint that rotates about the vertical is used in the experiment while the second and the third joints that form a parallel mechanism are in locked motion using high-gain controllers. As shown in Fig. 4.4, the operator interacts with the master robot while the slave robot is physically connected via a nonlinear spring to a stiff wall. For simplicity of the picture, in lieu of the physical wall and environment, symbols of the wall and the environment are displayed in Fig. 4.4.

The Phantom Omni robots are connected in daisy chain on a FireWire port and communicate with the same computer. The robots are interfaced with MATLAB
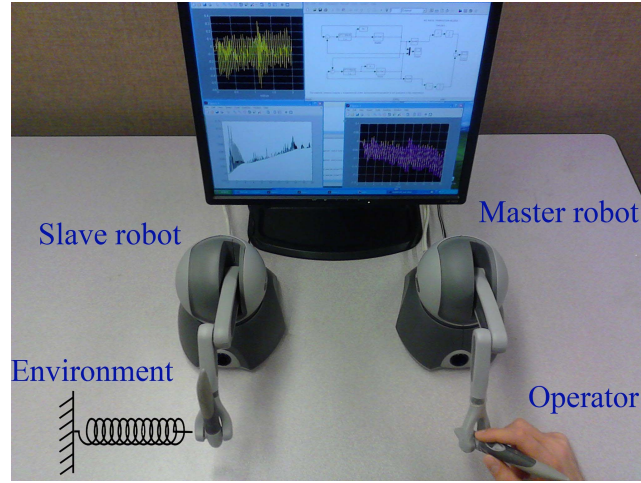
Figure 4.4: Experimental setup – The master arm is controlled by the human operator and the slave arm interacts with its environment.

Simulink®(from Mathworks, Natick, MA, USA) via a pair of QuARC®blocks (from Quanser Inc. Markham, ON, Canada). To have accurate sampling times, the simulation runs in the discrete-time and the sampling time of the Simulink is set to the value given for each experiment. The controller(4.2)has been implemented noting that all of the systems and operations of (4.2) are in discrete-time.

To be able to verify our absolute stability condition, the mass m and damping b of the robots had to be found through grey-box system identification in a separate experiment. The Omni robots were found to have small but non-negligible joint friction. The viscous friction term was lumped in the damping term and the Coulomb friction term was identified and feed-forward compensated in the controller. The values of the mass (inertia, as it corresponds to rotational motion) and the total damping were found to be $m = 1.503 \times 10^{-2} \pm 1.7 \times 10^{-4} \text{Kg.m}^2$ and $b = 4.624 \times 10^{-2} \pm 1.1 \times 10^{-3} \text{Kg.m}^2/\text{s}$. Also, in a separate experiment, the static model of the nonlinear spring acting as the slave environment was found. The experiment confirmed that the spring was a passive system due to non-negative dissipated energy.

Two series of experiment were conducted to verify the validity and accuracy of the theoretical absolute stability condition (4.40) for different scaling and controller

ratio values. In the first set, it is assumed that the position scaling and the controller ratio are $n_c = n_p = 1$, while in the second set $n_p = n_c = 3$. The absolute stability regions are shown in Fig. 4.5 and Fig. 4.6 with the above scaling factors. In each experiment, the controller gains, the sampling time, and the scaling factors are set to constant values and the master is manipulated by the human operator while the slave robot is interacting with the environment. Based on the given set of parameters and condition (4.40), a particular experiment will be expected from theory to lie in one of the absolute stability or potential instability regions in Fig. 4.5 and Fig. 4.6. In practice, as the operator derives the teleoperator, if the master and slave positions become unbounded or indefinitely oscillating, the teleoperation system judged to be unstable – such unstable experiments are marked by circles in Fig. 4.5 and Fig. 4.6. On the other hand, if the positions remain bounded, the teleoperation system is judged to be stable – such stable experiments are marked by stars in Fig. 4.5 and Fig. 4.6. It is expected that all of the experimentally-obtained circles must lie in the theoretically-arrived potential instability region. However, the stars may lie in either the absolute stability region or the potential instability region because it is possible to have a potentially unstable teleoperator that, when coupled to certain human operator and environment couplings, results in a stable teleoperation system.

It was theoretically argued in Remark 3 higher control gains result in a higher transparency of the teleoperation system. In a scaled teleoperation system, transparency requires the ratio of the positions to be n_p as described in (4.3) and, in the context of position error based control, the ratio of the forces to be n_c as in (4.34). Using the sampled-data teleoperation system, various controller gains were experimentally tested with the results shown in Fig. 4.7. For the fixed sampling time T=4 ms and the scaling factors $n_c = n_p = 3$, and $B = 0$, the controller gain K changed from 0.5 to 4.5. In each experiment, the operator moved the master while the slave was in free space. For simplicity of comparison of the position signals in the plots, the slave position has been scaled down by n_p. The mean square value of the
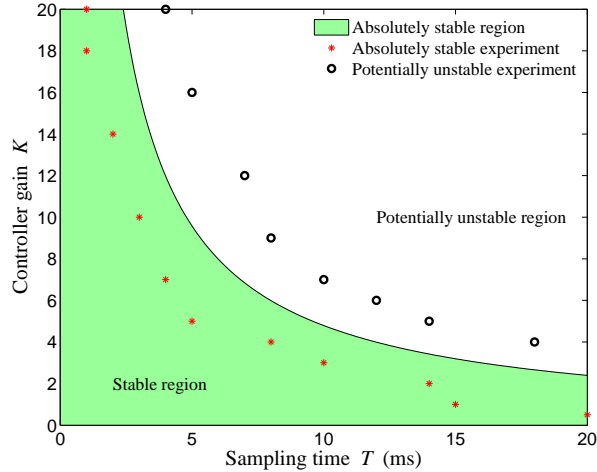
Figure 4.5: The theoretical absolute stability region in $K - T$ plane versus experimental data points obtained from a sampled-data teleoperator with $n_c = n_p = 1$.

position tracking error has been computed as a measure of the transparency of the teleoperation system. Provided that the sampling time T and the control gain K are in the absolute stability region of Fig. 4.6, increasing the controller gain decreases the mean square error, confirming that higher controller gains result in higher transparency. In Fig. 4.7-f, it is seen that the pair of (T, K) happens to be outside of the absolutely stable region of Fig. 4.6 and, consequently, having a higher controller gain did not result in higher transparency; instead the system became unstable. Thus, while absolute stability puts an upper bound on the control gains, obtaining good transparency will impose lower bounds on them. These emphasize the importance of the tradeoff between the stability and transparency of a teleoperation system.

In the experimental results of Fig. 4.8, examples of stable and unstable systems have been demonstrated when the sampling time increased from 2 ms to 6 ms. In this experiment, the scaling factors were $n_c = n_p = 3$ and the controller gain was $K = 4$. While the slave robot is in free space, the operator initially moved the master robot and then released it. As shown in Fig. 4.8, the positions of the master and the slave converge for $T = 2$ ms, which satisfies (4.37), while they oscillate indefinitely after the operator releases the master for $T = 6$ ms, which violates (4.37).

71
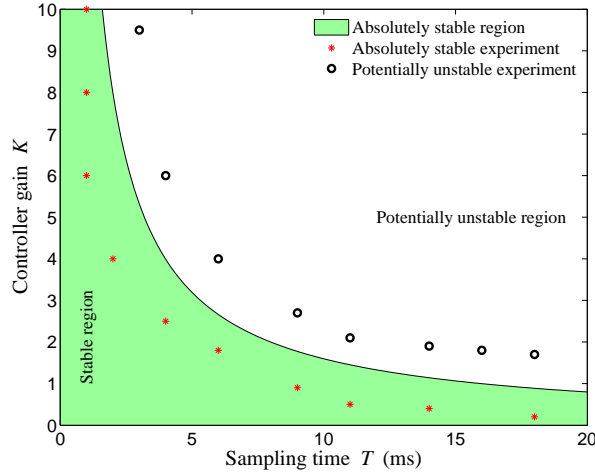
Figure 4.6: The theoretical absolute stability region in $K - T$ plane versus experimental data points obtained from a sampled-data teleoperator with $n_c = n_p = 3$.

4.6 Case study: effect of sampling time on system absolute stability and task performance in teleoperated flipping of a switch

To demonstrate the coupling between the absolute stability bound in (4.37) and the performance of a task carried out through a sampled-data teleoperation system, a task is considered in which a three-way slide switch is flipped by the operator. Trying to accomplish this task with a sampling time of 17 ms for the discrete-time teleoperation controller, experimental trials showed that the controller gains needed to be higher than the maximum value allowed by the stability bound in (4.37), which is not allowed. By reducing the sampling time, it is possible to increase the stability margin (i.e., the maximum admissible controller gain obtained from (4.37) and make it possible for the operator to perform the task successfully. In the following, the details of the task process and the effect of the sampling time on the system absolute stability and the operator task performance will be elaborated.

Fig. 4.9 shows a three-way slide switch. The objective of the task is to flip the
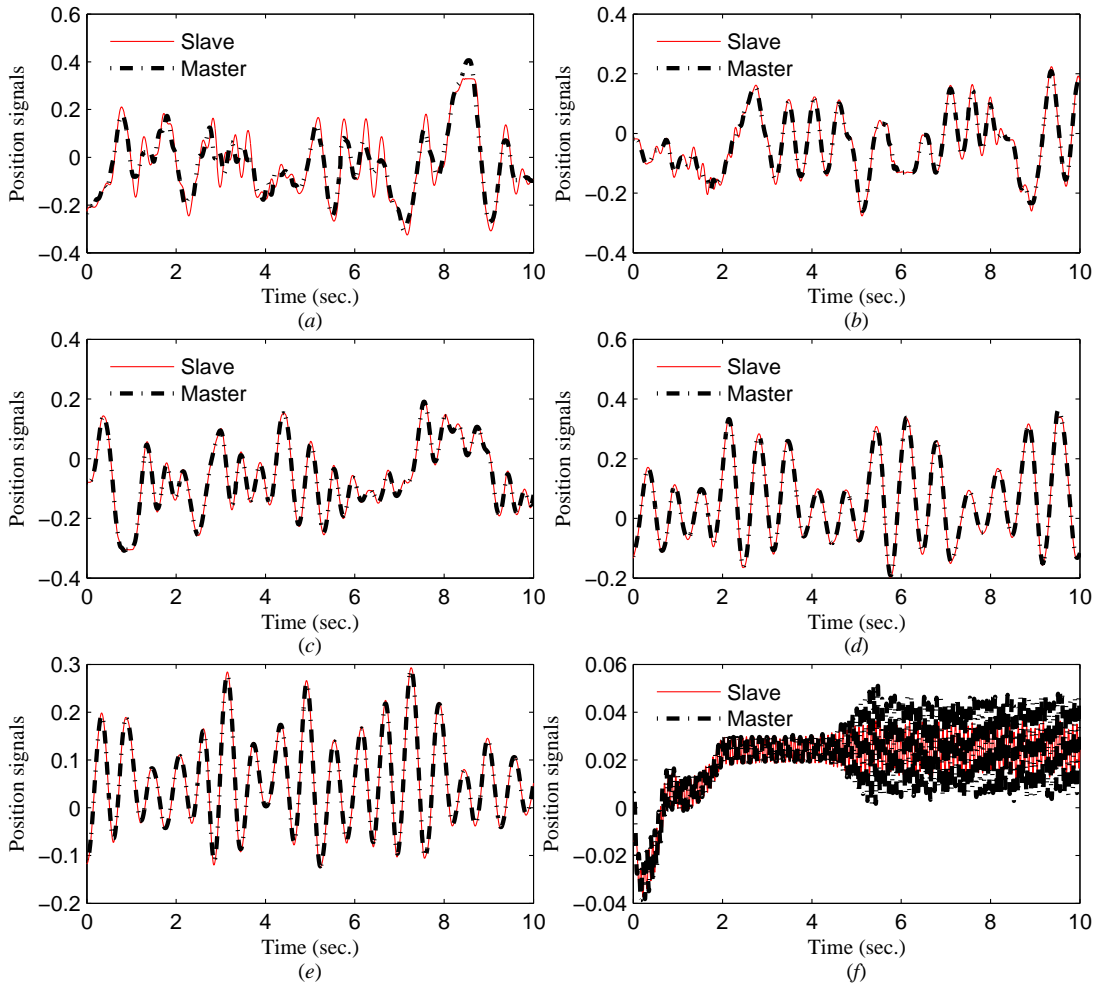
Figure 4.7: The positions of the master and the slave when the operator moved the master and the slave was in free space. The proportional controller gain was $K = 0.5$, $K = 1.5$, $K = 2.5$, $K = 3$, $K = 3.5$ and $K = 4.5$ for parts (a) to (f), respectively. The means of absolute value of the tracking errors are 2.20×10^{-3}, 1.59×10^{-4}, 2.86×10^{-5}, 2.43×10^{-5}, 1.22×10^{-5} and 2.59×10^{-4} rad, respectively.
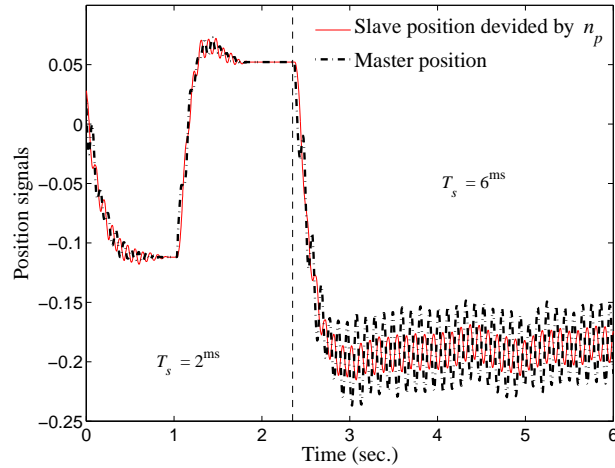
Figure 4.8: The position of the master and slave. The sampling time is $T = 2^{\text{ms}}$ in $0 < t \le 2.35^{ms}$ and $T = 6^{\text{ms}}$ in $2.35 < t < 6^{ms}$.
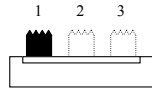
Figure 4.9: A three-way slide switch where the objective of the task is to flip it from state 1 to state 2 but not to state 3.

switch using the teleoperation system from state 1 to state 2 but not to state 3. For the operator to perform the task successfully, the teleoperation controller should ensure that the master/slave position tracking error is less than the position difference between states 2 and 3 of the switch. Such a small position error can only be reached when the teleoperation controller gains are selected sufficiently large (in general, large gains correspond to high teleoperation transparency). Increasing the controller gain, however, jeopardizes the system stability as the sampling time-dependent bound given in (4.37) indicates. However, by decreasing the sampling time one can always increase the stability margin of the system such that the admissible control gains are large enough to ensure satisfactory task performance. Otherwise, for a given sampling time, it may or may not be possible to achieve the required transparency while maintaining stability.

To demonstrate the above, a set of experiments is conducted on a teleoperation
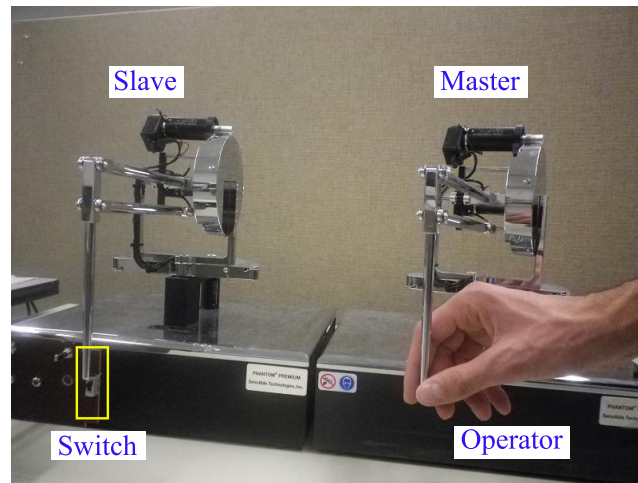
Figure 4.10: The experimental setup for flipping the three-way slide switch.

system consisting of two Phantom Premium haptic devices (Sensable Technologies, Inc., Wilmington, MA, USA) for flipping the three-way slide switch 4.10. Initially, the sampling time is set to 17 ms. It is observed that a proportional gain of 3 (for the master and the slave controllers) stabilizes the system but the user cannot successfully teleoperate the switch, failing to flip the switch from state 1 to state 2 without going to state 3. This phenomenon is caused by the relatively low control gain for the slave robot, which results in the accumulation of control actions (forces) until the position error builds up to a large enough threshold at which the slave control action can overcome the switch stiction. Increasing the controller gain from 3 to 5 for the same sampling time makes the teleoperation system unstable; it will be shown that a controller gain of 5 is large enough to ensure good transparency and satisfactory performance of the task, if the sampling time can be lowered. Thus, the only way to achieve the desired transparency is to decrease the sampling time as shown in Fig. 4.11.

The vertical axis in Fig. 4.11 shows the controller gain, which has a direct relationship to teleoperation transparency and operator task performance. The horizontal axis is the sampling time of the discrete-time controller. A transparency boundary exists in the form of a nearly horizontal line in this plane, above which the controller

75
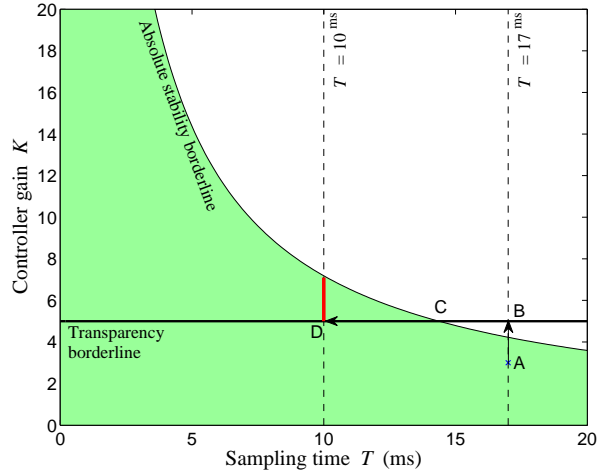
Figure 4.11: Transparency and absolute stability of the switching task. Point A corresponds to an absolutely stable but non-transparent teleoperation system, Point B corresponds to an unstable teleoperation system in which the controller gain meets the transparency requirement, Point C corresponds a teleoperation system with the largest sampling time satisfying both transparency and absolute stability conditions, and Point D corresponds to an absolutely stable and transparent teleoperation system

gains are high enough to ensure that the operator can correctly flip the switch. The absolute stability boundary of (4.37) is also shown as a curved line below which the controller gain is low enough to ensure the absolute stability. The dashed vertical line indicates a fixed sampling time, typically upper bounded by hardware limitations in the experimental setup. For our system with the sampling time of 17 ms, the vertical line is at a location where there is no overlap between the transparent and the absolutely stable segments of the dashed vertical line. Consequently, with the given sampling time, there is no choice for the controller gain to be stable and concurrently satisfy the transparency requirement. As the vertical line for the sampling time moves to the left, it reaches a point (at about 14.5 ms) where stability and transparency are simultaneously met, corresponding to the maximum allowed sampling time and the minimum allowed gain for the controller (point C in Fig. 4.11). As the vertical line moves further to the left, there is a segment of the line that sits below the absolute stability borderline and above the transparency borderline. By moving

to smaller sampling times, this segment of the vertical line expands, allowing us to achieve higher transparencies (by going to higher control gains without jeopardizing the stability). The above example illustrates that increasing the transparency while preserving the stability will be made possible by a reduction in the sampling time.

4.7 Conclusions and future work

In this chapter, a condition for absolute stability of a position error based, sampled-data, scaled teleoperation system has been found using the small gain theorem. The proposed analysis takes into account the exact models of the discretization components such as the zero-order-hold and the sampler. Instead of requiring the passivity of the teleoperator (i.e., the teleoperation system excluding the operator and the environment), absolute stability is merely concerned with the closed-loop stability of the teleoperation system having assumed the passivity of the environment and the human operator, and is less conservative than passivity. Unlike passivity, the absolute stability of a teleoperator allows the teleoperator to be non-passive and involve arbitrary scaling of position and/or force.

The derived absolute stability condition has been simplified for certain controller structures, arriving at bounds on the controller parameters, the sampling time, the master and the slave robot dampings, and the position and force scaling factors. The conditions have been verified in a set of experiments using a dual Phantom Omni teleoperation system. For future work, the condition will be extended to sampled-data scaled teleoperation systems that use the 4-channel control architectures, and when there is time delay in the communication channel between the master and the slave.

Chapter 5

Stability of Teleoperation Systems under Non-passive and Strictly-passive Operator and Environment [1]

5.1 Introduction

Stability analysis of a bilateral teleoperation system is challenging due to two typically unknown elements in its two ends: the human operator and the environment [69, 108, 109]. For analysis of stability, a teleoperation system is typically modeled as a two-port network teleoperator connected to the two one-port network terminations as shown in Fig. 5.1-a, where the teleoperator comprises the master, the slave, their controllers, and the communication channel and the terminations are the human operator and the environment (see Section 2.4.2). By definition, absolute stability

---

[1]This chapter has been submitted to the IEEE Transactions on Control Systems Technology [11]. Parts of this chapter have been presented in the 2012 IEEE/RSJ International Conference on Intelligent Robots and Systems, Vilamoura, Portugal [9]. Also parts of this chapter will be presented in two papers in the 2013 IEEE World Haptics Conference in Daejeon, Korea, 2013 [10, 12].

of a two-port network will guarantee the stability of the coupled system resulting from connecting the two-port network to two passive but otherwise arbitrary one-port network terminations. Equivalently, two-port network absolute stability requires that the driving-point impedance seen at one of the ports is passive when the other port is terminated to a passive one-port network (Fig. 5.1-b) [71]. Therefore, the notion of absolute stability has been applied to the stability analysis of coupled two-port networks with limited information about the terminations.
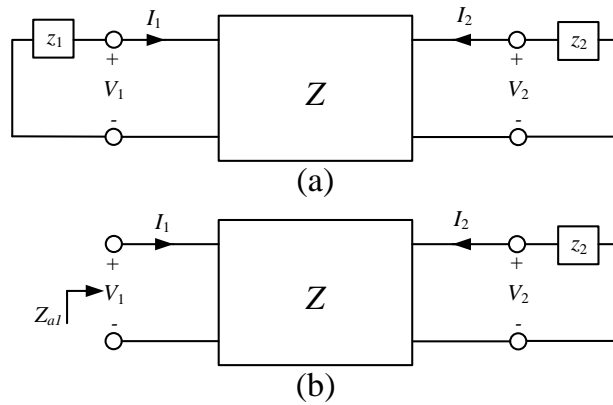
Figure 5.1: (a) A two-port network connected to two one-port network terminations, and (b) the driving-point impedance at port 1, $Z_{a1} = V_1/I_1$, when port 2 is terminated to a passive impedance z_2.

5.1.1 Llewellyn's absolute stability criterion

For stability analysis of a bilateral teleoperation system, sometimes the passivity of the teleoperator is investigated [97, 110, 2, 98], which is sufficient for its absolute stability [71] (see Section 2.4.3). The teleoperator's absolute stability is a less conservative condition compared to its passivity (see Section 2.4.4). Due to stability-transparency trade-offs in a bilateral teleoperation system, minimizing conservatism in stability analysis is important [66, 111, 112].

A well-known absolute stability criterion for two-port networks was proposed by Llewellyn [113] and applied to bilateral teleoperators [114, 115, 116]. Llewellyn's

absolute stability criterion gives closed-form conditions involving the immittance (impedance, admittance, hybrid, and transmission [117]) parameters of a two-port network for it to be absolutely stable [71, 118].

5.1.2 Assumption on termination passivity

Llewellyn's absolute stability criterion requires both of the terminations of the two-port network to be passive. Passivity of a linear time-invariant (LTI) system is equivalent to the positive-realness of its input-output relationship in the frequency domain (transfer function or impedance in the context of this thesis) [119]. Equivalently, a passive LTI system has an impedance with its Nyquist diagram entirely in the right half of the complex plane (RHP).

Expecting the passivity of both of the terminations of a teleoperation system can be unrealistic and overly restrictive in some applications (see Section 2.6). A two-port network's termination may simply be non-passive. On the other hand, a termination can be strictly-passive. Later in the chapter, we will discuss specific examples of such terminations for bilateral teleoperation systems. In this chapter, a powerful tool is developed for stability analysis of a two-port network coupled to a passive termination and a non-passive or strictly-passive termination with certain constraints on the termination's impedance.

Interestingly, to have a stable coupled system, it suffices if, after terminating the two-port network to a one-port network that is not necessarily passive, the driving-point impedance seen at the remaining (i.e., open) port is passive. This is because connecting a passive termination at the currently open port of this two-port network will inevitably result in a passive and thus stable system even though the opposite port might have been connected to a non-passive termination. As we will see later, this can be explained by the concepts of excess of passivity (EOP) and shortage of passivity (SOP) for feedback-interconnected systems. Briefly, when two systems are connected in a negative feedback loop, the stability of the interconnected system is

guaranteed if both systems are passive. If one of the system has EOP, the other system may have SOP without risking the instability of the interconnected system [79].

5.1.3   Leveraging termination knowledge in stability analysis

Utilizing knowledge about a termination in the analysis of stability of a coupled two-port network has been increasingly investigated by researchers. For instance, knowing a lower or upper bound on the impedance of a termination helps to model the termination as an arbitrary impedance coupled to a series or shunt impedance, respectively [115, 120]. In another work, notion of bounded impedance absolute stability (BIAS) is applied to a teleoperation system in the scattering domain and the resulted stability conditions are expressed as bounds on the reflection coefficients [121]. The teleoperation system can be modeled in the integral quadratic constraints (IQC) formulation to reestablish stability conditions with known bounds on the termination [122]. Also, recent work shows that conventional absolute stability criteria can be extended to strictly-passive [9] and non-passive terminations [10].

5.1.4   Examples of non-passive and strictly-passive terminations

For a human operator, non-passivity may occur in many cases. On the other hand, a typical environment may be strictly-passive in many applications. Examples of these are given below.

Let us consider an example of a non-passive termination in a master-slave teleoperation system. When the master is manipulated by a human operator, the operator is typically assumed to be passive. This assumption is valid for tasks that involve a relaxed arm such as sensing (or relaxed grasp) tasks [73, 12]. However, the human operator is non-passive in many other practical cases including in posture-maintenance

(i.e., rigid grasp) tasks [12] or trajectory following tasks [10]. This is intuitively understood by considering a teleoperator that has been designed to be passive. The interconnection of this passive teleoperator and a passive environment will be passive [107]. Therefore, the only source of net energy in the system can be the human operator. If the human operator is also passive, no active motion can exist in the system. Thus, the human operator must be generating energy, e.g., when following a trajectory. Another example of a non-passive termination in a teleoperation system is a non-passive environment. This happens when external forces enable the environment to do work on the teleoperator. For example, a beating heart in a surgical teleoperation system is an environment that emits energy. In another example, let us consider a teleoperation system with a strictly-passive termination. A mass-spring-damper system is output strictly-passive with excess of passivity equal to the system damping. In general, in the presence of viscous friction (i.e., damping) an otherwise passive environment becomes strictly-passive.

5.1.5 Methodology

In this chapter, a stability analysis tool is developed to investigate the stability of a two-port network coupled to a passive termination and either (a) a strictly-passive termination or (b) a non-passive termination. Llewellyn's absolute stability criterion is derived as a special case of the proposed stability criterion. While a passive impedance has a Nyquist diagram in the RHP, the Nyquist diagram of a strictly-passive impedance is placed only in a subset of the RHP. Conversely, the Nyquist diagram of a non-passive impedance trespasses the jω-axis and into the left half of the complex plane (LHP).

Input strictly-passive (ISP) and output strictly-passive (OSP) systems have Nyquist diagrams inside a right-shifted RHP and a disc to the right of and tangent to the origin, respectively [123, 124]. The borderlines of these regions are expressed by lines or circles in the complex plane. Similar to ISP and OSP systems, their non-passive

counterparts are defined as input non-passive (INP) and output non-passive (ONP) systems with Nyquist diagrams inside a left-shifted RHP and a disc to the left of and tangent to the origin, respectively. Since the notion of ONP does not correspond to useful physical systems, a more useful alternative is defined as a disc-like non-passive (DNP) system whose Nyquist diagram is placed inside a disc centered at the origin. The stability criterion proposed in this chapter applies to a two-port network connected to a passive termination and to another termination that is ISP, OSP, INP or DNP.

5.1.6 Advantages of the proposed stability criterion

Taking into account the SOP of a non-passive termination as proposed in this chapter will allow to predict the potential instability of a coupled two-port network where the conventional absolute stability conditions fails to do so. Also, the proposed stability criterion will help ensure the stability of a coupled two-port network terminated to a non-passive termination by choosing the controllers gains in a more stringent fashion compared to the conventional absolute stability condition. On the other hand, taking into account the EOP of a strictly-passive termination as proposed in this chapter will enable us to reduce conservatism in controller design and potentially enhance teleoperation performance compared to when the conventional absolute stability condition is used. In fact, strict-passivity of the terminations allows having a non-passive teleoperator while preserving coupled stability, which can help to improve performance.

5.1.7 Organization of the chapter

The chapter is organized as follows. First, mathematical background and definitions are presented in Section 5.2. In Section 5.3, Mobius transformations of regions in the complex plane are applied to find stability condition when a termination is ISP, OSP, INP, or DNP. While the results of Section 5.3 are applicable to any two-port

network, an important application of the new conditions is in bilateral teleoperation systems discussed in Section 5.4. A simulation study for a teleoperation system is presented in Section 5.5. In Section 5.6, the experimental results are presented for a teleoperation system. Finally, concluding remarks and future work are presented in Section 5.7.

5.2   Mathematical preliminaries

This section includes definitions and prerequisite theories that are used in the subsequent sections. Notions of passivity, absolute stability, positive realness, and strict-passivity are defined below. In the thesis, all the units are in SI unless specified otherwise.

Notation:

- **A**, a and $A(s)$ denote a matrix, a scalar and a variable in Laplace domain, respectively. Complex conjugate of a is denoted by $\bar{a}$.

- A circle in the complex plane is expressed as $\mathcal{C}(r, c)$, where $r \in \mathbb{R}$ is the radius and $c \in \mathbb{C}$ is the centre of the circle. The area inside this circle is denoted by the disc $\mathcal{D}(r, c)$.

Assumptions:

- The dynamics of the master and slave robots are LTI and known [2].

- The dynamics of the environment are LTI but not necessarily known. The human arm dynamics can be approximated with an LTI model [12].

- The communication link between the master and the slave has negligible time-delay.

---

[2]Feedback linearization (inverse dynamics) approach is used to make an internal loop which results in an LTI and decoupled approximation of the nonlinear and coupled dynamics the robot [125, 126].

5.2.1 Definitions of passivity and absolute stability

Definition 5.1. *[123, 79] A system with input $u(.)$ and output $y(.)$ where $u(t), y(t) \in \mathbb{R}^m$ is passive if there is a constant β such that*

$$\int_0^t y^T(\tau)u(\tau)d\tau \geq -\beta \tag{5.1}$$

for all functions $u(.)$ and all $t \geq 0$. The constant β is the energy stored in the system at time $t = 0$.

Definition 5.2. *[123, 127] A system with input $u(.)$ and output $y(.)$ where $u(t), y(t) \in \mathbb{R}^m$ is ISP if there are constants β and $\delta > 0$ such that*

$$\int_0^t y^T(\tau)u(\tau)d\tau \geq -\beta + \delta \int_0^t u^T(\tau)u(\tau)d\tau \tag{5.2}$$

for all functions $u(.)$ and all $t \geq 0$. The value δ is the EOP for the ISP system.

Definition 5.3. *[123] A system with input $u(.)$ and output $y(.)$ where $u(t), y(t) \in \mathbb{R}^m$ is OSP if there are constants β and $\epsilon > 0$ such that*

$$\int_0^t y^T(\tau)u(\tau)d\tau \geq -\beta + \epsilon \int_0^t y^T(\tau)y(\tau)d\tau \tag{5.3}$$

for all functions $u(.)$ and all $t \geq 0$. The value ϵ is the EOP for the OSP system.

Definition 5.4. *A system at initial rest with input $u(.)$ and output $y(.)$ where $u(t), y(t) \in \mathbb{R}^m$ is INP if there is constant $\eta > 0$ such that*

$$\int_0^t y^T(\tau)u(\tau)d\tau \geq -\eta \int_0^t u^T(\tau)u(\tau)d\tau \tag{5.4}$$

for all functions $u(.)$ and all $t \geq 0$. The value η is the SOP for the INP system.

Definition 5.5. *A system at initial rest with input $u(.)$ and output $y(.)$ where $u(t), y(t) \in$*

$\mathbb{R}^m$ *is ONP if there is constant $\upsilon > 0$ such that*

$$\int_0^t y^T(\tau)u(\tau)d\tau \geq -\upsilon \int_0^t y^T(\tau)y(\tau)d\tau \tag{5.5}$$

for all functions $u(.)$ and all $t \geq 0$. The value υ is the SOP for the ONP system.

Instead of ONP systems in Definition 5.5, we define a more useful class corresponding to DNP systems as below.

Definition 5.6. *An LTI system $G(s)$ is DNP with SOP of ρ if $|G(j\omega)| \leq 1/2\rho$.*

Definition 5.7. *[128] A $p \times p$ proper rational transfer function matrix $G(s)$ is positive real if*

- *all poles of all elements of $G(s)$ meet $\mathrm{Re}\{s\} \leq 0$,*

- *any pure imaginary pole $j\omega$ of any element of $G(s)$ is a simple pole and the residue matrix $\lim_{s \to \infty}(s - j\omega)G(s)$ is positive semidefinite Hermitian.*

- *for all real ω for which $j\omega$ is not a pole of any element of $G(s)$, the matrix $G(j\omega) + G^T(-j\omega)$ is positive semidefinite.*

5.2.2 Lemmas of passivity and absolute stability

For a scalar rational transfer function, the last part of Definition 5.7 reduces to $\mathrm{Re}G(j\omega) \geq 0$. The following lemma establishes the connection between passivity of a transfer function and the region covered by its Nyquist diagram in the complex plane.

Lemma 5.1. *[123, 129] Consider an LTI rational transfer function $G(s)$. Assume that all poles of $G(s)$ have negative real parts. The system is passive if and only if $\mathrm{Re}G(j\omega) \geq 0$ for all frequencies ω (Fig. 5.2-a).*

Similarly, Lemmas 5.2-5.3 below make the connection between EOP of ISP and OSP systems to the corresponding Nyquist diagram regions in the complex plane.
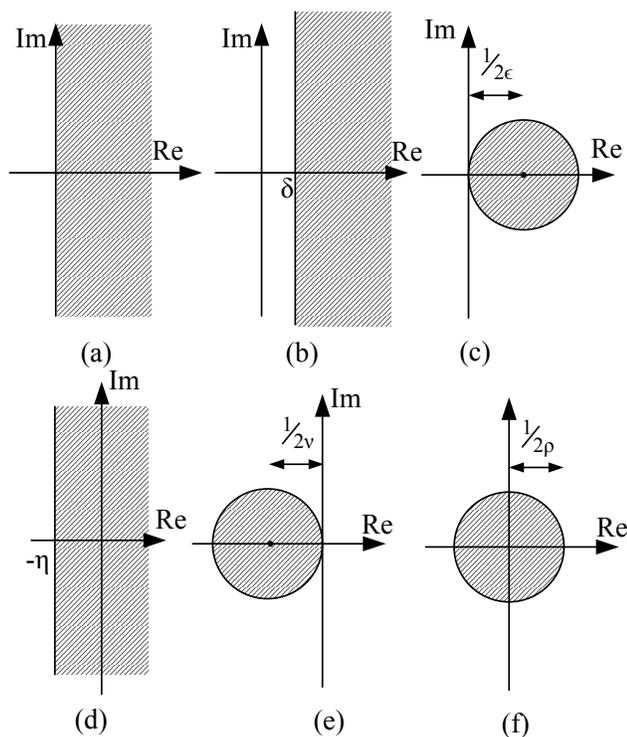
Figure 5.2: Nyquist diagrams of (a) a passive system, (b) an ISP system with EOP of δ, (c) an OSP system with EOP of ϵ, (d) an INP system with SOP of η, (e) an ONP system with SOP of υ, (f) a DNP system with SOP of ρ.

Lemma 5.2. *[123] Consider an LTI rational transfer function $G(s)$. Assume that all poles of $G(s)$ have negative real parts. The system is ISP with EOP of δ if and only if $\mathrm{Re}\,G(j\omega) \geq \delta$ for all frequencies ω (Fig. 5.2-b).*

Lemma 5.3. *[123] Consider an LTI rational transfer function $G(s)$. Assume that all poles of $G(s)$ have negative real parts. The system is OSP with EOP of ϵ if and only if the Nyquist diagram of $G(j\omega)$ is contained in the disc $\mathcal{D}(1/(2\epsilon), 1/(2\epsilon))$ for all frequencies ω (Fig. 5.2-c), i.e., $\mathrm{Re}\,G(j\omega) \geq \epsilon|G(j\omega)|^2$.*

Dual to the EOP of an ISP system (Lemma 5.2), we can relate the SOP of an INP system to its Nyquist diagram region. For example, if $G(s)$ is an INP system with SOP of η, then $\mathrm{Re}\,G(j\omega) \geq -\eta$ (Fig. 5.2-d).

Passivity has been vastly used in the teleoperation literature to ensure stability.

The connection between passivity and absolute stability is made via the following lemma.

Lemma 5.4. *A two-port network is absolutely stable if and only if for any passive but otherwise arbitrary termination of a port, the driving-point impedance at the other port is passive.*

Lemma 5.5. *In the complex plane of z, a line and a circle are expressed by the following unified formulation:*

$$Az\bar{z} + \bar{B}z + B\bar{z} + C = 0 \tag{5.6}$$

where A, B and C are scalar complex numbers, i.e., $A, B, C \in \mathbb{C}$. If $A = 0$, (5.6) reduces to the equation of a line. If $A \neq 0$, (5.6) expresses the following circle [130]:

$$\mathcal{C}(\frac{\sqrt{|B|^2 - AC}}{|A|}, -B/A) \tag{5.7}$$

5.3 Stability of two-port network with non-passive or strictly-passive terminations

Mappings of the regions in the impedance plane are introduced in Section 5.3.1. In Section 5.3.2 and Section 5.3.3, these mappings will be applied to find stability conditions for a two-port network with a non-passive and strictly-passive terminations, respectively.

5.3.1 Mapping of regions via Mobius transformation

A two-port network is expressed by its impedance Z matrix as

$$\begin{bmatrix} V_1(s) \\ V_2(s) \end{bmatrix} = \begin{bmatrix} Z_{11}(s) & Z_{12}(s) \\ Z_{21}(s) & Z_{22}(s) \end{bmatrix} \begin{bmatrix} I_1(s) \\ I_2(s) \end{bmatrix} \tag{5.8}$$

where the pairs (V_1, V_2) and (I_1, I_2) denote the voltages and currents at the two terminals. When port 2 is connected to a termination with impedance z_2 (Fig. 5.1-b), the driving-point impedance Z_{a1} at port 1 is expressed as

$$Z_{a1} = Z_{11} - \frac{Z_{12}Z_{21}}{Z_{22} + z_2} = \frac{z_2(Z_{11}) + (Z_{11}Z_{22} - Z_{12}Z_{21})}{z_2 + (Z_{22})} \tag{5.9}$$

In the following, the result of mapping two general areas representing the impedance z_2 – a rectangle and a disk – will be found in the Z_{a1} impedance plane.

5.3.1.1 Mapping of a rectangular impedance via Mobius transformation

In order to investigate the stability of a two-port network with ISP or INP terminations, we introduce the following theorem to study the mappings of such terminations.

Theorem 5.1. *Suppose that the termination z_2 has a rectangular shape in the complex impedance plane, namely $-a \leq \mathrm{Re} z_2 \leq b$, $-d \leq \mathrm{Im} z_2 \leq c$ as shown in Fig. 5.8-a. This region in the z_2 plane is mapped by the Mobius transformation (5.9) to a crescent-like region in the Z_{a1} plane defined by the outer circle*

$$\mathcal{C}\left(\frac{|Z_{12}Z_{21}|}{2(R_{22} - a)}, Z_{11} - \frac{Z_{12}Z_{21}}{2(R_{22} - a)}\right) \tag{5.10}$$

and the inner circle

$$\mathcal{C}\left(\frac{|Z_{12}Z_{21}|}{2(R_{22} + b)}, Z_{11} - \frac{Z_{12}Z_{21}}{2(R_{22} + b)}\right) \tag{5.11}$$

after excluding the following two discs:

$$\mathcal{D}\left(\frac{|Z_{12}Z_{21}|}{2c + 2I_{22}}, \frac{Z_{11} + jZ_{12}Z_{21}}{2c + 2I_{22}}\right) \tag{5.12}$$

$$\mathcal{D}\left(\frac{|Z_{12}Z_{21}|}{2d + 2I_{22}}, \frac{Z_{11} + jZ_{12}Z_{21}}{-2d + 2I_{22}}\right) \tag{5.13}$$

$\square$

Proof. The rectangular shape in the z_2 plane (Fig. 5.8-a) consists of four lines of $\text{Re}z_2 = -a$, $\text{Re}z_2 = b$, $\text{Im}z_2 = c$ and $\text{Im}z_2 = -d$. Each of these four lines will be transformed to a circle in the Z_{a1} plane. In the following, in Step 1 the mapping of the vertical line $\text{Re}z_2 = -a$ is found to be (5.10). Then, in Step 2, the mapping of the vertical line of $\text{Re}z_2 = b$ is found and it is shown to be inside and tangent to the circle of (5.10). Finally, in Step 3 the mappings of the two horizontal lines are found and the region inside the rectangles is transformed.

Step 1:

Let us consider the vertical line of $\text{Re}z_2 = -a$. The Mobius transformation (5.9) from z_2 plane into Z_{a1} plane is split to three transformations, namely a linear transformation ($\zeta_1 = z_2 + Z_{22}$), an inversion ($\zeta_2 = 1/\zeta_1$) and another linear transformation ($\zeta_3 = Z_{11} - Z_{12}Z_{21}\zeta_2$) [130].

The three transformations are considered separately:

1. The first transformation is a linear transformation as $\zeta_1 = z_2 + Z_{22}$ that translates the LHP to the right side by the real part of Z_{22}, i.e. $R_{22} - a$ (Fig. 5.3-b). The resulting line is expressed as $\text{Re}\{\zeta_1\} = (R_{22} - a)$, which can be converted to the general circle/line formulation as $\zeta_1 + \bar{\zeta}_1 = 2(R_{22} - a)$ (i.e. $A = 0$, $B = 1$ and $C = -2(R_{22} - a)$).

2. The second transformation is an inversion $\zeta_2 = 1/\zeta_1$. Substitution of the definition of the new transformation into result of step 1 reads as $1/\zeta_2 + 1/\bar{\zeta}_2 = 2(R_{22} - a)$, which can be expressed in the general form of $-2(R_{22}-a)\zeta_2\bar{\zeta}_2 + \zeta_2 + \bar{\zeta}_2 = 0$ (i.e. $A = -2(R_{22} - a)$, $B = 1$ and $C = 0$). This is an equation for a circle and hence this is a circle $\mathcal{C}(1/2(R_{22} - a), 1/2(R_{22} - a))$ (Fig. 5.3-c). It should be noted that $R_{22} - a$ has to be positive because the vertical line in Fig. 5.3b must be in the RHP.

3. The third transformation is $\zeta_3 = Z_{11} - Z_{12}Z_{21}\zeta_2$. Similar to the first transformation, the third transformation is a linear transformation (Fig. 5.3-d). For this

transformation the magnifying factor is $Z_{12}Z_{21}$ and translation is Z_{11}. Therefore, the circle will be expanded or contracted by factor of and $Z_{12}Z_{21}$ and the radius becomes $r_o = \frac{|Z_{12}Z_{21}|}{2(R_{22}-a)}$ and the centre of the circle will be translated to $c_o = Z_{11} - \frac{Z_{12}Z_{21}}{2(R_{22}-a)}$. The latter shows that a region expressed as $\mathrm{Re}z_2 \geq -a$ is mapped to a region inside a disc express as in (5.10).
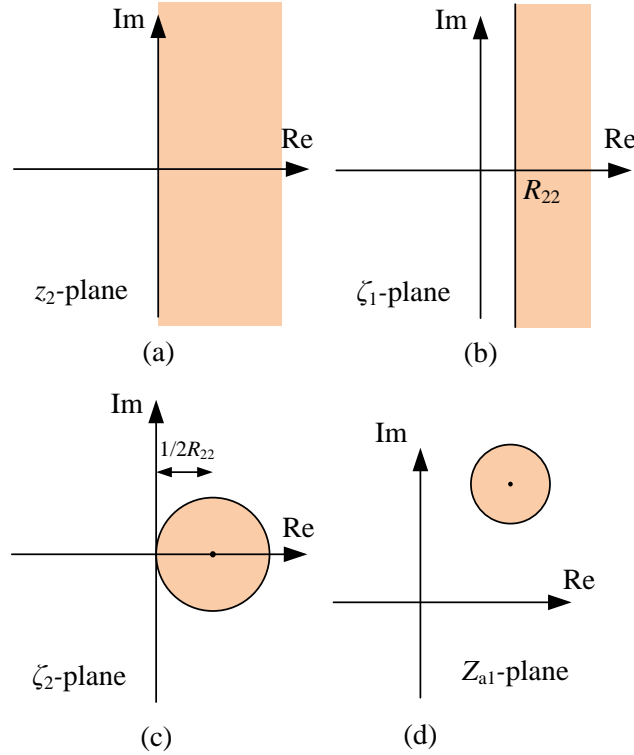
Figure 5.3: The Mobius transformation has been split into three transformations: from (a) to (b) is a linear transformation (horizontal translation), from (b) to (c) is an inversion, and from (c) to (d) is another linear transformation with expansion/contraction in addition to a translation.

Step 2:

Similar to Step 1, it is easy to show that the vertical line of $\mathrm{Re}z_2 = b$ is transformed to a circle of (5.11). In the following it is shown that the circle of (5.11) is enclosed by the circle of (5.11) and also the two circles are tangent at the furthest point from the origin. Consequently, the area between the two vertical lines of $\mathrm{Re}z_2 = -a$ and $\mathrm{Re}z_2 = b$ is transformed to a cresent as shown in Fig. 5.4.
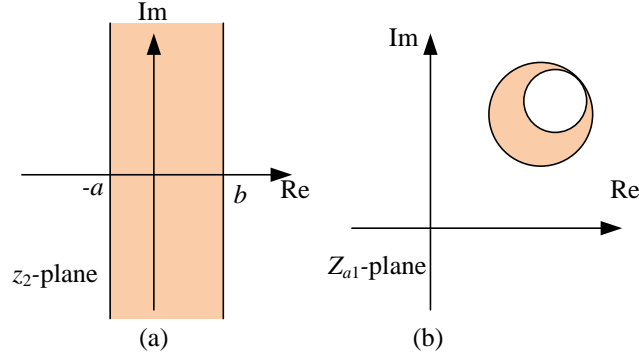
Figure 5.4: In analysis of the strip-like impedances the strip in the z_2-plane (a) is mapped to a rotated crescent in the Z_{a1}-plane (b).

In the following, it is proved that the circle corresponding to $\mathrm{Re}z_2 = b$ is entirely inside the circle corresponding to $\mathrm{Re}z_2 = -a$. The two circles of (5.10) and (5.11) resulted from expansions/contractions term $Z_{12}Z_{21}$ followed by a translation by Z_{11} in the Z_{a1}-plane. Consequently, as depicted in Fig. 5.5-a, an extension of the line connecting the centres of these two circles $(\overline{t_a t_b})$ goes through the origin. Another conclusion is that the length of the line segment between the centres of the two circles, i.e., $|\overline{t_a t_b}|$, is identical to the differences between to the radii of the two circles (i.e., $|{}^a r_o - {}^b r_o|$). Therefore, as shown in Fig. 5.5-a, the two circles must be tangent at their farthest points from the origin. Additionally, changing the bounds on the real part of z_2 will result in the circles shown in Fig. 5.5-b. As the real value of z_2 is allowed to increase, the radius of the smaller circles decreases. Also, as the real value of z_2 is allowed to decrease further into the negative values, the radius of the larger circles increases (not shown in Fig. 5.5-b).

Step 3:

In this step of the proof, it is shown that the horizontal lines of $\mathrm{Im}z_2 = c$ and $\mathrm{Im}z_2 = -d$ are transformed to circles of (5.12) and (5.13). Let us consider the horizontal line of $\mathrm{Im}z_2 = c$.

Similar to Step 1, the Mobius transformation (5.9) is split into three transformations, in which the first and the third are linear transformations and the second
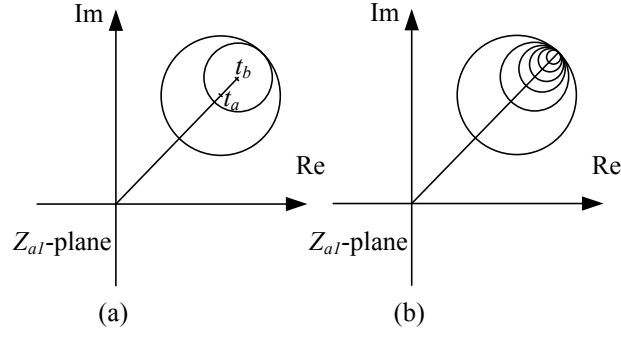
Figure 5.5: The vertical lines in the z_2-plane are mapped to circles in the Z_{a1}-plane. The vertical line at $\operatorname{Re} z_2 = -a$ is mapped to the larger circle in the Z_{a1}-plane while the vertical line at $\operatorname{Re} z_2 = b$ is mapped to the smaller circle (a). As the real value of z_2 is allowed to increase (i.e., larger b), the radius of the smaller circle decreases while the circles still share the same tangent point.

transformation is an inversion. The line $\operatorname{Im} z_2 = c$ is expressed as $z_2 + \bar{z}_2 = 2cj$ and the definition of the first transformation $\zeta_1 = z_2 + Z_{22}$ is substituted to yield the resulting line in ζ_1-plane as $\zeta_1 - \bar{\zeta}_1 = 2cj + 2I_{22}$, where $I_{22} = \operatorname{Im}\{Z_{22}\}$. If it is assumed that $I_{22} + c \geq 0$, substituting the definition of the second transformation $\zeta_2 = 1/\zeta_1$ one can find the transformed the circle in the ζ_2 plane to be $-(2c + 2I_{22})\zeta_2\bar{\zeta}_2 + j\zeta_2 - j\bar{\zeta}_2 = 0$, which has the general circle/line formulation with $A = -(2c + 2I_{22})$, $B = -j$ and $C = 0$. The equation in the ζ_2-plane is $\mathcal{C}(1/(2c + 2I_{22}), -j/(2c + 2I_{22}))$, which is a circle below the origin but tangent to the real axis at the origin. The third transformation $\zeta_3 = Z_{11} - Z_{12}Z_{21}\zeta_2$ bears a translation of Z_{11}, mirrors the circle, expands the circle with expansion factor of $|Z_{12}Z_{21}|$ and finally rotates the circle around Z_{11} about the angle of $Z_{12}Z_{21}$. The resulting circle in the Z_{a1}-plane is circle of (5.12).

As depicted in Fig. 5.6 by increasing the imaginary level c in z_2-plane makes the smaller circles in Z_{a1}-plane, where all of the circles have a tangent point in common at Z_{11}. The region corresponding the region lower than the upper limit of $\operatorname{Im} z_2 = c$ in the z_2-plane is transformed to the region outside of the disc expressed by (5.12) in the Z_{a1}-plane.

Similar to the above mapping for $\operatorname{Im} z_2 = c$, it is easy to show that the mapping
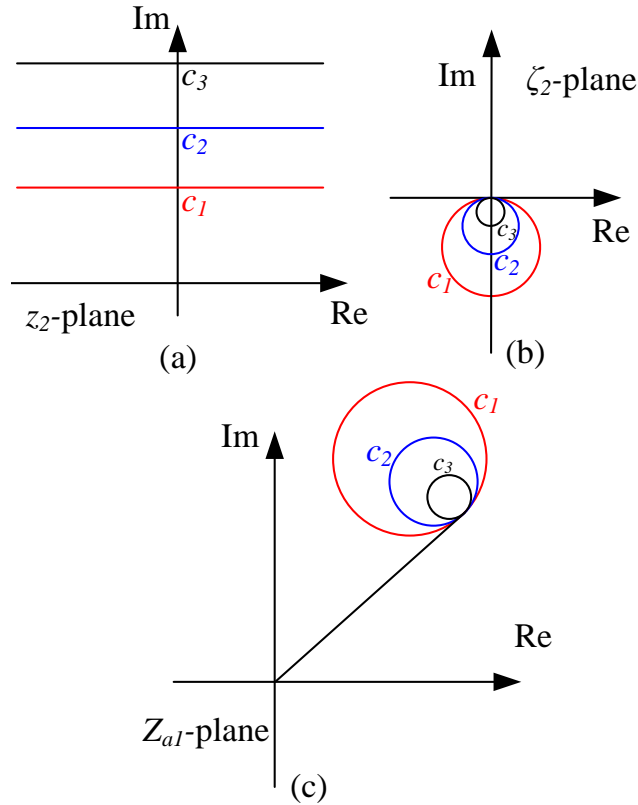
Figure 5.6: The horizontal lines in the z_2-plane are transformed into circles in the Z_{a1}-plane. As the horizontal line moves up, the radius of the circles decreases. Yet, all of the circles are tangent at one point.

of the horizontal line of $\text{Im}\,z_2 = -d$ is (5.13). The assumption of $I_{22} + c \geq 0$ is also replaced by $I_{22} - d \leq 0$.

Note that by increasing the limit on the imaginary part of the upper limit to infinity and decreasing the lower limit to minus infinity, the mapped region in the Z_{a1}-plane becomes the entire plane due to the fact that the radii of the circles decreases as the limit are going further from the real axis.

Combining the transformation of the four lines of Step 1, 2 and 3 the rectangle of Fig. 5.8-a in the z_2 plane is transformed to the portion of a crescent, where the two sides of the crescent are excluded from the region as shown in Fig. 5.8-b expressed with the circles of (5.10)-(5.13) in the Z_{a1} plane. □

The mapped region in the Z_{a1} plane is shown in Fig. 5.8-b.

94
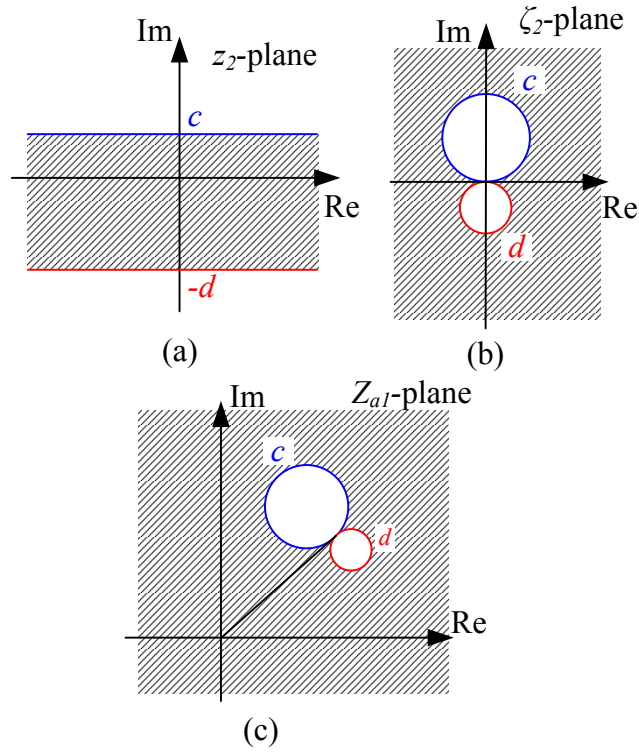
Figure 5.7: The area between the two horizontal lines in the z_2-plane are transformed into the hatched area in Z_{a1}-plane.

Remarks:

- The circles shown in Fig. 5.8 resemble a rotated and translated Smith Chart, which has been applied to investigating the stability of a bilateral teleoperation via reflection coefficients [131].

- By increasing the parameters a, b, c and d in Fig. 5.8-a, the outer circle of the crescent in Fig. 5.8-b enlarges, the inner circle shrinks, and the two discs on the top and bottom shrink.

5.3.1.2 Mapping of a disc impedance via Mobius transformation

In order to investigate the stability of two-port networks with DNP or OSP terminations, we introduce the following two theorems to study mappings of such termina-
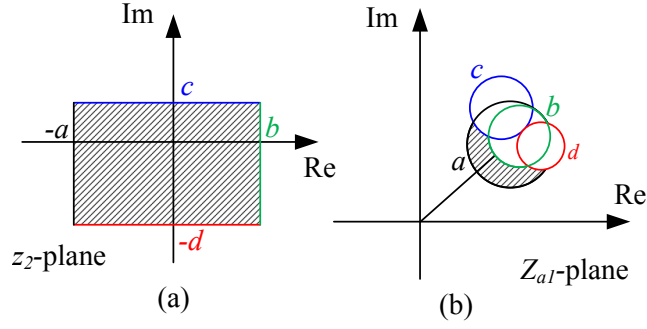
Figure 5.8: A rectangle in the z_2-plane (a) is transformed into the hatched region in the Z_{a1}-plane (b). The circles are marked in relation with the corresponding lines.

tions.

Theorem 5.2. *Suppose that the termination impedance z_2 is a disc defined by $\mathcal{D}(M, 0)$. This region is mapped by the Mobius transformation (5.9) to the following region in the Z_{a1}-plane:*

$$
\begin{cases}
\mathcal{D}(\dfrac{|Z_{12}Z_{21}|M^2}{||Z_{22}|^2 - M^2|}, \dfrac{-Z_{22}Z_{12}Z_{21}}{|Z_{22}|^2 - M^2} + Z_{11}), & \text{if } |Z_{22}| \neq M. \\[2ex]
\mathrm{Re}Z_{a1} > \left(R_{11} - \dfrac{\mathrm{Im}\{Z_{12}Z_{21}\}}{2R_{22}} \right), & \text{if } |Z_{22}| = M \text{ and } Z_{22} \in \mathbb{R}
\end{cases}
\tag{5.14}
$$

$\square$

Proof. As explained in the proof of Theorem 5.1 the Mobius transformation (5.9) is split to three transformations. (1) a linear transformation of $\zeta_1 = z_2 + Z_{22}$, (2) an inversion $\zeta_2 = 1/\zeta_1$, and (3) a linear transformation $\zeta_3 = Z_{11} - Z_{12}Z_{21}\zeta_2$. Lines or circles are expressed in the formulation in the complex plane.

The border of the disc is $\mathcal{C}(M, 0)$ in the z_2-plane and is expressed as $z_2\bar{z}_2 = M^2$ in the circle/line formulation. From the first transformation of $z_2 = \zeta_1 - Z_{22}$, substitution of z_2 is a shifted circle expressed as $\zeta_1\bar{\zeta}_1 - \bar{Z}_{22}\zeta_1 - Z_{22}\bar{\zeta}_1 + |Z_{22}|^2 - M^2 = 0$, which is a circle in the general expression with $A = 1$, $B = -\bar{Z}_{22}$ and $C = |Z_{22}|^2 - M^2$. The second transformation is substituted as $\zeta_1 = 1/\zeta_2$. After simplification the resulting shape is $1 - \bar{Z}_{22}\bar{\zeta}_2 - Z_{22}\zeta_2 + (|Z_{22}|^2 - M^2)\zeta_2\bar{\zeta}_2 = 0$. Now, this shape can be either

96

a circle or a line depending whether $|Z_{22}| = M$ or not. If $|Z_{22}| \neq M$ the mapped shape in the ζ_2-plane is a circle otherwise it is a line. These two cases are considered separately below.

- If $|Z_{22}| \neq M$, resulting shape is a circle $\mathcal{C}(\frac{M^2}{||Z_{22}|^2 - M^2|}, \frac{Z_{22}}{|Z_{22}|^2 - M^2})$. The third transformation shift this circle to another circle $\mathcal{C}(\frac{|Z_{12}Z_{21}|M^2}{||Z_{22}|^2 - M^2|}, \frac{-Z_{22}Z_{12}Z_{21}}{|Z_{22}|^2 - M^2} + Z_{11})$ and the mapped region is inside this circle.

- If $|Z_{22}| = M$, the result of the second transformation is a line $1 - \bar{Z}_{22}\bar{\zeta}_2 - Z_{22}\zeta_2 = 0$. This line is vertical only if the coefficient of $\bar{\zeta}_2$ is zero, which requires that Z_{22} to have no imaginary part, and otherwise the resulting region is a rotated and shifted half plane and hence there is no condition in which guarantees the region to be entirely in the RHP. With the assumption of $\mathrm{Im} Z_{22} = 0$, the mapped region in ζ_2-plane is a vertical line at $\zeta_2 = 1/2R_{22}$. The third transformation shifts this vertical line to $R_{11} - \mathrm{Im}\{Z_{12}Z_{21}\}/2R_{22}$. Therefore, the mapped region in the Z_{a1}-plane is the right hand side of this vertical line.
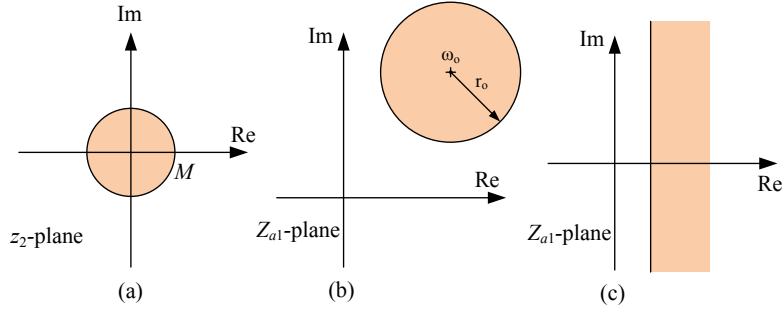
Figure 5.9: (a) a disc in the z_2-plane inside $\mathcal{C}(M, 0)$, (b) if $|Z_{22}| \neq M$, the mapped region is also a disc in the Z_{a1}-plane, (c) if $|Z_{22}| = M$, the mapped region is a shifted RHP.

□

While Theorem 5.2 finds the transformation of a disc-like region (corresponding to a DNP termination), the following theorem finds the transformation if the disc is shifted to the right by M (corresponding to an OSP termination).

Theorem 5.3. *Consider a Mobius transformation of (5.9). A disc in the z_2-plane inside of $\mathcal{C}(M, M)$ is mapped by the Mobius transformation (5.9) to the following region in the Z_{a1}-plane:*

$$
\begin{cases}
\mathcal{D}(\dfrac{|Z_{12}Z_{21}|M^2}{||Z_{22} + M|^2 - M^2|}, \dfrac{-Z_{22}Z_{12}Z_{21}}{|Z_{22} + M|^2 - M^2} + Z_{11}), & if\ |Z_{22} + M| \neq M. \\[4mm]
\mathrm{Re}Z_{a1} > \left(R_{11} - \dfrac{\mathrm{Im}\{Z_{12}Z_{21}\}}{2(R_{22} + M)} \right), & if\ |Z_{22}| = M\ and\ Z_{22} \in \mathbb{R}
\end{cases}
\tag{5.15}
$$

$\square$

Proof of Theorem 5.3 is similar to the proof of Theorem 5.2.

5.3.2 Stability of a two-port network with non-passive terminations

Shortage of passivity for a termination of a two-port network means that the coupled network may be unstable even if Llewellyn's conditions are met. Therefore, more stringent conditions for stability will be found in this section for two types of non-passive terminations.

5.3.2.1 Stability of a two-port network with an INP termination

Let us assume that a non-passive termination's impedance covers a rectangular area in the complex plane. If the region is partially in the LHP with bounds on the real and imaginary parts of the complex impedance, the termination is INP. In Theorem 5.4 below, the absolute stability condition for a two-port network with this INP termination is introduced.

Theorem 5.4. *Consider the two-port network (5.8) and assume that, as shown in Fig. 5.1-b, the driving-point impedance seen from port 1 is Z_{a1} while port 2 of the two-port network is terminated to an impedance z_2. Assume that z_2 is INP with*

$-a \leq \mathrm{Re}z_2 \leq b$ *and* $-d \leq \mathrm{Im}z_2 \leq c$ *as shown in Fig.* 5.8-a *with* $a, b, c, d \geq 0$. *If port 1 of the two-port network is terminated to a passive impedance, the necessary and sufficient condition for stability of the coupled system comprising the two-port network, the passive termination at port 1, and the INP termination at port 2 is*

(i) Z_{11} *and* Z_{22} *have no poles in the RHP,*

(ii) *Pure imaginary poles of* Z_{11} *and* Z_{22} *are simple and have positive residues, and*

(iii) *For all real positive frequencies* ω,

$$R_{11} \geq 0$$

$$R_{22} \geq a$$

$$2R_{11}R_{22} - \mathrm{Re}\{Z_{12}Z_{21}\} - |Z_{12}Z_{21}| - 2R_{11}a \;\; \geq 0 \qquad (5.16)$$

$\square$

Proof. Conditions (i) and (ii) are necessary conditions for ensuring positive realness of Z_{11} and Z_{22} in zero-impedance conditions for ports 2 and 1, respectively. Let us consider the third condition of Theorem 5.4. As shown in Fig. 5.1-b, the two-port network is connected to a passive impedance z_2 and the input impedance seen from the other port is assumed to be Z_{a1}. The two-port network will be absolutely stable if Z_{a1} is passive as well. The driving-point impedance Z_{a1} is expressed based on the two-port network impedance parameters Z_{ij}'s and the termination impedance z_2 as in (5.9).

The borderline of passivity in the z_2 complex plane is a vertical line at $-a$. If $\mathrm{Re}Z_{22} \geq a$, and for similar reason $\mathrm{Re}Z_{11} \geq 0$, Theorem 5.1 applies with $b = \infty$, $c = \infty$ and $d = \infty$. The passive region is mapped to a disc inside of $\mathcal{C}(|Z_{12}Z_{21}|/(2(R_{22} - a)), Z_{11} - Z_{12}Z_{21}/(2(R_{22} - a)))$. The condition for passivity of the driving-point

impedance Z_{a1} is that this disc with radius of r_o and centre of c_o must be entirely in the RHP, i.e., $\mathrm{Re}c_o - r_o \geq a$. Thus, the absolute stability becomes

$$\frac{2\mathrm{Re}Z_{11}\mathrm{Re}Z_{22} - \mathrm{Re}\{Z_{12}Z_{21}\} - |Z_{12}Z_{21}|}{2(R_{22} - a)} \geq 0 \tag{5.17}$$

This completes the proof. □

Remarks:

- The parameters b, c and d do not appear in the stability condition (5.16) due to the fact that the inner circle and the top and bottom circles in Fig. 5.8-b are not the source of any constraint when ensuring the passivity (i.e., the positive realness) of the driving-point impedance Z_{a1}. In other words, besides the parameters of the two-port network, stability depends only on the lower limit of the real part of the INP impedance z_2 (i.e., -a) for the two-port network.

- As a special case of Theorem 5.4, by setting $a = 0$, $b = \infty$, $c = \infty$ and $d = \infty$, the region covered by the impedance z_2 becomes the entire RHP (i.e., all passive impedances). Evidently, when $a = 0$, our stability condition (5.16) reduces to the well-known Llewellyn's absolute stability criterion for two passive terminations [118]:

$$R_{11} \geq 0$$
$$R_{22} \geq 0$$
$$2R_{11}R_{22} - \mathrm{Re}\{Z_{12}Z_{21}\} - |Z_{12}Z_{21}| \geq 0 \tag{5.18}$$

- The difference between the stability conditions (5.16) and (5.18) is in their second and third conditions. As expected, compared to (5.18), (5.16) is more stringent because $a \geq 0$ and it provides for stability of the two-port network coupled to an INP termination.

- a is indeed the SOP of the INP termination z_2 according to Definition 5.4 and the non-passive dual of Lemma 5.2.

5.3.2.2 Stability of a two-port network with a DNP termination

In many applications of bilateral teleoperation, the knowledge about the non-passive termination, e.g., human arm, can be translated to a maximum amplitude of its impedance [132, 133]. This maximum impedance is the same as the radius of the disc for a DNP termination, which is expressed as $|z_2| \leq M$. Passivity of a two-port network connected to a DNP termination can be studied using the following theorem.

Theorem 5.5. *Consider the two-port network system (5.8) and assume that, as shown in Fig. 5.1-b, the driving-point impedance seen from port 1 is Z_{a1} while port 2 of the two-port network is terminated to an impedance z_2. Assume that z_2 is DNP with $|z_2| \leq M$, where $M > 0$ is known. If port 1 of the two-port network is terminated to a passive impedance, the necessary and sufficient condition for stability of the coupled system comprising the two-port network, the passive termination at port 1, and the DNP termination at port 2 is*

(i) Z_{11} and Z_{22} have no poles in the RHP,

(ii) Pure imaginary poles of Z_{11} and Z_{22} are simple and have positive residues, and

(iii) For all real positive frequencies ω,

$$R_{11} \geq 0$$

$$R_{22} \geq 0$$

$$\begin{cases} R_{22}(|Z_{11}|^2 - M^2) - \mathrm{Re}\{Z_{11}Z_{12}Z_{21}\} - |Z_{12}Z_{21}|M \geq 0 & \text{if } |Z_{11}| > M. \\ -R_{22}(|Z_{11}|^2 - M^2) + \mathrm{Re}\{Z_{11}Z_{12}Z_{21}\} - |Z_{12}Z_{21}|M \geq 0 & \text{if } |Z_{11}| < M. \\ -2R_{22}R_{11} - \mathrm{Re}\{Z_{12}Z_{21}\} \geq 0 & \text{if } Z_{11} = M. \end{cases}$$

$$(5.19)$$

$\square$

Proof of Theorem 5.5 is similar to the proof of Theorem 5.4 with the difference that the region covered by the non-passive termination is now a disc, which requires using Theorem 5.2.

5.3.3 Stability of a two-port network with strictly-passive terminations

Having excess of passivity for a termination of a two-port network allows for more flexible stability conditions. Input and output strict-passivity of a termination are considered separately in the following two subsections.

5.3.3.1 Stability of a two-port network with an ISP termination

Theorem 5.6. *Consider the two-port network system (5.8) and assume that, as shown in Fig. 5.1-b, the driving-point impedance seen from port 1 is Z_{a1} while port 2 of the two-port network is terminated to an impedance z_2. Assume that z_2 is ISP with $\mathrm{Re} z_2 \geq \delta \geq 0$. If port 1 of the two-port network is terminated to a passive impedance, the necessary and sufficient condition for stability of the coupled system comprising the two-port network, the passive termination at port 1, and the ISP termination at port 2 is*

(i) Z_{11} and Z_{22} have no poles in the RHP,

(ii) Pure imaginary poles of Z_{11} and Z_{22} are simple and have positive residues, and

(iii) For all real positive frequencies ω,

$$R_{11} \geq 0$$
$$R_{22} \geq -\delta$$
$$2R_{11}R_{22} - \mathrm{Re}\{Z_{12}Z_{21}\} - |Z_{12}Z_{21}| + 2R_{11}\delta \geq 0 \qquad (5.20)$$

$\square$

Proof of Theorem 5.6 is similar to the proof of Theorem 5.4 with the difference that $\delta = -a$.

Remark:

- The last condition in (5.20) for coupled stability of a two-port network with an ISP termination can be compared to its non-passive counterpart in (5.16). It is clear that the latter is more conservative. Intuitively, for coupled stability, the two-port network should absorb more energy when connected to a non-passive termination than when connected to a strictly-passive termination.

5.3.3.2 Stability of a two-port network with an OSP termination

In many applications of bilateral teleoperation, the only knowledge about the strictly-passive termination is that its Nyquist diagram is a disc that is centered on the positive segment of the real axis and is tangent to the imaginary axis at the origin. This disc can be expressed as $\text{Re}G(j\omega) \geq \epsilon|G(j\omega)|^2$, where ϵ is EOP of the OSP termination. If $\epsilon = 0$, the termination becomes passive as its Nyquist diagram will be in the RHP.

Theorem 5.7. *Consider the two-port network system (5.8) and assume that, as shown in Fig. 5.1-b, the driving-point impedance seen from port 1 is Z_{a1} while port 2 of the two-port network is terminated to an impedance z_2. Assume that z_2 is OSP with $\text{Re}z_2 \geq \epsilon|z_2|^2$, where $\epsilon > 0$ is known. If port 1 of the two-port network is terminated to a passive impedance, the necessary and sufficient condition for stability of the coupled system comprising the two-port network, the passive termination at port 1, and the OSP termination at port 2 is*

(i) *Z_{11} and Z_{22} have no poles in the RHP,*

(ii) *Pure imaginary poles of Z_{11} and Z_{22} are simple and have positive residues, and*

103

(iii) For all real positive frequencies ω,

$$R_{11} \geq 0$$

$$R_{22} \geq 0$$

$$R_{22}(|Z_{11} + M|^2 - M^2) - \text{Re}\{(Z_{11} + M)Z_{12}Z_{21}\} - |Z_{12}Z_{21}|M \geq 0 \quad (5.21)$$

$$|Z_{11} + M| > M \quad (5.22)$$

$\square$

where $M = 1/(2\epsilon)$. Proof of Theorem 5.7 is similar to the proof of Theorem 5.4 with the difference that the region occupied by the Nyquist diagram of the termination is now a disc, which requires using Theorem 5.3.

5.4 Application to bilateral teleoperation

The coupled stability conditions presented in Sections 5.3 are valid for any two-port network. In this section, the two-port network is assumed to be a bilateral teleoperator. In this context, the voltage-current pair (V,I) for the impedance matrix (5.8) is replaced by the force-velocity pair (F,sX). The coupled stability theorems in Section 5.3 for strictly-passive and non-passive terminations will be applied to a teleoperator coupled with a non-passive human operator and a strictly-passive environment.

5.4.1 Modelling of bilateral teleoperation systems

For a 1 degree-of-freedom, bilateral teleoperation system, the master and the slave robots are modelled as LTI systems

$$
\begin{aligned}
sX_m(s) &= \frac{1}{m_m s + b_m}(F_h(s) - F_m(s)) \\
sX_s(s) &= \frac{1}{m_s s + b_s}(F_e(s) - F_s(s))
\end{aligned}
\quad (5.23)
$$

Also, the operator and the environment are modeled as

$$F_h(s) = \tilde{F}_h(s) - sZ_h(s)X_m(s) \qquad (5.24)$$

$$F_e(s) = \tilde{F}_e(s) + sZ_e(s)X_s(s) \qquad (5.25)$$

In the above, F, Z and X denote the force, the impedance and the position, respectively. Also, the subscripts h, e, m and s denote the operator, the environment, the master and the slave, respectively. Furthermore, $\tilde{F}$ represents the exogenous force.
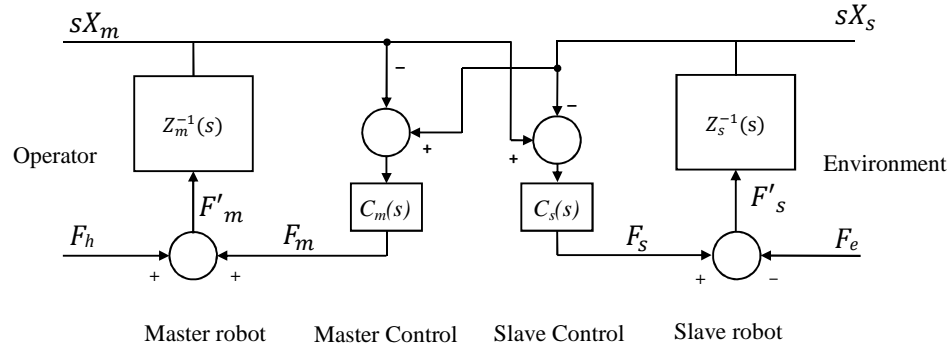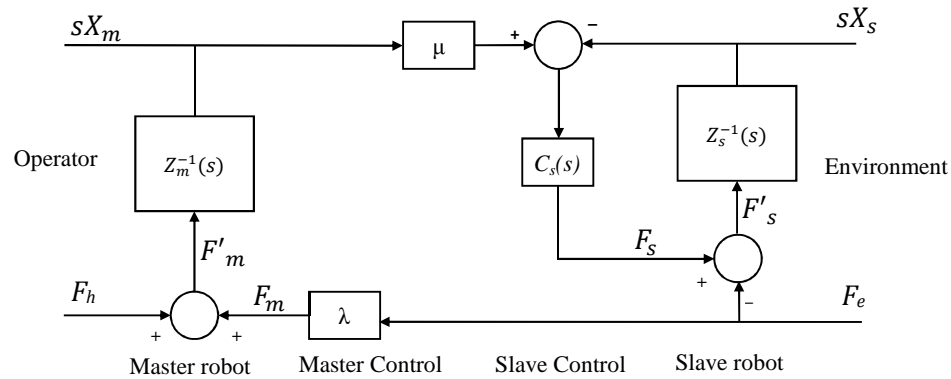

Figure 5.10: A bilateral teleoperation system, (a) with PEB control, and (b) DFR control.

Bilateral teleoperation systems with position error based (PEB) and direct force reflecting (DFR) controllers are shown in Fig. 5.10. For the PEB architecture, the teleoperation controllers and the impedance matrix of the teleoperator are shown in

105

Table 5.1, where $F_{m,s}$ are the controller outputs. In this case, the controllers of the master and the slave are $C_s(s) = k_{p_s}/s + k_{v_s}$ and $C_m(s) = k_{p_m}/s + k_{v_m}$, respectively, where $k_{v_m}, k_{v_s}, k_{p_m}, k_{p_s} \geq 0$. For the DFR architecture, the slave robot's position controller may be PD[3] (named DFR(PD) architecture) or P+D (named DFR(P+D) architecture) [134]. The difference between these two is that position controller for the slave robot; see Table 5.1. The controllers and the impedance matrices of these two DFR controllers are shown in Table 5.1, where μ and λ are the position and force scaling factors.

Table 5.1: Controllers of bilateral teleoperation systems and their impedance matrices

Controller	Control law	Impedance matrix
PEB	$\begin{cases} F_m(s) = C_m(s)(X_s(s) - X_m(s)) \\ F_s(s) = C_s(s)(X_m(s) - X_s(s)) \end{cases}$	$\begin{bmatrix} Z_{tm} & C_m \\ C_s & Z_{ts} \end{bmatrix}$
DFR(PD)	$\begin{cases} F'_m(s) = F_h(s) - \lambda F_e(s) \\ F'_s(s) = C_s(s)(\mu X_m(s) - X_s(s)) - F_e(s) \end{cases}$	$\begin{bmatrix} Z_m + \mu\lambda C_s & \lambda Z_{ts} \\ \mu C_s & Z_{ts} \end{bmatrix}$
DFR(P+D)	$\begin{cases} F'_m(s) = F_h(s) - \lambda F_e(s) \\ F'_s(s) = k_p(\mu X_m(s) - X_s(s)) - sk_v X_s(s) - F_e(s) \end{cases}$	$\begin{bmatrix} Z_m + \frac{\mu\lambda k_p}{s} & \lambda Z_{ts} \\ \frac{\mu k_p}{s} & Z_{ts} \end{bmatrix}$

5.4.2 Teleoperation system stability conditions for passive, INP and ISP terminations

---

[3]Note that the impedance matrix (5.8) relates velocity to force (instead of position to force); this fact changes the representation of the position controller from PD to PI.

Table 5.2: Stability conditions for different choices of teleoperation system control architecture and different choice of terminations

Control	Passive	INP	ISP
PEB	$b_m b_s + b_m k_{v_s} + b_s k_{v_m} \geq \dfrac{\left(k_{v_m} k_{p_s} - k_{p_m} k_{v_s}\right)^2}{4 k_{p_m} k_{p_s}}$	$\left(k_{v_m} + b_m\right)\left(b_s - \eta\right) + b_m k_{v_s} \geq \dfrac{\left(k_{v_m} k_{p_s} - k_{p_m} k_{v_s}\right)^2}{4 k_{p_m} k_{p_s}}$ & $b_s + k_{v_s} \geq \eta$	$\left(k_{v_m} + b_m\right)\left(b_s + \delta\right) + b_m k_{v_s} \geq \dfrac{\left(k_{v_m} k_{p_s} - k_{p_m} k_{v_s}\right)^2}{4 k_{p_m} k_{p_s}}$
DFR (PD)	None	None	None
DFR (P+D)	$\mu\lambda \leq \dfrac{4 b_m}{b_s + k_v}$ & $\mu\lambda \leq \dfrac{b_m\left(b_s + k_v\right)}{m_s k_p}$	$\mu\lambda \leq \dfrac{4 b_m\left(b_s + k_v - \eta\right)}{\left(b_s + k_v\right)^2}$ & $\mu\lambda \leq \dfrac{b_m\left(b_s + k_v - \eta\right)}{m_s k_p}$ & $b_s + k_v \geq \eta$	$\mu\lambda \leq \dfrac{4 b_m\left(b_s + k_v + \delta\right)}{\left(b_s + k_v\right)^2}$ & $\mu\lambda \leq \dfrac{b_m\left(b_s + k_v + \delta\right)}{m_s k_p}$

Table 5.2 compares the necessary and sufficient stability conditions for the PEB, DFR(PD) and DFR(P+D) controlled teleoperation systems when one of the ports is connected a passive, INP or ISP termination. These conditions have resulted from substituting the impedance matrices of PEB, DFR(PD) and DFR(P+D) controlled teleoperation systems from Table 5.1 into the stability conditions (5.16), (5.18) and (5.20) for INP, passive and ISP terminations, respectively. Note that the position scaling factor μ and the force scaling factor λ appear together in the stability conditions.

Discussions:

- Consider the (PEB, passive) entry of Table 5.2. The teleoperation system stability requires a lower bound on the robots damping terms b_m and b_s and bounds on the master and slave controllers gains. A sufficient condition for stability of this system is to have the master and the slave controllers proportional to each other:

$$\frac{k_{p_s}}{k_{v_s}} = \frac{k_{p_m}}{k_{v_m}} \tag{5.26}$$

  The condition (5.26) is both necessary and sufficient for coupled stability if the master and the slave dynamics only involves masses, i.e., $b_m = b_s = 0$.

- The (PEB, INP) entry of Table 5.2 is similar to the (PEB, Passive) entry of Table 5.2 with the exception that b_s is replaced by $b_s - \eta$, where η is the SOP for the INP termination. The physical interpretation of the above fact is that the SOP of the INP termination (connected at port 2) reduces the effective damping of the corresponding robot (the slave robot), which has to be greater than a lower bound in order to ensure stability. In other words, SOP of the INP termination necessitates higher damping for the robot and makes the stability condition harder to satisfy. If the robot damping is not high enough to make up for the SOP of the INP termination, the derivative term of the controllers must be selected high enough to overcome non-passivity of the termination.

- For the (PEB, INP) entry of Table 5.2, also note that the robot damping terms b_m and b_s cannot be both zero because it causes the left hand side of the first inequality to be negative. This result has an intuitive interpretation. In the (PEB, Passive) case with no damping terms for the master and the slave robots, we saw that the only choice for the controllers was (5.26). The non-passivity of the termination should make this choice even more limited. However, no freedom is left in the controller parameter space. Therefore, the termination cannot be non-passive.

- The (PEB, ISP) entry of Table 5.2 is similar to the (PEB, Passive) entry of Table 5.2 with the exception that b_s is replaced by $b_s + \delta$, where δ is the EOP for the ISP termination. The physical interpretation of the above fact is that the EOP of the ISP termination (connected at port 2) increases the effective damping of the corresponding robot (the slave robot), which has to be greater than a lower bound in order to ensure stability. In other words, EOP of the ISP termination relaxes the lower bound requirement on the robot damping and makes the stability condition easier to satisfy. Also, the robot damping terms b_m and b_s are allowed to be both zero and the controller gain do not necessarily have to be chosen according to (5.26).

- The INP column of Table 5.2 includes conditions that are expectedly more limiting than their counterparts in the Passive column. In fact, the more non-passive the termination, the more restrictive the stability condition for the coupled system. Conversely, the ISP column of Table 5.2 has stability conditions that are less restrictive that their counterparts in the Passive column. In fact, the more passive the termination, the more relaxed the stability condition for the coupled system.

- With the DFR(PD) controller (i.e., force reflection for the master and PD position controller for the slave), substituting the impedance matrix $\mathbf{Z_{PD}}$ into the

stability conditions (5.18), (5.16) and (5.20) yields conditions that never hold for $\omega = 0$. This fact has previously been reported in [93]. However, with the DFR(P+D) controller (i.e., force reflection for the master and a P position controller and internal damping for the slave), there does exist a range of controller gains for stability; this has also previously been reported in [134]. Similar to the PEB controller, in the DFR(P+D) case the effective damping of the robot is reduced or increased by the non-passivity or excess of passivity of the termination, making the stability conditions more restrictive or more relaxed, respectively.

5.4.3 Teleoperation system stability conditions for DNP and OSP terminations

Substituting the impedance matrices of PEB, DFR(PD) and DFR(P+D) controlled teleoperation systems from Table 5.1 into the stability conditions of DNP and OSP termination, i.e., (5.19) and (5.21), results in conditions of the following form

$$\mathcal{N}(\omega) = N_8\omega^8 + N_6\omega^6 + N_4\omega^4 + N_2\omega^2 + N_0 \geq 0 \tag{5.27}$$

where N_i's, $i = 0, 2, 4, 6, 8$, are functions of system parameters $m_m, b_m, m_s, b_s, \mu, \lambda, k_v, k_p$ and M. For the DNP termination, $N_0 \geq 0$ corresponding to $\omega = 0$ yields necessary conditions for stability that are shown in Table 5.3. For the OSP termination, N_0 is always non-negative for PEB, DFR(PD) and DFR(P+D) controllers. Furthermore, in (5.27), the high frequency component N_8 is non-negative for both DNP and OSP. The terms N_2, N_4 and N_6 may have sign changes depending on the parameters that are involved.

In order to find stability bound, the stability conditions found in Theorems 5.5 and 5.7 can be tested over a range of frequencies of interest for a haptic teleoperation system, e.g., 0-100 rad/sec. If the condition $\mathcal{N}(\omega) \geq 0$ is satisfied for the entire range of frequencies, the coupled system is considered stable. An example of the

Table 5.3: Necessary conditions for stability of the teleoperation system with DNP termination for PEB, DFR(PD) and DFR(P+D) controllers.

Controller	Condition for having $N_0 \geq 0$
PEB	$M \leq \dfrac{b_s k_{p_m} + b_m k_{p_s} + 2k_{p_s} k_{v_m} + 2k_{p_m} k_{v_s}}{k_{p_s}}$
DFR(PD)	$M \leq b_m + 2\mu\lambda(Bs + 2Kv)$
DFR(P+D)	$M \leq b_m + 2\mu\lambda(Bs + Kv)$

stability index $\mathcal{N}(\omega)$ for the benchmark teleoperator, a DFR(PD) controller, and a DNP termination with various values of disk radius M is plotted in Fig. 5.11. The parameter of the teleoperation system are $m_m = 0.015$, $b_m = 0.01822$, $m_s = 0.15$, $b_s = 0.1822$, $k_p = 10$, $k_v = 2$ and $\mu\lambda = 0.02$. In this example, the maximum value of disk radius M of the DNP termination is found to be 4.92. Any higher M for the DNP termination can cause instability.
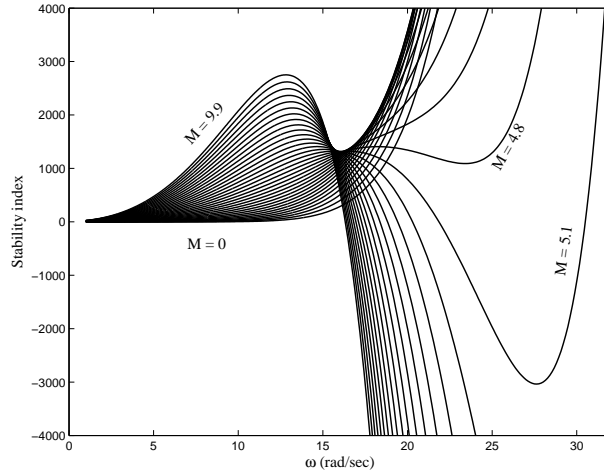

Figure 5.11: The stability index is evaluated for different values of the disc radius for a range of frequencies.

5.5 Simulation study

A bilateral teleoperation system with PEB control (Fig. 5.10-a) is simulated in MAT-LAB/Simulink. Whereas in the experiment in Section 5.6, we will be limited to

111

having two identical master and slave robots, in the simulations in this section we have the liberty of verifying the proposed stability criteria when the master and the slave robots have different models. The selected model parameters are $m_m = 0.015$ and $b_m = 0.0182$ for the master and $m_s = 0.15$ and $b_m = 0.182$ for the slave. Table 5.4 compares the theoretical stability conditions (Theory columns) with the simulation results (Simulation Column). In each row of Table 5.4, the PEB control gains, the operator impedance, and the environment impedance are changed and the robots positions are monitored for boundedness to detect instability. In each Theory column of the table, the theoretical stability conditions in Sections 5.4.2 and 5.4.3 are evaluated and the results are listed as either absolutely stable (Abs. Stab.) or potentially unstable (Pot. Unst.).

In Table 5.4, the terminations are $G_P = \frac{1}{s+1}$, $G_{ISP} = \frac{s+0.5}{s+1}$, $G_{OSP} = \frac{1}{s+1}$, $G_{INP} = \frac{s-0.5}{s+1}$ and $G_{DNP} = \frac{s-1}{s+1}$. The Nyquist diagrams in Fig. 5.12 show that the EOP values of the ISP and OSP terminations are 0.5 and 1, respectively. Also, the SOP values of the INP and DNP terminations are 0.5 and 0.5, respectively. In all cases, the human operator exogenous force $\tilde{F}_h(s)$ is assumed to be a sine wave with a magnitude of 1 and frequency of 2π rad/sec and the environment exogenous force $\tilde{F}_e(s)$ is assumed to be zero.

Table 5.4: Comparing stability of teleoperation systems in theory and simulation.

| # | Control gains | | | | Terminations | | Theory | | | | | Simulation |
	k_{p_m}	k_{v_m}	k_{p_s}	k_{v_s}	Z_h	Z_e	(PEB, Passive)	(PEB, INP)	(PEB, DNP)	(PEB, ISP)	(PEB, OSP)	
1	10	2	20	2	G_P	G_{OSP}	Abs. Stab.	-	-	-	Abs. Stab.	Stable
2	40	2	10	2	G_P	G_{OSP}	Pot. Unst.	-	-	-	Abs. Stab.	Stable
3	10	1	20	2	G_P	G_{ISP}	Abs. Stab.	-	-	Abs. Stab.	-	Stable
4	20	1	20	2	G_P	G_{ISP}	Pot. Unst.	-	-	Abs. Stab.	-	Stable
5	5	1	20	2	G_{DNP}	G_P	Pot. Unst.	-	Pot. Unst.	-	-	Unstable
6	5	1	20	4	G_{DNP}	G_P	Abs. Stab.	-	Pot. Unst.	-	-	Unstable
7	10	2	40	2	G_{INP}	G_P	Pot. Unst.	Pot. Unst.	-	-	-	Unstable
8	20	2	30	5	G_{INP}	G_P	Abs. Stab.	Pot. Unst.	-	-	-	Unstable

From rows 1 and 3 of the table, we see that if stability in simulations is shown for a set of control gains under the assumption that the terminations are passive, replacing a passive termination with a strictly-passive termination (ISP or OSP) does not alter the result. Conversely, if instability in simulations is shown for a set of control gains under the assumption that the terminations are passive, replacing a passive termination with a non-passive termination may not alter the result; while rows 5 and 7 show two cases of this.

Rows 6 and 8 show that the theoretical stability condition for passive terminations (i.e., Llewellyn's criterion) listed under the column (PEB, passive) expectedly fails to recognize instability if that occurs because of a non-passive termination. Conversely, Rows 2 and 4 show that the theoretical stability condition for passive terminations (i.e., Llewellyn's criterion) listed under the column (PEB, passive) fails to recognize stability if that occurs because of a strictly-passive termination. In fact, when a termination is strictly-passive, the teleoperation system may be stable even when the teleoperator is recognized by Llewellyn's criterion to be potentially unstable; our proposed stability criterion informs us about this, thus providing an opportunity to leverage higher control gains for improved transparency while preserving stability.

5.6 Experimental results

In order to test the stability conditions, experiments are conducted on a pair of Phantom Premium 1.5A haptic devices (Geomagic Inc., Wilmington, MA), which form a bilateral teleoperation system. In the following, two sets of experiments are shown for a strictly-passive termination and a non-passive termination. Typically, it is the environment termination that is strictly-passive while it is the human operator termination that is non-passive.
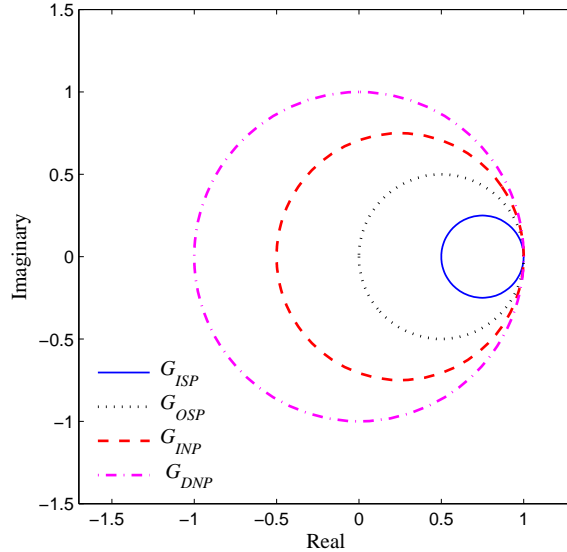
Figure 5.12: Nyquist diagrams of a ISP, OSP, INP and DNP terminations.

5.6.1 Experiments involving a strictly-passive environment

5.6.1.1 Experimental setup

We use the 1-DOF bilateral teleoperation system shown on Fig. 5.13 comprising two 3-joint Phantom Premium 1.5A robots as the master and as the slave. The sampling period for the robot is $T_s = 1ms$. Out of the three joints of each robot, the first (x) is teleoperated. In this direction, the robot dynamics was identified as a mass-damper with a mass of $m_m = m_s = 0.015$ and a damper of $b_m = b_s = 0.01822$ [5]. The third joint (z) is locked using high-gain control. The second joint (y) is used for a purpose explained below. In the experiments, the environment is designed to be strictly-passive. To design such an environment, the slave robot's end-effector is connected via two springs from opposite sides to a stiff wall and at the same time slides a block of wood on the table. While the spring is passive (lossless), the wood-table viscous friction (acting as a damper) makes the environment strictly-passive. The viscous friction and, therefore, the EOP of the strictly-passive environment can by controlled

115
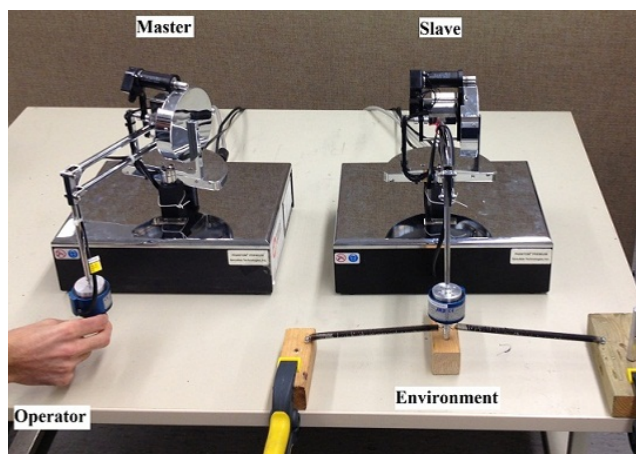
Figure 5.13: The experimental setup for testing ISP environment.

by changing the perpendicular force, which comes from the robot's second joint (y), on the wood block by the slave robot. In the following experiments, the environment either has a low EOP ($\tau_y = 0$) or high EOP ($\tau_y = 0.2$ N.m). Using the definition of the EOP (5.2), in an experiment the values of EOP are identified to be 0.74 and 0.90, respectively. In the following, both PEB (Fig. 5.10-a) and DFR (Fig. 5.10-b) controllers are used in the above-mentioned bilateral teleoperation system and in each case the theoretical stability conditions are verified experimentally.

5.6.1.2 PEB architecture

The bilateral teleoperation system with PEB architecture (Fig. 5.10-a) is tested for different control gains. The experimentally-obtained positions of the master and the slave are shown in Fig. 5.14 when the control gains change according to Table 5.5. The top and the bottom rows of Fig. 5.14 correspond to EOP values of 0.74 and 0.90 for the ISP environment, respectively.

116
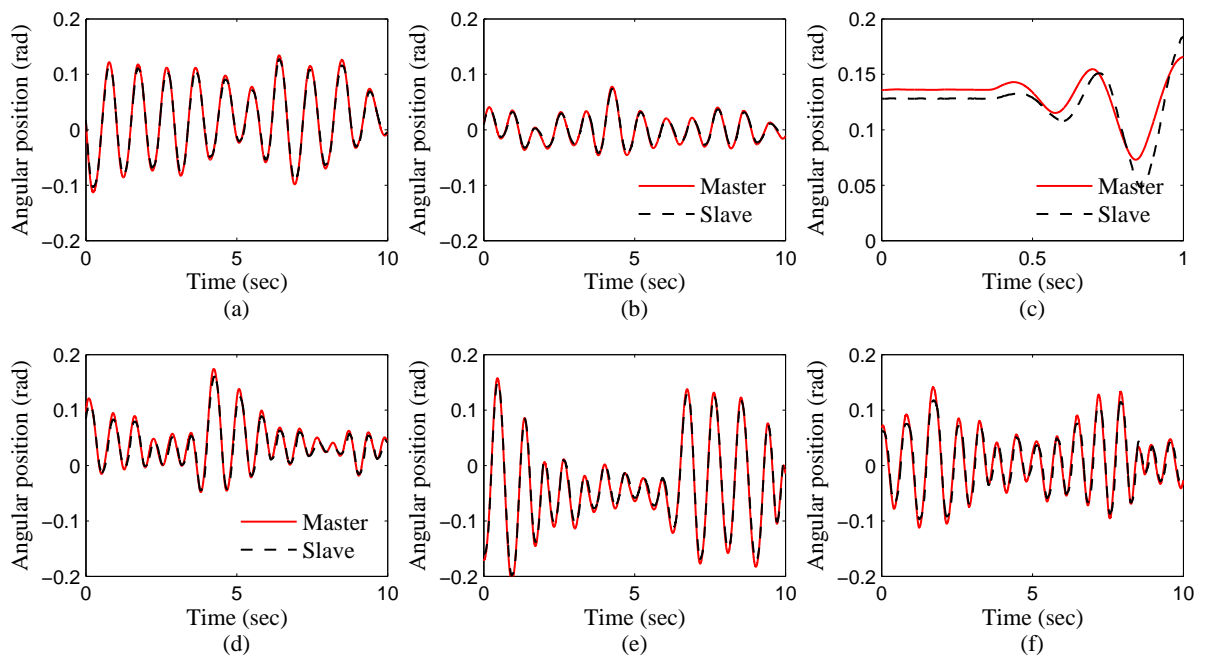
Figure 5.14: Master-slave positions for strictly-passive environment with PEB architecture. Top row has $\tau_y = 0$ and and bottom row has torque of $\tau_y = 0.2$ N.m. The controller gains are given in Table 5.5.

Table 5.5: Stability condition for the bilateral teleoperation system with PEB controllers

#	Figure	Controller gains				EOP	Theory		Experiment	Tracking Error
		k_{p_m}	k_{v_m}	k_{p_s}	k_{v_s}		(PEB, Passive)	(PEB, ISP)		
1	Fig. 5.14-a	20	2	30	2	0.74	Pot. Unst.	Abs. Stab.	Stable	0.49858
2	Fig. 5.14-b	20	2	40	2	0.74	Pot. Unst.	Abs. Stab.	Stable	0.27401
3	Fig. 5.14-c	1	2	40	2	0.74	Pot. Unst.	Pot. Unst.	Unstable	-
4	Fig. 5.14-d	20	2	30	2	0.90	Pot. Unst.	Abs. Stab.	Stable	0.70815
5	Fig. 5.14-e	20	2	40	2	0.90	Pot. Unst.	Abs. Stab.	Stable	0.61674
6	Fig. 5.14-f	10	2	20	2	0.90	Pot. Unst.	Abs. Stab.	Stable	1.0726

In Table 5.5, each row shows a selection of control gains for the PEB controller. These controller gains and the robot model have been substituted in the stability conditions of Table 5.2. In particular, the stability condition in the (PEB, Passive) entry of Table 5.2 has led to the stability conclusion (i.e., stable or unstable) listed in the (PEB, Passive) column of Table 5.5. Similarly, the stability condition in the (PEB, ISP) entry of Table 5.2 has led to the stability conclusion listed in the (PEB, ISP) column of Table 5.5. Furthermore, the cases of actual instability of the system manifested by growing or sustained oscillations is observed and listed in the Experiment column of Table 5.5. The last column shows the Euclidean norm of the position tracking error between the master and the slave.

Comparing the controller gains in rows 1 and 2 of Table 5.5, it is seen that increasing the controller gain k_{p_s} leads to a lower tracking error; in general, higher control gains improve performance but undermine the stability of the system. The same phenomenon can be seen when comparing rows 4 and 5. On the other hand, reducing the controller gain k_{p_m} from row 2 to row 3 or from row 5 to row 6 results in an increase in the tracking error.

In all of the 6 experiments of Fig. 5.14, the conventional (Llewellyn's) stability criterion, i.e., the condition listed in the (PEB, Passive) entry of Table 5.2, predicts that the teleoperation system is unstable; see the (PEB, Passive) column of Table 5.5. In practice, however, EOP of the ISP termination causes the teleoperation system to be stable; see the Experiment column of Table 5.5. This is because the conventional stability condition in the (PEB, Passive) entry of Table 5.2 is conservative because it guarantees stability of the two-port network for *any* passive termination regardless of its EOP value (which can be as little as zero for a lossless termination). In reality, excess of passivity in a termination allows for tolerating a shortage of passivity in the two-port network such that coupled stability is preserved. Allowing a non-passive two-port network (teleoperator) gives us the flexibility to design less conservative and better performing controllers by increasing the controller gains.

119

5.6.1.3 DFR architecture

The bilateral teleoperation system with a DFR architecture (Fig. 5.10-b) involves a 6-DOF force/torque JR3 force sensor ®(Woodland, CA) and can have different control gains. The force sensor has an internal low-pass filter with a cutoff frequency at 31.25 Hz. Here, a DFR(P+D) controller as described in the last row of Table 5.1 is used and hence the stability condition in the last row of Table 5.2 applies. In Table 5.6, each row shows a selection of control gains for the DFR(P+D) controller. These controller gains and the robot model have been substituted in the stability conditions of Table 5.2. In particular, the stability condition in the (DFR(P+D), Passive) entry of Table 5.2 has led to the stability conclusion (i.e., stable or unstable) listed in the (DFR(P+D), Passive) column of Table 5.6. Similarly, the stability condition in the (DFR(P+D), ISP) entry of Table 5.2 has led to the stability conclusion listed in the (DFR(P+D), ISP) column of Table 5.6. Furthermore, the cases of actual instability of the system manifested by growing or sustained oscillations is observed and listed in the Experiment column of Table 5.6.

Table 5.6: Experiments on a teleoperation system with a DFR controller. The scaling factors are $\lambda = 0.2$ and $\mu = 0.5$.

| # | Controller | | EOP | Theory | | Experiment |
	k_p	k_v		(DFR, passive)	(DFR, ISP)	
1	10	1	0.74	Pot. Unst.	Abs. Stab.	Stable
2	10	2	0.74	Pot. Unst.	Abs. Stab.	Stable
3	20	2	0.74	Pot. Unst.	Abs. Stab.	Stable
4	20	5	0.74	Pot. Unst.	Abs. Stab.	Stable
5	10	1	0.90	Pot. Unst.	Abs. Stab.	Stable
6	10	2	0.90	Pot. Unst.	Abs. Stab.	Stable
7	20	2	0.90	Pot. Unst.	Abs. Stab.	Stable
8	20	5	0.90	Pot. Unst.	Abs. Stab.	Stable

In Fig. 5.15, a comparison between DFR(P+D) and DFR(PD) controllers are made. For both controllers, the parameters and gains are EOP = 0.74, $\lambda = 0.5$, $\mu = 1$, $K_p = 20$, and $k_v = 0.1$. In the experiments, the DFR(P+D) controller (Fig. 5.15-a) is stable while the DFR(PD) experiment (Fig. 5.15-b) is unstable. This

is in agreement with the stability conditions given in the (DFR(P+D), ISP) and (DFR(PD), ISP) entries of Table 5.2.
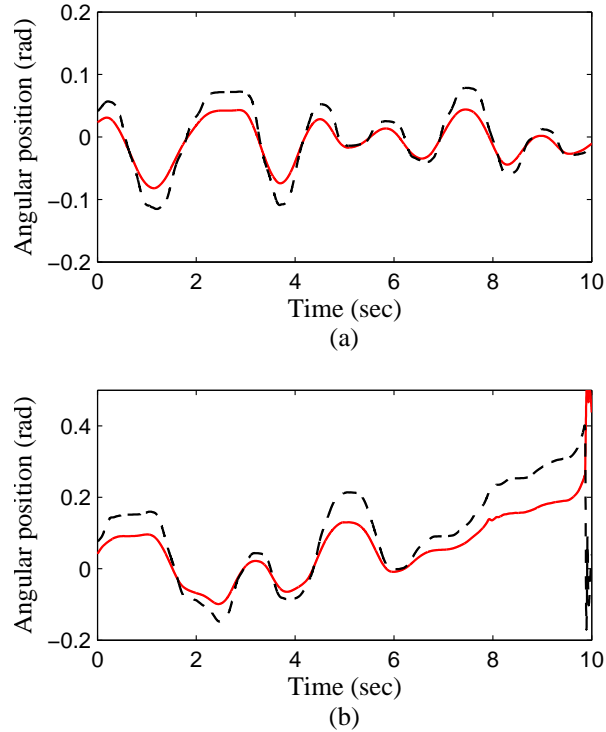
Figure 5.15: Master-slave positions for an ISP environment in DFR teleoperation with (a) a DFR(P+D) controller, and (b) a DFR(PD) controller.

5.6.2 Experiments involving a non-passive operator

5.6.2.1 Experimental setup

Typically, the master is manipulated by a human operator. For reasons described in the following, in this set of experiments, the master is connected to another robot whose task is to manipulate the master. The robot that takes the place of the human operator is called operator emulating robot (OER). Experiments involving a human operator are not easily reproducible due to the fact that every person's arm has a unique physical characteristics. Even for the same human operator, the hand

121

impedance and passivity/activity varies from the beginning to the end of the experiment. Consequently, instead of a human operator, an OER is used to manipulate the master. The OER comprises a controller that allows us to achieve a desired SOP level while ensuring the non-passivity of the OER. In our experimental setup, the OER is a Phantom Omni and is coupled to the master robot as depicted in Fig. 5.16.
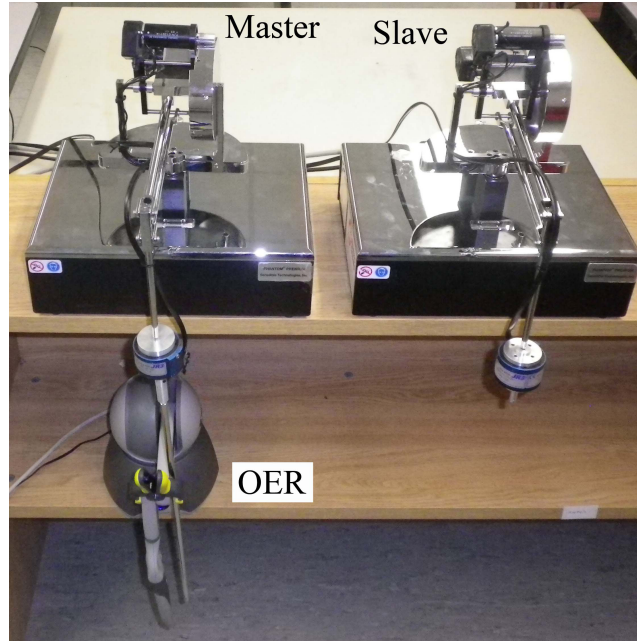
Figure 5.16: An OER is used as a human operator in a bilateral teleoperation systems.

5.6.2.2 PEB architecture

The teleoperation system of Fig. 5.16 was controlled using a PEB controller. Two sets of controller gains were used: (a) $k_{p_m} = 10$, $k_{v_m} = 2$, $k_{p_m} = 10$ and $k_{v_m} = 2$, and (b) $k_{p_m} = 30$, $k_{v_m} = 2$, $k_{p_m} = 10$ and $k_{v_m} = 2$. In a separate experiment, the SOP of the OER was identified to be $\eta = 0.745$. Based on this non-passivity, the stability condition of the (PEB, INP) of Table 5.2 is checked for the two controller gain sets. The stability condition for passive terminations, i.e., the (PEB, Passive) entry of Table 5.2, identifies the system with the first set of control gains as stable and with the second set of gains as unstable. However, both sets of control gains make

the system become unstable in practice. The (PEB, INP) condition of Table 5.2 truly identifies both of the cases as unstable, which is in agreement with practice.

5.7 Conclusions and future work

Conventional stability analysis for two-port network systems relies on the assumption that the one-port network terminations for the two-port network are passive. In the context of bilateral teleoperation systems, where the terminations are the human operator and the environment, this assumption is less than accurate. As a result, the conventional stability analysis will be either invalid (when a termination is non-passive) or overly conservative (when a termination is strictly passive). In this chapter, a powerful stability analysis tool has been developed based on complex-plane Mobius transformations of the termination impedance. The new stability criterion is able to give accurate assessment of (or conditions) for coupled two-port network stability in the presence of a non-passive termination when the conventional stability analysis may fail to identify potential instability. Conversely, the new stability criterion can provide more flexibility in control design in the presence of a strictly-passive termination and, therefore, help to achieve transparency improvement. Although the resulting stability conditions are valid for any two-port network, they are applied to PEB-controlled and DFR-controlled bilateral teleoperation systems and are tested both in simulations and experiments. In the future, the proposed approach can be extended to cases where both terminations of a two-port network are non-passive or strictly-passive. For example, a non-passive human operator may teleoperate a robot interacting with a non-passive (e.g., a beating heart) or a strictly-passive environment (e.g., any environment modeled as a mass-spring-damper). Another useful direction is to extend the approach presented here to multi-port network systems, which represent multilateral haptic teleoperation systems.

Chapter 6

Conclusions and Future Directions

6.1 Conclusions

In the context of stability analysis for bilateral teleoperation systems, conventional passivity and absolute stability analyses involve assumptions that may stop the control design from simultaneously achieving stability and maximum transparency. Specifically, two assumptions are typically made in these stability analyses. The first simplifying assumption is that the entire teleoperation system operates in continuous-time even though we know that the controller implementation inevitably includes discretization components. The second simplifying assumption is about the passivity of the teleoperator terminations, which can be violated (for a non-passive termination) or not restrictive enough (for a strictly-passive termination).

To address the sampled-data teleoperator passivity analysis problem, in this thesis, a passivity criterion was proposed for a bilateral teleoperator that included discrete-time, position-error-based controllers for the master and the slave. The sampled-data system included the exact models of the discretization components, i.e., the zero-order-hold and the sampler. Parseval's theorem was applied to convert the time-domain passivity criterion into the frequency domain. The controllers of the master and the slave must be selected to be inversely proportional to the position scaling in

order to have a closed-form passivity condition. The passivity criterion resulted in a lower bound on the robots damping terms, an upper bound on the sampling time, and bounds on the controller gains. When the master and slave controllers were selected to be PD controllers, the bounds on the gains become upper bounds. This passivity criterion gives guidelines to tune the controller gains while ensuring the stability of the coupled sampled-data teleoperation system. Computer simulations and experiments with a teleoperation system comprising a pair of Phantom Omni robots validated the new passivity criterion.

The above passivity condition was then improved to a less-conservative absolute stability condition in order to obtain a more transparent and still stable teleoperation system. The small gain theorem was applied to find a criterion for absolute stability of a scaled teleoperation system with position-error-based controllers implemented in discrete-time. In lieu of requiring the passivity of the two-port network teleoperator, absolute stability only ensures the stability of the coupled teleoperation system. As a result of reduction in the conservatism compared to the passivity analysis, the absolute stability analysis of a two-port network teleoperator allows the controllers to be selected arbitrarily. In other words, unlike passivity, in absolute stability the controllers do not have to be selected to be inversely proportional to the position scaling. When the controller architecture is known, substituting the controller into the derived absolute stability criterion simplifies to bounds on the controller gains, the sampling time, the master and the slave robot dampings, and the position and force scalings. The resulting criterion was verified through experiments on a teleoperation system including a pair of Phantom Omni robots.

The passivity and absolute stability analyses for two-port networks assume that the terminations are passive. In a teleoperation system, assuming that the terminations of the teleoperator are passive is less than accurate. Therefore, satisfying the conventional absolute stability condition may not guarantee stability (due to a non-passive termination) or may be overly conservative (due to a strictly-passive termination).

A new stability analysis tool is developed for two-port networks using Mobius transformations of the termination impedance in the complex-plane, which considers the excess of passivity or the shortage of passivity of a termination. In the presence of a strictly-passive termination, the new stability criterion provides more flexibility in control design, which can be used to improve transparency. Although the resulting stability conditions are valid for any two-port network, they were applied to a bilateral teleoperation system with a position-error-based or direct-force-reflection controller. The resulting conditions were tested on a pair of Phantom Premium robots.

6.2 Future directions

6.2.1 Passivity and absolute stability analyses for sampled-data teleoperation systems with other control architectures

The passivity and absolute stability conditions developed in the thesis apply to the position-error-based control architecture. The position-error-based control architecture is used in many applications especially when mounting a force sensor at the slave end-effector is not plausible, for instance, due to the confined space or the tool sterilization requirements in the surgical tools. However, in some other applications including material handling, it is feasible to integrate a force sensor at the tip of the slave robot. To benefit from having this force sensor, the control architecture for the sampled-data teleoperation system should be based on the direct force reflection or the four-channel control schemes. The passivity and absolute stability criteria for the sampled-data teleoperation system can therefore be extended to these different control architectures in the future.

6.2.2 Stability analysis for two-port networks when both terminations are non-passive or strictly-passive

The proposed approach for the stability analysis of a two-port network with a non-passive or strictly-passive termination can be extended to cases where both terminations are non-passive or strictly-passive. For example, a non-passive human operator may teleoperate a robot interacting with a non-passive environment (e.g., a beating heart) or a strictly-passive environment (e.g., an environment modeled as a mass-spring-damper). Similar to the reasons given for the stability analysis of a two-port network with a non-passive or strictly-passive termination, non-passivity of terminations can jeopardize the stability of the coupled teleoperation system. Conversely, strict-passivity of terminations allows having more flexibility in the control design. When a two-port network is connected to a non-passive termination and another strictly-passive termination, their impacts may simply cancel out. These issues remain to be studied in the future.

6.2.3 Stability analysis for multi-port networks when terminations are non-passive or strictly-passive

A growing trend in teleoperation research is to extend the current bilateral teleoperation systems to multi-lateral teleoperation systems. For instance, in a trilateral teleoperation system, besides having a human operator and an environment, there is a third termination. In most applications, the third termination is a second human operator that performs a remote task in collaboration with the first human operator. One of the main applications of this dual-user tele-cooperation system is in training of operators (tele-mentoring). For instance, user 1 can be an expert surgeon while user 2 is a protégé. The contribution of each user to the remote task can be tuned by an authority factor. This factor is a number between zero and 1 – zero for a fully expert-controlled system and 1 for a fully protégé-controlled system. As an extension

to the stability analysis of two-port networks with non-passive or strictly-passive terminations, stability of multi-lateral tele-cooperation systems can be analyzed in the future.

6.2.4 Integral quadratic constraints framework for stability analysis of bilateral teleoperation systems

The mathematical framework used in the thesis enabled us to consider non-idealities of teleoperation systems and to investigate their impacts on stability. Another framework to consider is the integral quadratic constraints, which may prove useful in finding the sampled-data passivity and sampled-data absolute stability criteria in a unified formulation. In addition, it may be applied to investigate stability when the terminations are either non-passive or strictly-passive. Applying the integral quadratic constraints has the drawback that it neglects the information regarding the impedance shape of the non-passive or strictly-passive termination. Studying relative advantages and disadvantages remains as future work.

Bibliography

[1] P. F. Hokayem and M. W. Spong. Bilateral teleoperation: An historical survey. *Automatica*, 42(12):2035–2057, 2006. doi: 10.1016/j.automatica.2006.06.027.

[2] G. Niemeyer and J. J. E. Slotine. Telemanipulation with time delays. *International Journal of Robotics Research*, 23(9):873–890, 2004. doi: 10.1177/0278364904045563.

[3] S. Salcudean. Control for teleoperation and haptic interfaces. In Bruno Siciliano and Kimon Valavanis, editors, *Control Problems in Robotics and Automation*, volume 230 of *Lecture Notes in Control and Information Sciences*, pages 51–66. Springer Berlin / Heidelberg, 1998.

[4] P. Arcara and C. Melchiorri. Control schemes for teleoperation with time delay: A comparative study. *Robotics and Autonomous Systems*, (38):49–64, 2002.

[5] A. Jazayeri and M. Tavakoli. A passivity criterion for sampled-data bilateral teleoperation systems. *IEEE Transactions on Haptics*, (2012), 2012. doi: 10.1109/TOH.2012.73.

[6] A. Jazayeri and M. Tavakoli. A passivity criterion for sampled-data bilateral teleoperation systems. In *Proceedings of World Haptics Conference*, Istanbul, Turkey, 2011.

[7] A. Jazayeri and M. Tavakoli. Absolute stability analysis of sampled-data scaled bilateral teleoperation systems. *Control Engineering Practice*, 21(8):1053–1064, 2013.

[8] A. Jazayeri and M. Tavakoli. Stability analysis of sampled-data teleoperation systems. In *Proceedings of Conference on Decision and Control*, pages 3608–3613, Atlanta, GA, 2010.

[9] A. Jazayeri and M. Tavakoli. Revisiting Llewellyns absolute stability criterion for bilateral teleoperation systems under non-passive operator or environment. In *Proceedings of the 2012 IEEE/RSJ International Conference on Intelligent Robots and Systems (IROS)*, volume 1, pages 70–75, Vilamoura, Portugal, 2012.

[10] A. Jazayeri, M. Dyck, and M. Tavakoli. Stability analysis of teleoperation systems under strictly passive and non-passive operator. In *Proceedings of the IEEE World Haptics Conference*, Daejeon, Korea, 2013.

[11] A. Jazayeri and M. Tavakoli. Bilateral teleoperation system stability with non-passive and strictly-passive operator or environment. *IEEE Transactions on Control Systems Technology*, 2013 submitted.

[12] M. Dyck, A. Jazayeri, and M. Tavakoli. Is the human operator in a teleoperation system passive? In *Proceedings of the IEEE World Haptics Conference*, Daejeon, Korea, 2013.

[13] T. B. Sheridan. Telerobotics. *Automatica*, 25(4):487–507, 1989.

[14] W. R. Ferrell and T. B. Sheridan. Supervisory control of remote manipulation. *Spectrum, IEEE*, 4(10):81–88, 1967. doi: 10.1109/MSPEC.1967.5217126.

[15] W. S. Kim A. K. Bejczy, S. Venema. Role of computer graphics in space telerobotics: Preview and predictive displays. *Cooperative Intelligent Robotics in Space*, 1387:365–377, 1990.

[16] G. Niemeyer and J.-J. E. Slotine. Toward bilateral internet teleoperation. *Beyond webcams: An introduction to online robots*, pages 193–214, 2001.

[17] G. Niemeyer, C. Preusche, and G. Hirzinger. Telerobotics. *Springer Handbook of Robotics*, pages 1339–1350, 2008.

[18] J. Cui, S. Tosunoglu, R. Roberts, C. Moore, and D. W. Repperger. A review of teleoperation system control. In *Proceedings of the Florida Conference on Recent Advances in Robotics*, 2003.

[19] R. A. Faust. *Robotics in Surgery: History, Current And Future Applications.* Nova Science Pub Inc, New York, 2006. ISBN 1600213863.

[20] M. Ghodoussi, S. E. Butner, and Y. Wang. Robotic surgery – the transatlantic case. In *Proceedings of the IEEE International Conference on Robotics and Automation*, volume 2, pages 1882–1888, 2002.

[21] S. E. Butner and M. Ghodoussi. Transforming a surgical robot for human telesurgery. *IEEE Transactions on Robotics and Automation*, 19(5):818–824, 2003. doi: 10.1109/TRA.2003.817214.

[22] S. Lee, G. Bekey, and A. K. Bejczy. Computer control of space-borne teleoperators with sensory feedback. In *Proceedings of the IEEE International Conference on Robotics and Automation*, volume 2, pages 205–214, 1985.

[23] L. M. Jenkins. Telerobotic work system-space robotics application. In *Proceedings of the IEEE International Conference on Robotics and Automation*, volume 3, pages 804–806, 1986.

[24] A. K. Bejczy and Z. Szakaly. Universal computer control systems (uccs) for space telerobots. In *Proceedings of the IEEE International Conference on Robotics and Automation*, volume 4, pages 318–324, 1987.

[25] Y. Tsumaki and M. M. Uchiyama. A model-based space teleoperation system with robustness against modeling errors. In *Proceedings of the IEEE Conference on Robotics and Automation*, volume 2, pages 1594–1599 vol.2, 1997.

[26] M. Nohmi. Space teleoperation using force reflection of communication time delay. In *Proceedings of the IEEE/RSJ International Conference on Intelligent Robots and Systems*, volume 3, pages 2809–2814 vol.3, 2003.

[27] T. Xia, S. Leonard, A. Deguet, L. Whitcomb, and P. Kazanzides. Augmented reality environment with virtual fixtures for robotic telemanipulation in space. In *Proceedings of the IEEE/RSJ International Conference on Intelligent Robots and Systems*, pages 5059–5064, 2012.

[28] W.-K. Yoon, T. Goshozono, H. Kawabe, M. Kinami, Y. Tsumaki, M. Uchiyama, M. Oda, and T. Doi. Model-based space robot teleoperation of ets-vii manipulator. *IEEE Transactions on Robotics and Automation*, 20(3):602–612, 2004. doi: 10.1109/TRA.2004.824700.

[29] X. Wang, H. Liu, W. Xu, B. Liang, and Y. Zhang. A ground-based validation system of teleoperation for a space robot. *International Journal of Advanced Robotic Systems*, 9(115), 2012.

[30] G. Hirzinger. The space and telerobotic concepts of the dfvlr rotex. In *Proceedings of the IEEE International Conference on Robotics and Automation*, volume 4, pages 443–449, 1987.

[31] G. Hirzinger, J. Heindl, and K. Landzettel. Predictive and knowledge-based telerobotic control concepts. In *Proceedings of the IEEE International Conference on Robotics and Automation*, pages 1768–1777 vol.3, 1989.

[32] G. Hirzinger, B. Brunner, J. Dietrich, and J. Heindl. Sensor-based space robotics-rotex and its telerobotic features. *IEEE Transactions on Robotics and Automation*, 9(5):649–663, 1993.

[33] N.Y. Lii, Zhaopeng Chen, B. Pleintinger, C.H. Borst, G. Hirzinger, and A. Schiele. Toward understanding the effects of visual- and force-feedback on robotic hand grasping performance for space teleoperation. In *Proceedings of the IEEE/RSJ International Conference on Intelligent Robots and Systems*, pages 3745–3752, 2010.

[34] T. B. Sheridan. Teleoperation, telerobotics and telepresence: A progress report. *Control Engineering Practice*, 3(2):205–214, 1995.

[35] T. Imaida, Y. Yokokohji, T. Doi, M. Oda, and T. Yoshikawa. Ground-space bilateral teleoperation of ets-vii robot arm by direct bilateral coupling under

7-s time delay condition. *IEEE Transactions on Robotics and Automation*, 20 (3):499–511, 2004. doi: 10.1109/TRA.2004.825271.

[36] R. Uhrich. Terminus controlled deep ocean manipulator. In *Proceedings of IEEE International Conference on Engineering in the Ocean Environment*, pages 301–304, 1973.

[37] T. B. Sheridan and W. L. Verplank. Human and computer control of undersea teleoperators. Technical report, DTIC Document, 1978.

[38] C. Domingues, M. Essabbah, N. Cheaib, S. Otmane, A. Dinis, et al. Human-robot-interfaces based on mixed reality for underwater robot teleoperation. In *Proceedings of IFAC Conference on Manoeuvring and Control of Marine Craft*, 2012.

[39] J. Funda and R. P. Paul. A symbolic teleoperator interface for time-delayed underwater robot manipulation. In *Proceedings of Ocean Technologies and Opportunities in the Pacific for the 90's*, pages 1526–1533, 1991.

[40] T. Hirabayashi, J. Akizono, T. Yamamoto, H. Sakai, and H. Yano. Teleoperation of construction machines with haptic information for underwater applications. *Automation in construction*, 15(5):563–570, 2006.

[41] R. H. Taylor and D. Stoianovici. Medical robotics in computer-integrated surgery. *IEEE Transactions on Robotics and Automation*, 19:765–781, 2003.

[42] S. Najarian, M. Fallahnezhad, and E. Afshari. Advances in medical robotic systems with specific applications in surgery – a review. *Journal of Medical Engineering & Technology*, 35(1):19–33, 2011.

[43] J. Funda, R. H. Taylor, B. Eldridge, S. Gomory, and K. G. Gruben. Constrained cartesian motion control for teleoperated surgical robots. *IEEE Transactions on Robotics and Automation*, 12(3):453–465, 1996.

[44] G. S. Guthart and J. K. Salisbury. The intuitive (TM) telesurgery system: overview and application. In *Proceedings of the IEEE International Conference on Robotics and Automation*, volume 1, pages 618–621, 2000.

[45] G. T. Sung and I. S. Gill. Robotic laparoscopic surgery: a comparison of the da Vinci and Zeus systems. *Urology*, 58(6):893–898, 2001.

[46] E. O. Kwon, T. C. Bautista, J. M. Blumberg, H. Jung, K. Tamaddon, S. R. Aboseif, S. G. Williams, and G. W. Chien. Rapid implementation of a robot-assisted prostatectomy program in a large health maintenance organization setting. *Journal of Endourology*, 24(3):461–465, 2010.

[47] R. W. Holloway, S. D. Patel, and S. Ahmad. Robotic surgery in gynecology. *Scandinavian Journal of Surgery*, 98(2):96, 2009.

[48] R. S. McClure, B. Kiaii, R. J. Novick, R. Rayman, S. Swinamer, K. Kodera, and A. H. Menkis. Computer-enhanced telemanipulation in mitral valve repair: preliminary experience in canada with the da vinci robotic system. *Canadian journal of surgery*, 49(3):193, 2006.

[49] L. Nifong, V. F. Chu, B. M. Bailey, D. M. Maziarz, V. L. Sorrell, D. Holbert, and W. R. Chitwood. Robotic mitral valve repair: experience with the da vinci system. *The Annals of thoracic surgery*, 75(2):438–443, 2003.

[50] G. R. Sutherland, I. Latour, and A. D. Greer. Integrating an image-guided robot with intraoperative mri. *IEEE Engineering in Medicine and Biology Magazine*, 27(3):59–65, 2008.

[51] W. Wei and Y. Kui. Teleoperated manipulator for leak detection of sealed radioactive sources. In *Proceedings of the IEEE International Conference on Robotics and Automation*, volume 2, pages 1682–1687, 2004.

[52] J. Barrio, F. Suarez-Ruiz, M. Ferre, and R. Aracil. A rate-position haptic controller for large telemanipulation workspaces. In *Proceedings of the IEEE/RSJ International Conference on Intelligent Robots and Systems*, pages 58–63, 2012.

[53] S. Lee, G. Sukhatme, G. J. Kim, and C.-M. Park. Haptic teleoperation of a mobile robot: a user study. *Presence: Teleoperators & Virtual Environments*, 14(3):345–365, 2005.

[54] N. Diolaiti and C. Melchiorri. Teleoperation of a mobile robot through haptic feedback. In *Proceedings of IEEE International Workshop on Haptic Virtual Environments and Their Applications*, pages 67–72, 2002.

[55] O. Linda and M. Manic. Self-organizing fuzzy haptic teleoperation of mobile robot using sparse sonar data. *IEEE Transactions on Industrial Electronics*, 58 (8):3187–3195, 2011.

[56] O. J. Rösch, K. Schilling, and H. Roth. Haptic interfaces for the remote control of mobile robots. *Control Engineering Practice*, 10(11):1309–1313, 2002.

[57] S.-G. Hong, J.-J. Lee, and S. Kim. Generating artificial force for feedback control of teleoperated mobile robots. In *Proceedings of the IEEE/RSJ International Conference on Intelligent Robots and Systems*, volume 3, pages 1721–1726, 1999.

[58] J. Lim, J. Ko, and J. Lee. Internet-based teleoperation of a mobile robot with force-reflection. In *Proceedings of IEEE Conference on Control Applications*, volume 1, pages 680–685, 2003.

[59] A. H. Herdocia, A. Shademan, and M. Jagersand. Unimodal asymmetric interface for teleoperation of mobile manipulators: A user study. In *Proceedings of the IEEE/RSJ International Conference on Intelligent Robots and Systems*, pages 5214–5219, 2012.

[60] H. V. Quang, I. Farkhatdinov, and J.-H. Ryu. Passivity of delayed bilateral teleoperation of mobile robots with ambiguous causalities: Time domain passivity approach. In *Proceedings of the IEEE/RSJ International Conference on Intelligent Robots and Systems*, pages 2635–2640, 2012.

[61] A. Y. Mersha, S. Stramigioli, and R. Carloni. Switching-based mapping and control for haptic teleoperation of aerial robots. In *Proceedings of the IEEE/RSJ International Conference on Intelligent Robots and Systems*, pages 2629–2634, 2012.

[62] D. Lee, A. Franchi, P. R. Giordano, H. I. Son, and H. H. Bulthoff. Haptic teleoperation of multiple unmanned aerial vehicles over the internet. In *Proceedings of the IEEE International Conference on Robotics and Automation*, pages 1341–1347, 2011.

[63] S. Stramigioli, R. Mahony, and P. Corke. A novel approach to haptic teleoperation of aerial robot vehicles. In *Proceedings of the IEEE International Conference on Robotics and Automation*, pages 5302–5308, 2010.

[64] M. Bergamasco, A. Frisoli, and C. Avizzano. Exoskeletons as man-machine interface systems for teleoperation and interaction in virtual environments. *Advances in Telerobotics*, pages 61–76, 2007.

[65] S. F. Atashzar, I. G. Polushin, and R. V. Patel. Networked teleoperation with non-passive environment: Application to tele-rehabilitation. In *Proceedings of the IEEE/RSJ International Conference on Intelligent Robots and Systems*, pages 5125–5130, 2012.

[66] D. A. Lawrence. Stability and transparency in bilateral teleoperation. *IEEE Transactions on Robotics & Automation*, 9:624–637, 1993. doi: 10.1109/CDC. 1992.371336.

[67] Y. Yokokohji and T. Yoshikawa. Bilateral control of master-slave manipulators for ideal kinesthetic coupling–formulation and experiment. *IEEE Transactions on Robotics and Automation*, 10(5):605–620, 1994.

[68] K. B. Fite, L. Shao, and M. Goldfarb. Loop shaping for transparency and stability robustness in bilateral telemanipulation. *IEEE Transactions on Robotics and Automation*, 20(3):620–624, 2004. doi: 10.1109/TRA.2004.825474.

[69] B. Hannaford and L. Wood. Performance evaluation of a 6 axis high fidelity generalized force reflecting teleoperator. In *Proceedings of JPL/NASA Conference on Space Telerobotics*, pages 89–97, Pasadena, CA, 1989.

[70] A. Aziminejad, M. Tavakoli, R. V. Patel, and M. Moallem. Transparent time-delayed bilateral teleoperation using wave variables. *IEEE Transactions on Control Systems Technology*, 16(3):548–555, 2008. doi: 10.1109/TCST.2007. 908222.

[71] S. S. Haykin. *Active Network Theory*. Addison-Wesley, Reading, MA, 1970.

[72] B. Hannaford. A design framework for teleoperators with kinesthetic feedback. *IEEE Transactions on Robotics and Automation*, 5:426–434, 1989.

[73] N. Hogan. Controlling impedance at the man/machine interface. In *Proceedings of IEEE International Conference on Robotics and Automation*, pages 1626–1631 vol.3, 1989.

[74] V. Mendez and M. Tavakoli. A passivity criterion for n-port multilateral haptic systems. In *Proceedings of Conference on Decision and Control*, pages 3608–3613, Atlanta, GA, 2010.

[75] G. M. H. Leung and B. A. Francis. Bilateral control of teleoperators with time delay through a digital communication channel. In *Proceedings of the Thirtieth Annual Allerton Conference on Communication, Control and Computing*, pages 692–701, 1992.

[76] M. Tavakoli, A. Aziminejad, R. V. Patel, and M. Moallem. Discrete-time bilateral teleoperation: modelling and stability analysis. *Control Theory and Applications, IET*, 2(6):496–512, 2008. doi: 10.1049/iet-cta:20070195.

[77] R. B. Gillespie and M. Cutkosky. Stable user-specific rendering of the virtual wall. In *Proceedings of the ASME International Mechanical Engineering Conference and Exposition*, volume 58, pages 397–406, Atlanta, GA, 1996.

[78] J. Artigas, C. Preusche, G. Hirzinger, G. Borghesan, and C. Melchiorri. Bilateral energy transfer in delayed teleoperation on the time domain. In *IEEE International Conference on Robotics and Automation*, pages 671–676, 2008.

[79] R. Sepulchre, M. Jankovic, and P. V. Kokotovic. *Constructive nonlinear control*. Springer, 2012. ISBN 0201558661.

[80] P. F. Hokayem and M. W. Spong. Bilateral teleoperation: An historical survey. *Automatica*, 42(12):2035–2057, 2006.

[81] R. J. Anderson and M. W. Spong. Asymptotic Stability for Force Reflecting Teleoperators with Time Delay. *The International Journal of Robotics Research*, 11(2):135–149, 1992. doi: 10.1177/027836499201100204.

[82] J. E. Colgate and G. G. Schenkel. Passivity of a class of sampled-data systems: Application to haptic interfaces. *Journal of Robotic Systems*, 14(1):37–47, 1997.

[83] J. J. Gil, A. Avello, A. Rubio, and J. Florez. Stability analysis of a 1 DOF haptic interface using the routh-hurwitz criterion. *IEEE Transactions on Control Systems Technology*, 12(4):583–588, 2004.

[84] N. Diolaiti, G. Niemeyer, F. Barbagli, and J. K. Salisbury. Stability of haptic rendering: discretization, quantization, time delay, and coulomb effects. *IEEE Transactions on Robotics*, 22(2):256–268, 2006.

[85] J. J. Abbott and A. M. Okamura. Effects of position quantization and sampling rate on virtual wall passivity. *IEEE Transactions on Robotics*, 21(5):952–964, 2005.

[86] P. Berestesky, N. Chopra, and M. W. Spong. Discrete time passivity in bilateral teleoperation over the Internet. In *Proceedings of International Conference on Robotics and Automation*, pages 4557–4564, New Orleans, LA, 2004.

[87] K. Kosuge and H. Murayama. Bilateral feedback control of telemanipulator via computer network in discrete time domain. In *Proceedings of IEEE International Conference on Robotics and Automation*, volume 3, pages 2219–2224, 1997.

[88] J. H. Ryu, D. S. Kwon, and B. Hannaford. Stable teleoperation with time-domain passivity control. *IEEE Transactions on Robotics and Automation*, 20 (2):365–373, 2004. doi: 10.1109/TRA.2004.824689.

[89] S. Stramigioli, C. Secchi, A. J. van der Schaft, and C. Fantuzzi. A novel theory for sample data system passivity. In *Proceedings of the IEEE/RSJ International Conference on Intelligent Robots and Systems*, pages 1936–1941, Lausanne, Switzerland, 2002.

[90] K. Ogata. *Discrete-Time Control Systems*. Prentice Hall, 2nd edition, 1995. ISBN 0130342815.

[91] M. S. Fadali and A. Visioli. *Digital control engineering: analysis and design*. Electronics & Electrical. Academic/Elsevier, 2009. ISBN 9780123744982.

[92] A. V. Oppenheim, A. S. Willsky, and I. T. Young. *Signals and systems*. Prentice-Hall signal processing series. Prentice-Hall International, 1996. ISBN 9780138111755.

[93] M. Tavakoli, A. Aziminejad, R.V. Patel, and M. Moallem. High-fidelity bilateral teleoperation systems and the effect of multimodal haptics. *IEEE Transactions on Systems, Man and Cybernetics – Part B*, 37(6):1512–1528, 2007. doi: 10.1109/TSMCB.2007.903700.

[94] E. Naerum and B. Hannaford. Global transparency analysis of the lawrence teleoperator architecture. In *Proceedings of IEEE International Conference on Robotics and Automation*, pages 4344–4349, 2009.

[95] K. Hashtrudi-Zaad and S. E. Salcudean. Transparency in time delay systems and the effect of local force feedback for transparent teleoperation. *IEEE Transactions on Robotics and Automation*, 18(1):108–114, 2002.

[96] Y. Matsuoka and R. D. Howe. Hand impedance change during learning of a novel contact task. In *World Congress on Medical Physics and Biomedical Engineering*, 2000.

[97] R. J. Anderson and M. W. Spong. Bilateral control of teleoperators with time delay. *IEEE Transactions on Automatic Control*, 34(5):494 –501, 1989. doi: 10.1109/9.24201.

[98] E. Nuno, L. Basanez, and R. Ortega. Passivity-based control for bilateral teleoperation: A tutorial. *Automatica*, 47(3):485–495, 2011. doi: 10.1016/j.automatica.2011.01.004.

[99] M. Mahvash and A. M. Okamura. Enhancing transparency of a position-exchange teleoperator. *World Haptics Conference*, pages 470–475, 2007.

[100] H. C. Cho and J. H. Park. Stable bilateral teleoperation under a time delay using a robust impedance control. *Mechatronics*, 15(5):611–625, 2005.

[101] J. J. Abbott and A. M. Okamura. Analysis of virtual fixture contact stability for telemanipulation. In *Proceedings of IEEE/RSJ International Conference on Intelligent Robots and Systems*, volume 3, pages 2699–2706, 2003.

[102] A. Haddadi and K. Hashtrudi-Zaad. Least conservative robust stability condition for linear bilateral teleoperation control systems. In *Proceedings of the EuroHaptics conference and Symposium on Haptic Interfaces for Virtual Environment and Teleoperator Systems. World Haptics*, pages 220–225, 2009.

[103] K. Kosuge, T. Itoh, and T. Fukuda. Scaled telemanipulation with communication time delay. In *Proceedings of the IEEE Conference on Robotics and Automation*, volume 3, pages 2019–2024 vol.3, 1996.

[104] H. C. Cho and J. H. Park. Impedance controller design of Internet-based teleoperation using absolute stability concept. In *IEEE/RSJ International Conference on Intelligent Robots and Systems, 2002*, volume 3, pages 2256–2261 vol.3, 2002.

[105] M. Boukhnifer and A. Ferreira. Wave-based passive control for transparent micro-teleoperation system. *Robotics and Autonomous Systems*, 54(7):601–615, 2006.

[106] P. X. Liu and J. Sheng. A review of bilateral sampled-data control of teleoperators. In *IEEE International Conference on Robotics and Biomimetics, 2004.*, pages 385–390, 2004.

[107] A. v. d. Schaft. *L2-Gain and Passivity in Nonlinear Control*. Springer-Verlag New York, Inc., Secaucus, NJ, USA, 2nd edition, 1999. ISBN 1852330732.

[108] J. Yan and S.E. Salcudean. Teleoperation controller design using h_∞-optimization with application to motion-scaling. *IEEE Transactions on Control Systems Technology*, 4(3):244–258, 1996. doi: 10.1109/87.491198.

[109] P. F. Hokayem and M. W. Spong. Bilateral teleoperation: An historical survey. *Automatica*, 42(12):2035–2057, 2006. doi: 10.1016/j.automatica.2006.06.027.

[110] D. Lee and M.W. Spong. Passive bilateral teleoperation with constant time delay. *IEEE Transactions on Robotics*, 22(2):269 –281, April 2006. doi: 10. 1109/TRO.2005.862037.

[111] J. Li, M. Tavakoli, V. Mendez, and Q. Huang. Conservatism of passivity criteria for stability analysis of trilateral haptic systems. In *Proceedings of the IEEE World Haptics Conference 2013*, Daejeon, Korea, 2013.

[112] J. Kim, P. H. Chang, and H.-S. Park. Two-channel transparency-optimized control architectures in bilateral teleoperation with time delay. *IEEE Transactions on Control Systems Technology*, 21(1):40–51, 2013. doi: 10.1109/TCST. 2011.2172945.

[113] F. B. Llewellyn. Some fundamental properties of transmission systems. *Proceedings of the IRE*, 40(3):271–283, 1952.

[114] R. J. Adams and B. Hannaford. Stable haptic interaction with virtual environments. *IEEE Transactions on Robotics and Automation*, 15(3):465–474, 1999.

[115] K. Hashtrudi-Zaad and S. E. Salcudean. Analysis of control architectures for teleoperation systems with impedance/admittance master and slave manipulators. *The International Journal of Robotics Research*, 20(6):419–445, 2001.

[116] A. Aziminejad, M. Tavakoli, R. V. Patel, and M. Moallem. Transparent time-delayed bilateral teleoperation using wave variables. *IEEE Transactions on Control Systems Technology*, 16(3):548–555, 2008. doi: 10.1109/TCST.2007. 908222.

[117] I. Aliaga, A. Rubio, and E. Sanchez. Experimental quantitative comparison of different control architectures for master-slave teleoperation. *IEEE Transactions on Control Systems Technology*, 12(1):2–11, 2004.

[118] W. H. Ku. Stability of linear active nonreciprocal n-ports. *Journal of the Franklin Institute*, 276(3):207–224, 1963. doi: 10.1016/0016-0032(63)90383-1.

[119] H. Marquez. *Nonlinear Control Systems: Analysis and Design.* Wiley-Interscience, 2003. ISBN 0471427993.

[120] R. J. Adams and B. Hannaford. Control law design for haptic interfaces to virtual reality. *IEEE Transactions on Control Systems Technology*, 10(1):3–13, 2002. doi: 10.1109/87.974333.

[121] A. Haddadi and K. Hashtrudi-Zaad. Robust stability of teleoperation systems with time delay: A new approach. *IEEE Transactions on Haptics*, (99), 2012. doi: 10.1109/TOH.2012.52.

[122] I. Polat and C. W. Scherer. Stability analysis for bilateral teleoperation: An IQC formulation. *IEEE Transactions on Robotics*, 28(6):1294–1308, 2012. doi: 10.1109/TRO.2012.2209230.

[123] R. Lozano, B. Maschke, B. Brogliato, and O. Egeland. *Dissipative Systems Analysis and Control: Theory and Applications.* Springer-Verlag New York, Inc., Secaucus, NJ, USA, 2007. ISBN 184628516X.

[124] J. W. Hill and J. F. Jensen. Telepresence technology in medicine: Principles and applications. *Proceedings of the IEEE*, 86(3):569–80, 1998. doi: 10.1109/5.662880.

[125] M. W. Spong and M. Vidyasagar. *Robot Dynamics and Control.* John Wiley & Sons, 2008.

[126] A. Isidori. *Nonlinear control systems*, volume 2. Springer Verlag, 1999.

[127] D. J. Hill and P. J. Moylan. Stability results for nonlinear feedback systems. *Automatica*, 13(4):377–382, 1977. doi: 10.1016/0005-1098(77)90020-6.

[128] H. Khalil. *Nonlinear Systems.* Prentice Hall, 3rd edition, 2001. ISBN 0130673897.

[129] J. J. E. Slotine and W. Li. *Applied nonlinear control.* Prentice-Hall Englewood Cliffs, NJ, 1991.

[130] N. Levinson and R. M. Redheffer. *Complex Variables.* McGraw-Hill, 1970. ISBN 0816251045.

[131] A. Haddadi and K. Hashtrudi-Zaad. Bounded-impedance absolute stability of bilateral teleoperation control systems. *IEEE Transactions on Haptics*, 3(1):15 –27, 2010. doi: 10.1109/TOH.2009.48.

[132] F. C.T. van der Helm, A. C. Schouten, E. de Vlugt, and G. G. Brouwn. Identification of intrinsic and reflexive components of human arm dynamics during postural control. *Journal of neuroscience methods*, 119(1):1–14, 2002. doi: 10.1016/S0165-0270(02)00147-4.

[133] K. Park, , and P. H. Chang. Stochastic estimation of human shoulder impedance with robots: An experimental design. In *Proceedings of the IEEE International Conference on Rehabilitation Robotics*, volume 2011, pages 1–8, 2011.

[134] B. Willaert, B. Corteville, D. Reynaerts, H. van Brussel, and E. B. van der Poorten. A mechatronic analysis of the classical position-force controller based on bounded environment passivity. *The International Journal of Robotics Research*, 30(4):444–462, 2011. doi: 10.1177/0278364910378334.

[135] M. C. Cavusoglu and D. Feygin. Kinematics and dynamics of phantom model 1.5, haptic interface. Technical Report UCB/ERL M01/15, EECS Department, University of California, Berkeley, 2001.

[136] E. Naerum, J. Cornella, and O.J. Elle. Wavelet networks for estimation of coupled friction in robotic manipulators. In *Proceedings of IEEE International Conference on Robotics and Automation, 2008*, pages 862–867, 2008.

[137] Lennart Ljung. *System Identification: Theory for the User (2nd Edition)*. Prentice Hall, 2 edition, January 1999. ISBN 0136566952.

Appendix A

Stability of continuous-time teleoperation with DFR control

The controller defined in (4.2) is a PEB controller, which is the most commonly used controlled due to the fact that it does not require force measurement. In another controller method, the slave environment contact forces are measured and transmitted to the master side, which is known as direct force reflecting (DFR) control. In the following it will be shown that the absolute stability analysis of the continuous-time teleoperation system with a DFR control is not satisfied and hence the absolute stability of the sampled-data teleoperation system is not satisfied. For a continuous-time bilateral teleoperation system the hybrid matrix for the DFR (also known as force-position) control reads as

$$H = \begin{bmatrix} Z_m & 1 \\ -\frac{C_s}{Z_{ts}} & \frac{1}{Z_{ts}} \end{bmatrix} \tag{A.1}$$

where $Z_{ts} = Z_s + C_s$, Z_s and Z_m are the impedance of the slave robots, and C_s is the slave controller. It can be seen that free motion force tracking is achieved $H_{12} = 1$ but free-motion impedance which is ideally zero cannot be accomplished $H_{11} \neq 0$. Obviously, the free-motion impedance H_{11} in the DFR case is closer to zero compared to the PEB controller 3.63. As it can be seen, for both PEB and DFR controllers the hybrid matrices cannot reach the values of the ideal transparency matrix because of H_{12} and H_{22} values, which emphasizes that for ideal transparency at least three channel of the 4-channel controllers are required.

Theorem A.1. *The teleoperation system with a DFR controller is absolutely stable if the controller derivative and proportional gains are positive, i.e. $k_{v_s}, k_{p_s} > 0$ and also $|C_s| \gg |Z_s|$.*

Proof. The Llewelly'n absolute stability criterion described in Section 2.4.4, is valid for all immitance parameters including hybrid matrix **H**. In the following the hybrid matrix A.1 will be tested in the Llewellyn's criterion.

First, H_{11} has no poles and the characteristic polynomial for H_{22} is $M_s s^2 + k_{v_s} s + k_{p_s}$, which has no RHP poles if $k_{v_s}, k_{p_s} > 0$. Also, $\mathrm{Re}\, H_{11} = 0$ and $\mathrm{Re}\, H_{22}$ is

$$\mathrm{Re}\, H_{22} = \frac{k_{v_s}}{k_{v_s}^2 + (-k_{p_s}/\omega + M_s\omega)^2} \tag{A.2}$$

which is non-negative if $k_{v_s} > 0$. In addition, the third condition in (2.2) yields

$$\mathrm{Re}\left(\frac{C_s}{C_s + Z_s}\right) - \left|\frac{C_s}{C_s + Z_s}\right| \geq 0 \tag{A.3}$$

which is possible only when the controller C_s is greater than the impedance of the slave robot $|C_s| \gg |Z_s|$. $\square$

Based on the Theorem (A.1), the continuous-time teleoperation system with DFR

controller is absolutely stable only if the controller gains are set to be infinity. For a sampled-data system, since discretization does not make an unstable system stable, the sampled-data equivalent system is not stable.

Appendix B

Phantom Omni modelling and identification

In this appendix dynamic model of the Phantom Omni has been shown and the parameters have been determined through grey box system identification. The first joint is the yaw angle and rotates the rest of the robot around the vertical axis. The other two joints form a parallel, cable driven mechanism in which the actuators are lumped on the main rotating body of the robot.

The dynamic model of the robot is

$$M_I(q)\ddot{q} + C_I(q,\dot{q})\dot{q} + F_r(\dot{q}) + G(q) = \tau \tag{B.1}$$

where $M_I(q)$ is the inertial term of the robot, $C_I(q,\dot{q})$ is the Coriolis and Centrifugial term, $F_r(\dot{q})$ is the friction term and $G(q)$ is the gravity term. The right hand side is the torque output vector. Also, q is the state vector $q = [\theta_1 \ \theta_2 \ \theta_3]^T$.

The values for the terms $M_I(q)$, $C_I(q,\dot{q})$ and $G(q)$ are derived in [135] for Phantom Premium which has the same structure as Phantom Omni. The friction term $F_r(\dot{q})$

comprises two terms

$$F_r(\dot{q}) = F_v \dot{q} + F_d(\dot{q}) \tag{B.2}$$

where F_v is Viscous coefficient which is assumed to be a diagonal matrix – uncoupled friction on the three joints. Also, $F_d(\dot{q})$ is the dynamic friction term which is a diagonal matrix function of signum of the velocity vector $F_d(\dot{q}) = \text{diag}(K_{d,i}\text{sgn}(\dot{q}_i))$. Using system identification for Phantom Omni robot, in [136] the values of dynamic friction term have been found to be

$$K_d = [1.980e - 2, \; 2.011e - 2, \; 1.689e - 2]^T \tag{B.3}$$

In the experiment of Chapter 3, the second and the third joints of the robot have been controlled by a stiff controller and the experiment is done on the first joint of the robot. The robot dynamic matrices will result in

$$M_{11}\ddot{\theta}_1 + K_{d,1}\text{sgn}(\dot{\theta}_1) + \text{K}_{v,1}\dot{\theta}_1 = \tau \tag{B.4}$$

The parameters of the linear terms of (B.4) have been found through system identification [137]: $M_{11} = 1.503 \times 10^{-2} \pm 1.7 \times 10^{-4}\text{Kg.m}^2$ and $K_{v,1} = 4.624 \times 10^{-2} \pm 1.1 \times 10^{-3}\text{Kg.s.m}^2$ and the parameter of the nonlinear term is $K_d(1)$ in (B.3). The latter term is internally compensated (as a feedforward term) in the dynamic model for the experimental results. For the linear terms M_{11} and $K_{v,1}$, the identification signals is a multiple sine with parameters of Table B.1.

Table B.1: Parameters of the multisine identification signal

Frequency (rad/sec)	Amplitude
1.884	0.017
3.142	0.02
4.712	0.18
6.283	0.34

Appendix C

Force observer

Passivity of the experiments have been determined using the time-domain passivity definition (3.41). While in the simulation, the signals are available for calculation the energy integral, in the experiments, it is required to estimate the forces from the robot model and the measured signals. To achieve this goal, this appendix discusses a force observer method. It should be noted that calculating the energy integral is done offline and after the experiments and the estimated force using this method is not used in the control loop for feedback.

The robot dynamic model (3.32) may be used to estimate the hand force knowing the master position and the applied master force:

$$f_h = f_m - m_m \ddot{x}_m - b_m \dot{x}_m \tag{C.1}$$

However, the direct method requires the acceleration of the master robot, which may be noisy because of the differentiation. To overcome this problem, a force observer is used in the following.

$$\dot{\hat{f}}_h = -l(x_m, \dot{x}_m)\hat{f}_h + l(x_m, \dot{x}_m)(f_m - m_m \ddot{x}_m - b_m \dot{x}_m) \tag{C.2}$$

where $\hat{f}_h$ is the estimated hand force and $l(x_m, \dot{x}_m)$ is the observer gain. The observer error is defined as $e_h = f_h - \hat{f}_h$, which leads to

$$\dot{e}_h = \dot{f}_h - \dot{\hat{f}}_h = \dot{f}_h + l(x_m, \dot{x}_m)\hat{f}_h - l(x_m, \dot{x}_m)f_h \tag{C.3}$$

The auxiliary variable z is defined as

$$z = \hat{f}_h - p(x_m, \dot{x}_m) \tag{C.4}$$

where $p(x_m, \dot{x}_m)$ is determined based on the observer gain as

$$\frac{d}{dt}p(x_m, \dot{x}_m) = l(x_m, \dot{x}_m)m_m\ddot{x}_m \tag{C.5}$$